Ubiquitous IoT through space communications

Zheng Zhou

THÈSE

En vue de l'obtention du

DOCTORAT DE L'UNIVERSITÉ FÉDÉRALE TOULOUSE MIDI-PYRÉNÉES

Délivré par :
l'Université Toulouse 3 Paul Sabatier (UT3 Paul Sabatier)

Présentée et soutenue le *28/10/2024* **par :**

Zheng ZHOU

Ubiquitous IoT through space communications

JURY

D. DRAGOMIRESCU	Professeure des universités	Présidente du Jury
D. DONSEZ	Professeur des universités	Rapporteur
C. PHAM	Professeur des universités	Rapporteur
M. PALATTELLA	Principal scientist	Examinateur
J. DECROIX	Ingénieur	Invité
N. ACCETTURA	Chargé de recherche	Co-directeur de thèse
P. BERTHOU	Professeur des universités	Directeur de thèse

École doctorale et spécialité :
MITT : Domaine STIC : Réseaux, Télécoms, Systèmes et Architecture
Unité de Recherche :
Laboratoire d'analyse et d'architecture des systèmes
Directeur(s) de Thèse :
Pascal BERTHOU et *Nicola ACCETTURA*
Rapporteurs :
Didier DONSEZ et *Congduc PHAM*

Acknowledgments

These three years of my PhD journey have passed in the blink of an eye. This period has been a precious chapter in my life, during which I grew academically and matured my personality. It has been a time filled with challenges but even more so with achievements. I want to express my deepest gratitude to everyone who has supported, encouraged, and helped me.

First and foremost, I would like to thank my supervisors, Nicola Accettura and Pascal Berthou, for their trust and guidance during these three years. I am thankful for their encouragement and insightful advice during challenging times. I also thank the jury members for their invaluable feedback and suggestions. Additionally, I would like to thank all the researchers at SARA for their support and expertise.

I would like to thank all the PhD students at SARA, who became like family while I lived alone in France. Their support, kindness, and companionship helped me through difficult times. I am genuinely thankful for their warmth and encouragement.

I would like to thank my family and friends back home. I am profoundly grateful to my parents for your love and selfless support. Your faith in me has always been my greatest motivation. I am also grateful to my friends for their constant encouragement.

Finally, I would like to thank Yiyao Zhai. During these three years, your presence has been a constant source of motivation and comfort. This journey would not have been the same without you.

Abstract

In recent years, Low-Power Wide-Area Networks (LPWAN) have emerged as a critical enabling technology for the Internet of Things (IoT) since they offer a cheap and affordable solution for connecting very low-power devices over long distances. Among various LPWAN technologies, Narrowband IoT (NB-IoT) has become a widely favored solution, particularly for applications requiring wide coverage and reliable communication. However, with the growing need to extend IoT connectivity to remote and underserved areas, there is an increasing interest in integrating NB-IoT with satellite networks, specifically Low Earth Orbit (LEO) satellites. This integration presents unique challenges due to satellite communication's dynamic nature, including issues related to synchronization and the management of a high density of User Equipments (UE) during the random access procedure, etc. In response to these challenges, this thesis makes several key contributions. First, a comprehensive framework based on key performance indicators (KPIs), such as reliability, latency, throughput, and energy efficiency, has been developed to evaluate and optimize IoT communications via satellite systematically. This framework provides a structured approach to balancing the trade-offs inherent in satellite-based IoT networks. Next, the thesis introduces a novel method for downlink synchronization that operates without relying on the Global Navigation Satellite System (GNSS), thereby reducing energy consumption and improving synchronization accuracy in LEO satellite environments. Building on this, a GNSS-free wake-up strategy is proposed to enhance energy efficiency, especially in scenarios with intermittent satellite coverage. This strategy allows UEs to conserve power by managing their active and sleep states, extending battery life without compromising communication reliability. Finally, the thesis addresses the challenge of random access in high-density environments by proposing an early detection method to reduce collisions during the random access procedure. This method improves the network's capacity to handle many UEs, ensuring that more UEs can access the network with fewer collisions. Together, these contributions offer a comprehensive set of solutions to overcome the limitations of current NB-IoT and LEO satellite integration strategies, paving the way for more efficient and scalable IoT networks in challenging environments.

Keywords: IoT, LPWAN, Satellite

Résumé

Ces dernières années, LPWAN sont devenus une technologie clé pour l'IoT, car ils offrent une solution abordable pour connecter des dispositifs à très faible consommation d'énergie sur de longues distances. Parmi les différentes technologies LPWAN, NB-IoT est devenu une solution largement privilégiée, en particulier pour les applications nécessitant une large couverture et une communication fiable. Cependant, avec le besoin croissant d'étendre la connectivité IoT aux zones reculées et mal desservies, l'intégration du NB-IoT avec les réseaux satellites, en particulier les satellites LEO, suscite un intérêt croissant. Cette intégration présente des défis uniques en raison de la nature dynamique des communications par satellite, notamment en ce qui concerne la synchronisation et la gestion d'une densité élevée de UEs lors de la procédure d'accès aléatoire, etc. En réponse à ces défis, cette thèse apporte plusieurs contributions clés. Tout d'abord, un cadre complet basé sur des KPIs, tels que la fiabilité, la latence, le débit et l'efficacité énergétique, a été développé pour évaluer et optimiser systématiquement les communications IoT via satellite. Ce cadre offre une approche structurée pour équilibrer les compromis inhérents aux réseaux IoT basés sur les satellites. Ensuite, la thèse introduit une méthode novatrice de synchronisation descendante qui fonctionne sans dépendre du GNSS, réduisant ainsi la consommation d'énergie et améliorant la précision de la synchronisation dans les environnements de LEO. En s'appuyant sur cela, une stratégie de réveil sans GNSS est proposée pour améliorer l'efficacité énergétique, notamment dans les scénarios de couverture satellite intermittente. Cette stratégie permet aux UEs d'économiser de l'énergie en gérant leurs états actifs et en veille, prolongeant ainsi la durée de vie de la batterie sans compromettre la fiabilité des communications. Enfin, la thèse aborde le défi de l'accès aléatoire dans les environnements à haute densité en proposant une méthode de détection précoce pour réduire les collisions lors de la procédure d'accès aléatoire. Cette méthode améliore la capacité du réseau à gérer un grand nombre de UEs, garantissant que davantage de UEs peuvent accéder au réseau avec moins de collisions. Ensemble, ces contributions offrent un ensemble complet de solutions pour surmonter les limitations des stratégies actuelles d'intégration du NB-IoT et des satellites LEO, ouvrant la voie à des réseaux IoT plus efficaces et évolutifs dans des environnements difficiles.

Mots clés : IoT, LPWAN, Satellite

Contents

List of Figures

List of Tables

Glossary

3GPP 3rd Generation Partnership Project

ABP Activation Before Personalization

ACK Acknowledgment

AoA Angle of Arrival

AWGN Additive White Gaussian Noise

CE Coverage Enhancement

CP Control Plane

CSS Chirp Spread Spectrum

DtS Direct-to-Satellite

E-UTRAN Evolved Universal Terrestrial Radio Access Network

EDT Early Data Transmission

eMTC enhanced Machine Type Communication

eNB Evolved Node B

EPC Evolved Packet Core

ETSI European Telecommunications Standard

FCC Federal Communications Commission

FDMA Frequency Division Multiple Access

GEO Geostationary Earth Orbit

GNSS Global Navigation Satellite Systems

GSM Global System for Mobile

ISL inter-satellite link

ISM Industrial, Scientific, and Medical

KPI Key Performance Indicator

LEO Low Earth Orbit

LNS LoRaWAN Network Server

LoRa Long Range

LPWAN Low-Power Wide-Area Network

LTE Long Term Evolution

MEO Medium Earth Orbit

MIB Master Information Block

NB-IoT Narrowband Internet of Thing

NPDCCH Narrowband Physical Downlink Control Channel

NPDSCH Narrowband Physical Downlink Shared Channel

NPRACH Narrowband Physical Random Access Channel

NPSS Narrowband Primary Synchronization Signal

NPUSCH Narrowband Physical Uplink Shared Channel

NSSS Narrowband Secondary Synchronization Signal

NTN Non-Terrestrial Networks

OFDMA Orthogonal Frequency-Division Multiple Access

OTAA Over The Air Activation

PRB Physical Resources Block

RAO Random Access Opportunity

RE Resource Element

RFID Radio Frequency IDentification

SC-FDMA Single Carrier-Frequency Division Multiple Access

SF Spreading Factor

SIB System Information Block

TA Timing Advance

TDMA Time Division Multiple Access

TLE Two-Line Element

UE User Equipment

UP User Plane

URL Uniform Resource Locator

UTC Coordinated Universal Time

Introduction

– Version française plus bas –

Over the last years, with the scale of the Internet of Things (IoT) expanding and the consequent sprout of a bigger and bigger variety of IoT applications [Al-Fuqaha 2015b], Low-Power Wide-Area Networks (LPWANs) have gained the interest of researchers and practitioners for their easy and low-cost deployments based on long-distance wireless communications [Mekki 2019]. Many LPWAN technologies have been developed recently. The unlicensed spectrum was recently populated by loss-tolerant LPWAN technologies, quickly dominating the IoT landscape and market due to their easy deployment. Among them, Sigfox [Sigfox 2010] and the Long Range (LoRa) technology [Semtech 2009]. At the same time, the Narrowband IoT (NB-IoT) technology is gaining widespread attention because its synchronization and resource allocation strategy make it exceptionally effective in applications requiring high reliability and connection quality [Migabo 2020]. Designed by the 3rd Generation Partnership Project (3GPP) since Release 13, NB-IoT works over the licensed spectrum. It inherits and simplifies most of the features of Long Term Evolution (LTE), thus being compatible with existing infrastructure and significantly reducing deployment complexity [3GPP 2015].

However, there are significant limitations regarding geographic coverage in traditional ground networks. Thereby, backhauling IoT devices with satellite networks has emerged as a significant advancement towards the objective of global connectivity [Palattella 2018]. Remarkably, the Direct-to-Satellite (DtS) architecture [Fraire 2019] represents the most challenging network scenario since battery-operated LPWAN devices on the ground are meant to communicate with satellites in their visibility directly. Compared to the Medium Earth Orbit (MEO) or Geostationary Earth Orbit (GEO) satellites, Low Earth Orbit (LEO) satellites are particularly advantageous for DtS IoT communications because of their closer distance to the Earth's surface. Specifically, closer distances translate into lower propagation delay, and this is a desired feature for real-time data transmission applications. Furthermore, the implied higher strength of received signals permits more efficient communications with very low-power devices [Centenaro 2021b]. More recently, the research on CubeSat LEO satellites has greatly reduced their costs [Poghosyan 2017, Yaqoob 2022].

However, the high maneuverability of LEO satellites introduces significant variability in both the Doppler effect and the propagation delay, which presents a major challenge for maintaining NB-IoT networks synchronized [Mannoni 2022]. The current mainstream solution involves using Global Navigation Satellite Systems (GNSS) to locate devices while simultaneously calculating their relative position to the satellite to pre-compensate for frequency and delay. However, this approach significantly increases the energy consumption of IoT devices, as GNSS modules

need to operate continuously to provide real-time positioning and timing information. Additionally, in the absence of a global coverage satellite constellation, availability also poses a significant challenge. Most IoT devices do not frequently transmit data, and when they do need to transmit, there may not be a satellite within range, leading to wasted energy. This intermittent connectivity issue causes devices to consume power while waiting for a transmission opportunity, thus reducing the overall energy efficiency. Therefore, improving transmission scheduling strategies is crucial for enhancing the performance of IoT networks backhauled by LEO satellites. Finally, due to satellites' significantly larger coverage area compared to traditional terrestrial networks, the random access phase of NB-IoT can result in a large number of devices attempting to connect simultaneously, leading to channel congestion and high collision rates. To effectively manage these challenges, more advanced access control needs to be developed to ensure reliable connections and efficient data transmission.

The primary objective of this thesis is to investigate the integration of NB-IoT with LEO satellites, addressing key challenges such as Doppler shift, synchronization, and energy efficiency. This research aims to develop and validate methodologies for lightweight synchronization of NB-IoT devices with LEO satellites through Doppler prediction and to propose a wake-up strategy that enables GNSS-free NB-IoT communication with sparse LEO satellite constellations, thereby reducing energy consumption and enhancing device autonomy. Additionally, the thesis explores leveraging timing advance (TA) values for collision detection and resolution in scenarios where multiple devices communicate simultaneously with a satellite. The performance of the proposed solutions is evaluated through extensive simulations. The aim is to ensure reliable, efficient, and scalable NB-IoT DtS communication, ultimately facilitating the deployment of IoT devices in the most remote and inaccessible regions of the world.

Organisation of the thesis

This thesis is organized into five chapters. Chapter 1 provides a comprehensive overview of LPWAN technologies, focusing on LoRa and NB-IoT, and discusses the characteristics and advantages of LEO satellites for IoT applications. This chapter also reviews existing literature and identifies key challenges such as the Doppler effect, synchronization, and energy efficiency and explores the trade-offs between reliability, capacity, latency, and energy efficiency in LPWAN connectivity through LEO satellites. Chapter 2 delves into lightweight synchronization methodologies for NB-IoT devices with LEO satellites through Doppler prediction without using GNSS, presenting detailed methodologies and simulation results. Chapter 3 introduces a GNSS-free wake-up strategy for NB-IoT devices. This strategy allows devices to estimate satellite passes and wake up only when necessary, significantly reducing energy consumption. Chapter 4 discusses the use of TA values for collision detection and resolution in scenarios where multiple devices communicate

simultaneously with a satellite. Finally, the conclusion chapter summarizes the key contributions of the thesis, discusses the implications of the research findings, and outlines potential directions for future work.

Au cours des dernières années, avec l'expansion de l'IoT et l'apparition consécutive d'une variété de plus en plus grande d'applications IoT, LPWAN ont suscité l'intérêt des chercheurs et des praticiens pour leurs déploiements faciles et peu coûteux basés sur des communications sans fil à longue distance. De nombreuses technologies LPWAN ont été développées récemment. Le spectre non licencié a été récemment peuplé par des technologies LPWAN tolérantes aux pertes, dominant rapidement le paysage et le marché de l'IoT en raison de leur déploiement facile. Parmi elles, Sigfox et la technologie LoRa. Parallèlement, la technologie NB-IoT suscite une attention croissante en raison de sa stratégie de synchronisation et d'allocation des ressources, ce qui la rend exceptionnellement efficace dans les applications nécessitant une grande fiabilité et qualité de connexion. Conçue par 3GPP depuis la Release 13, la NB-IoT fonctionne sur le spectre licencié. Elle hérite et simplifie la plupart des caractéristiques de LTE, étant ainsi compatible avec l'infrastructure existante et réduisant considérablement la complexité du déploiement.

Cependant, il existe des limitations significatives en ce qui concerne la couverture géographique dans les réseaux terrestres traditionnels. Ainsi, le raccordement des appareils IoT aux réseaux satellitaires est apparu comme une avancée significative vers l'objectif de la connectivité mondiale. Notamment, l'architecture DtS représente le scénario réseau le plus exigeant, car les dispositifs LPWAN fonctionnant sur batterie au sol sont censés communiquer directement avec les satellites dans leur champ de vision. Comparés aux satellites en MEO ou GEO, les satellites en LEO sont particulièrement avantageux pour les communications IoT DtS en raison de leur proximité avec la surface terrestre. Plus précisément, cette proximité se traduit par un délai de propagation plus faible, ce qui est une caractéristique

souhaitée pour les applications de transmission de données en temps réel. De plus, la plus grande force du signal reçu permet des communications plus efficaces avec des dispositifs très basse consommation. Plus récemment, la recherche sur les satellites LEO CubeSat a considérablement réduit leurs coûts.

Cependant, la grande manœuvrabilité des satellites LEO introduit une variabilité significative à la fois dans l'effet Doppler et le délai de propagation, ce qui représente un défi majeur pour le maintien de la synchronisation des réseaux NB-IoT. La solution actuelle consiste à utiliser des GNSS pour localiser les appareils tout en calculant simultanément leur position relative par rapport au satellite pour précompenser la fréquence et le délai. Cependant, cette approche augmente considérablement la consommation d'énergie des appareils IoT, car les modules GNSS doivent fonctionner en continu pour fournir des informations de positionnement et de synchronisation en temps réel. De plus, en l'absence d'une constellation de satellites à couverture mondiale, la disponibilité pose également un défi majeur. La plupart des appareils IoT ne transmettent pas fréquemment de données, et lorsqu'ils ont besoin de transmettre, il se peut qu'il n'y ait pas de satellite à portée, ce qui entraîne une perte d'énergie. Ce problème de connectivité intermittente oblige les appareils à consommer de l'énergie en attendant une opportunité de transmission, réduisant ainsi l'efficacité énergétique globale. Par conséquent, l'amélioration des stratégies de planification des transmissions est cruciale pour améliorer les performances des réseaux IoT via satellites LEO. Enfin, en raison de la couverture nettement plus large des satellites par rapport aux réseaux terrestres traditionnels, la phase d'accès aléatoire du NB-IoT peut entraîner un grand nombre d'appareils tentant de se connecter simultanément, ce qui provoque une congestion du canal et des taux de collision élevés. Pour gérer efficacement ces défis, un contrôle d'accès plus avancé doit être développé afin d'assurer des connexions fiables et une transmission de données efficace.

L'objectif principal de ce manuscrit est d'étudier l'intégration du NB-IoT avec les satellites LEO, en abordant les défis clés tels que le décalage Doppler, la synchronisation et l'efficacité énergétique. Cette recherche vise à développer et valider des méthodologies pour la synchronisation légère des appareils NB-IoT avec les satellites LEO par la prédiction Doppler, et à proposer une stratégie de réveil permettant une communication NB-IoT sans GNSS avec des constellations de satellites LEO clairsemées, réduisant ainsi la consommation d'énergie et améliorant l'autonomie des appareils. De plus, le manuscrit explore l'utilisation des valeurs d'avance de temps (TA) pour la détection et la résolution des collisions dans les scénarios où plusieurs appareils communiquent simultanément avec un satellite. Les performances des solutions proposées sont évaluées par le biais de simulations approfondies. L'objectif est d'assurer une communication DtS NB-IoT fiable, efficace et évolutive, facilitant ainsi le déploiement d'appareils IoT dans les régions les plus reculées et inaccessibles du monde.

Ce manuscrit est organisé en cinq chapitres. Le Chapitre 1 offre une vue d'ensemble complète des technologies LPWAN, en se concentrant sur LoRa et NB-IoT, et discute des caractéristiques et avantages des satellites LEO pour les appli-

cations IoT. Ce chapitre passe également en revue la littérature existante, identifie les principaux défis tels que l'effet Doppler, la synchronisation et l'efficacité énergétique, et explore les compromis entre fiabilité, capacité, latence et efficacité énergétique dans la connectivité LPWAN via les satellites LEO. Le Chapitre 2 se penche sur les méthodologies de synchronisation légère pour les appareils NB-IoT avec les satellites LEO grâce à la prédiction Doppler sans utiliser le GNSS, en présentant des méthodologies détaillées et des résultats de simulation. Le Chapitre 3 introduit une stratégie de réveil sans GNSS pour les appareils NB-IoT. Cette stratégie permet aux appareils d'estimer les passages des satellites et de se réveiller uniquement lorsque cela est nécessaire, réduisant ainsi considérablement la consommation d'énergie. Le Chapitre 4 de l'utilisation des valeurs TA pour la détection et la résolution des collisions dans les scénarios où plusieurs appareils communiquent simultanément avec un satellite. Enfin, la conclusion résume les principales contributions du manuscrit, discute des implications des résultats de recherche, et propose des orientations potentielles pour les travaux futurs.

Chapter 1

Background and thesis problematic

Ce chapitre présente une analyse approfondie des protocoles NB-IoT et LoRaWAN et de leur intégration avec les satellites LEO. L'objectif principal est d'évaluer leurs performances en termes de fiabilité, latence, débit et efficacité énergétique, et de proposer une approche méthodologique pour concevoir un réseau optimisé. Contrairement aux réseaux terrestres, les communications par satellite posent des défis uniques tels que l'effet Doppler, les délais de transmission prolongés et la gestion de l'énergie. Ce chapitre met en évidence les avantages et les inconvénients de chaque protocole dans le contexte des communications par satellite et propose des solutions pour surmonter les défis techniques, en mettant l'accent sur l'importance d'une approche équilibrée pour optimiser les KPIs

Contents

The emergence of an IoT infrastructure based on LPWAN backhauled by satellites has opened up new avenues for connectivity, providing an affordable and viable solution for remote and inaccessible areas. However, this approach still faces a lot of challenges. This chapter presents a comprehensive overview of the background and the main issues addressed in this thesis, focusing on the architecture and challenges of integrating satellite and terrestrial networks for IoT applications. The rest of the chapter is organized as follows. Sec.1.1 introduces the concept of IoT, providing a foundation for understanding the broader context of this thesis. Sec.1.2 delves into

LPWAN technologies, including LoRaWAN and NB-IoT. Sec.1.3 explores Direct-to-Satellite IoT, discussing network architectures, different satellite orbits for DtS IoT, and the associated research challenges. Finally, Sec.1.4 introduces the key performance indicators used to evaluate the performance of satellite IoT networks and builds a general framework for the following research.

1.1 Internet of Things

The Internet of Things is a technological paradigm enabling various physical devices, such as vehicles, home appliances, sensors, etc., being connected through the Internet. The core idea underneath the IoT is to achieve data collection, transmission, and processing even in real time through physical devices, software, and other techniques [Atzori 2010, Gubbi 2012].

IoT has found diverse applications across various sectors based on this foundational capability. In healthcare, real-time health data monitoring can provide patients with personalized care and timely medical intervention [Selvaraj 2019]. Also, in the industrial sector, IoT can monitor equipment conditions, predict failures, and facilitate preventive maintenance, thereby reducing maintenance costs [Xu 2014]. Beyond these examples, IoT also plays a critical role in environmental monitoring, smart grids, and other applications essential for building smart cities. These technologies enable efficient resource management, improve urban infrastructure, and enhance the overall quality of life in urban areas [Zanella 2014]. In addition to smart cities, IoT has also found valuable applications in other fields, particularly in remote and rural areas, such as agriculture [Mowla 2023], forest fire prevention, wildlife monitoring [Choudhary 2020], etc.

Since the concept of IoT was introduced in the 1990s [Ashton 2009], its technological development has steadily advanced. Initially, IoT emerged with Radio Frequency IDentification (RFID) technology to meet the demands of fast logistics. As costs decreased and technology evolved, IoT expanded into vertical market applications such as monitoring, security, and transportation [Lv 2021] and enabled the localization of people or objects [Asaad 2021]. Since the 2020s, with miniaturized electronics and 5G development, IoT has evolved towards a ubiquitous network infrastructure allowing remote operation and monitoring, where a Uniform Resource Locator (URL) can identify every smart device [Jamshed 2022].

The types of IoT communication technologies have also increased to support the growing range of applications [Al-Fuqaha 2015a]. There are many ways to differentiate between different types of communication technologies, and the two most basic are wired and wireless. Wired technologies include Ethernet, Modbus, etc. Furthermore, wireless technologies can be further differentiated by their transmission distance. Short-range wireless technologies typically work within a distance of 100 meters or less. Examples include Bluetooth, Wi-Fi, ZigBee, etc [Borgia 2014]. It is commonly used in applications like connecting smartphones to speakers, home automation systems, and personal area networks. Medium-range wireless technologies

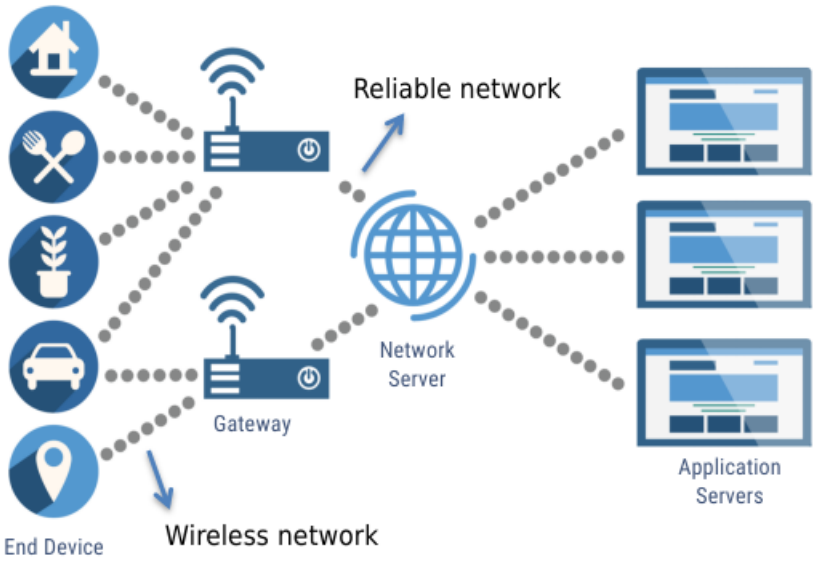

Figure 1.1: Architecture of LPWAN

generally operate within a distance of up to several kilometers. Examples include LTE-Advanced and 5G, which are used in mobile communications, smart city infrastructure, and remote monitoring systems where devices need to connect over larger areas but not over extremely long distances [Stiller 2020]. Long-range wireless technologies typically operate over distances ranging from several kilometers to tens of kilometers, making them ideal for applications such as smart agriculture, remote environmental monitoring, and wide-area IoT deployments. Due to the long distances, recharging or replacing device batteries is often difficult, leading to the development of Low Power Wide Area Networks (LPWAN). The latter are designed to address these challenges by offering low power consumption and extended battery life, making it a key focus of this thesis. They will be explored in detail in the next section.

1.2 Low-Power Wide-Area Networks

LPWANs are designed to connect a large number of low-power devices across large areas, enabling the communication necessary for a wide range of IoT applications. The architecture of LPWAN can be understood through its key components, as showed in Fig. 1.1.

Starting from the *end devices*, which are deployed in various applications introduced in Sec. 1.1. These devices are characterized by low power consumption, enabling them to operate for extended periods on battery power. Then, end devices are able to communicate with *gateways* through a wireless network. This network supports long-range communication, which will be introduced later, allowing devices located far from the gateway to connect with it. Gateways act as intermediaries

between end devices and the network server. They receive data from multiple end devices over the wireless network and forward it to the *network server* over a reliable network connection. The reliable network segment ensures that data transmitted from gateways to the network server is done reliably and securely. This network is often based on robust communication technologies like Ethernet, cellular networks, or satellite links. The network server is the central component that manages the entire LPWAN. It handles data processing, device management, and communication protocols, ensuring that data from end devices is correctly processed and routed to the appropriate application servers. Finally, *application servers* are where the collected data is processed, analyzed, and utilized. They provide the interface for users to interact with the data and derive actionable insights.

In summary, LPWANs offer a scalable and efficient way to connect numerous low-power IoT devices over large distances. In the following sections, two LPWAN protocols that have garnered significant attention will be introduced in detail: LoRa and NB-IoT.

1.2.1 LoRaWAN

In detail, **LoRa** was introduced by Semtech Corporation [1] and adopts a *Chirp Spread Spectrum* (CSS) modulation scheme to enable long-range communication even in noisy environments [Knight 2016]. Herein, a narrowband input signal is spread over a wider bandwidth and immediately transmitted; then, it can be correctly decoded very far away, even if severely attenuated. The LoRa modulation further enables the use of several Spreading Factors (SFs) to increase the ability of the receiver to decode simultaneous signal transmissions on the same frequency channel. Each SF is associated with a specific data rate, transmission range, and energy consumption. Such communications happen on the *unlicensed* Industrial, Scientific, and Medical (ISM) *band*, thus competing for the use of the radio resources with other interfering technologies operating in the same frequency bands. The enormous interest of companies in such cutting-edge technology pushed for the creation of the LoRa Alliance, which aims to promote LoRa and design a Medium Access Control (MAC) layer capable of managing the communication resource exploitation in LoRa Wide Area Networks (LoRaWAN).

From the architectural point of view, for LoRaWAN, low-power End Devices (EDs) communicate through LoRa links with all the LoRaWAN Gateways in their transmission range. The LoRaWAN Network Server (LNS) totally controls the gateways. They encapsulate uplink LoRa frames received by EDs within TCP/IP packets and forward them to the LNS. The gateways also forward the downlink traffic from LNS to EDs. In fact, the LoRaWAN MAC protocol is established between any ED and the LNS. In turn, the LNS can be interconnected with several application servers.

The LoRaWAN protocol adopts an ALOHA-based random access scheme [Polonelli 2019] as Medium Access Control Protocol. End devices

[1] Semtech: https://www.semtech.com/lora

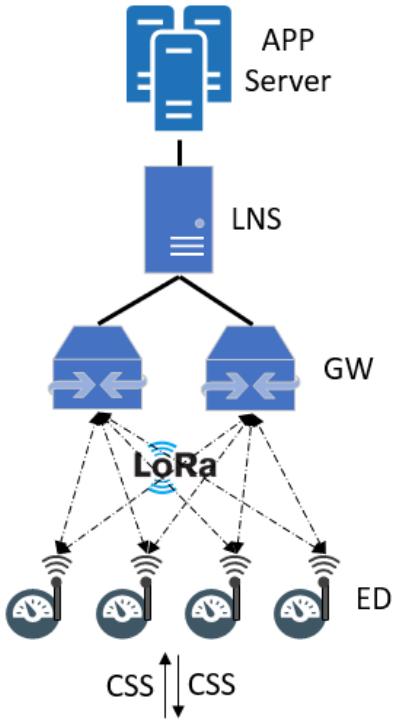

Figure 1.2: Architecture of LoRaWAN

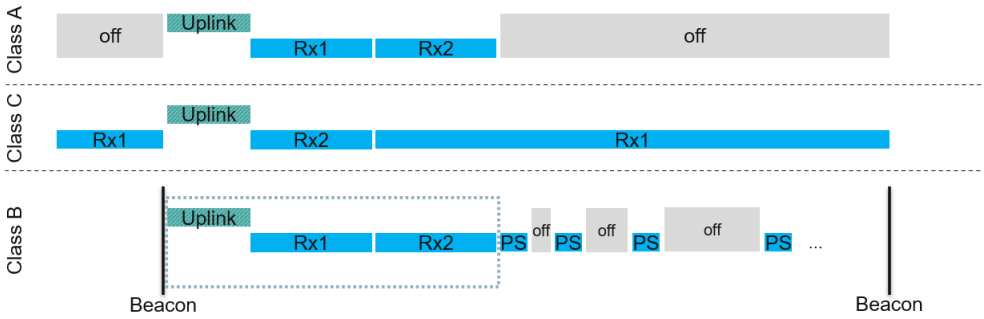

Figure 1.3: Different classes of LoRaWAN

(EDs) transmit without listening and sensing the channel before. The LoRa EDs can operate in three different communication classes, illustrated in Figure 1.3. Class A is the simplest mode and the default class, supported by all the EDs. After each uplink transmission, two receive windows, $Rx1$ and $Rx2$, are opened, allowing the ED to receive downlink traffic from the LNS through the gateway. The ED waits for $1s$ before opening the $Rx1$. If the ED cannot receive a downlink in the $Rx1$, it opens the $Rx2$ after an additional delay of $1s$. The ED switches into sleep mode after $Rx2$, till the next uplink has started. Class C is like Class A, with the difference that the receiving windows are never closed and stay open until

the next uplink. Thus, class C is less energy-efficient than Class A. In Class B, the EDs use beacon messages sent from the gateway to synchronize with the LNS. It allows the EDs to open additional receive windows, named ping slots, without the need for prior uplink transmission. Since ED must be in RX mode during the ping slots, Class B implies additional energy consumption compared to Class A. It must be noticed that Class B devices still operate like Class A devices for uplink transmissions.

In a LoRaWAN network, EDs do not negotiate resource allocation with a gateway like NB-IoT, but they still need to join the network before being able to transmit data. To this aim, they should exchange some keys with the LNS, and ensure the secure data exchange over the end-to-end system. Two different join procedures are supported by the standard: Activation Before Personalization (ABP) and Over The Air Activation (OTAA). In the ABP, the keys are pre-stored in the ED. When a message is to be sent, the keys are sent along with the data and authenticated by the LNS. Instead, in the OTAA mode, the EDs need to send a *join request* and receive *join accept* from the LNS, before being accepted in the network.

However, since LoRa uses the unlicensed ISM band, the duty cycle must be configured to limit the maximum amount of data each device can upload daily while respecting access policies. In Europe, the European Telecommunications Standards (ETSI) Institute enforces per sub-band duty-cycle policies ranging from 0.1% to 10% [ETSI 2018]. In the Federal Communications Commission (FCC) regions, a maximum ToA of $400ms$ is imposed for the uplink transmissions, while the duty cycle is not restricted. Finally, concerning the bandwidth, 125 kHz can be adopted in both regions, while 250 kHz and 500 kHz are allowed in the ETSI and FCC regions, respectively.

1.2.2 NB-IoT

Instead, **NB-IoT** employs a *narrow band modulation* and works into the *licensed spectrum*. It was conceived by 3GPP and proposed for the first time in Release 13 [3GPP 2015] to make current cellular networks ready to support IoT applications with low cost, low power consumption, and low data rates. The development of the NB-IoT standard was initially based on the existing LTE functionalities. Such an approach (i.e., leveraging existing technology) minimized the development effort and shortened the time to market. The NB-IoT specification is still evolving, and the most recent releases, i.e., Rel-17 and Rel-18, focus on IoT over Non-Terrestrial Networks (NTN) to provide broader global coverage. Their objective is to address the challenges inherent to the integration of NB-IoT over ground-to-satellite links, i.e., initial synchronization, high propagation delays, Doppler variation rate, high paging load with a considerable number of users, etc. Several companies, like Sateliot[2], Ligado [3], and GateHouse[4], have invested in designing and developing global

[2]Sateliot: https://sateliot.space/en/
[3]Ligado: https://ligado.com/
[4]Gatehouse: https://gatehouse.com/

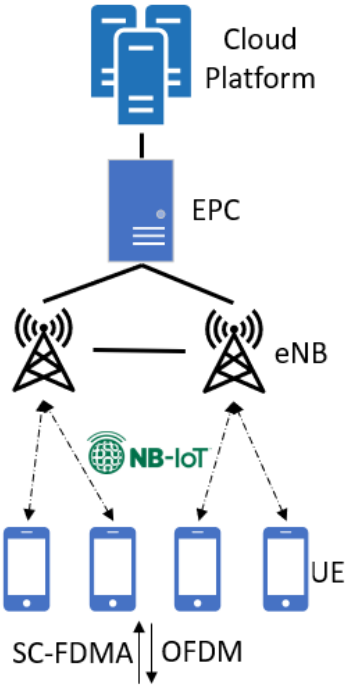

Figure 1.4: Architecture of NB-IoT

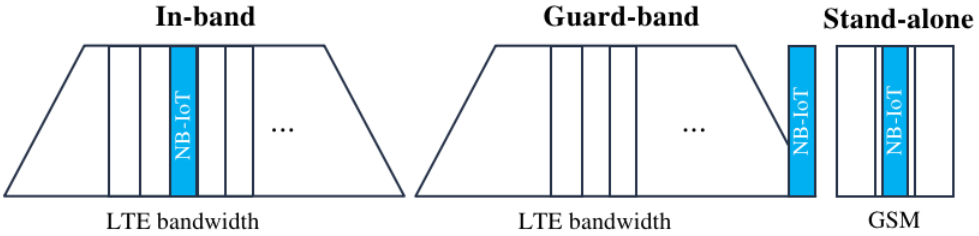

Figure 1.5: Three deployment modes of NB-IoT

NB-IoT satellite networks and can already offer such service.

Similar to LoRaWAN, the NB-IoT network architecture can be divided into two main parts: the core network, namely the Evolved Packet Core (EPC), and the access network, namely the Evolved Universal Terrestrial Radio Access Network (E-UTRAN). EPC is responsible for transmitting the collected IoT data to the cloud platform for further processing and managing mobile devices [3GPP 2015].

The access network includes the User Equipment (UE) and the evolved Node B (eNB). Clearly, an NB-IoT UE plays the same network role as a LoRaWAN ED. Indeed, UEs and EDs are equipped with one or more sensors, a microcontroller, and a radio transceiver, and they are in charge of collecting and transmitting IoT data to the Internet through respectively the EPC and the LNS. Instead, the eNB (as the LoRa gateway) is the base station connecting the UE to the core network.

Like LTE, and differently from LoRa, NB-IoT adopts two different modula-

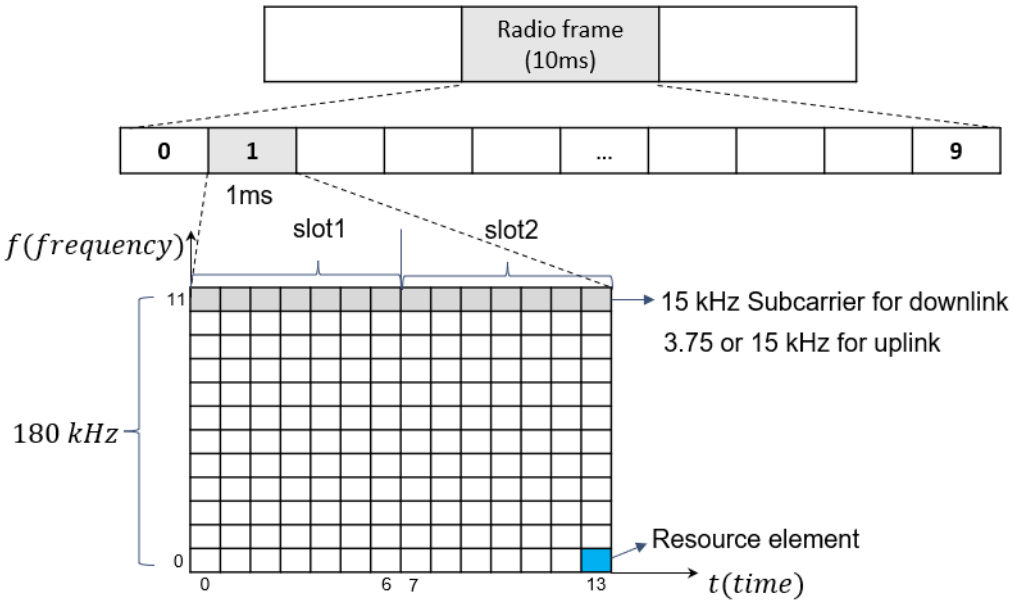

Figure 1.6: Radio Frame of NB-IoT

tion schemes for downlink and uplink messages, respectively Orthogonal Frequency-Division Multiple Access (OFDMA), and Single Carrier-Frequency Division Multiple Access (SC-FDMA). NB-IoT occupies the 180 kHz frequency band, corresponding to a block of resources in the LTE bandwidth. NB-IoT supports three deployment modes, illustrated in Figure 1.5. The In-band mode occupies one of the Physical Resources Blocks (PRBs) of LTE. The Guard-band mode occupies only the protection band of LTE. In the stand-alone mode, NB-IoT can be deployed in any frequency spectrum, such as Global System for Mobile (GSM) frequency bands.

Figure 1.6 illustrates the structure of NB-IoT radio frame. Each radio frame has a duration of 10 ms and is divided into 10 subframes. Each subframe is made up of 2 slots. One subframe consists of 12 x 14 Resource Elements (REs) with a 15 kHz subcarrier for downlink (3.75 kHz or 15 kHz for uplink). 3GPP has defined several channels and signals with distinct functions for uplink and downlink, as described hereafter.

For the downlink, two synchronization signals, Narrowband Primary Synchronization Signal (NPSS) and Narrowband Secondary Synchronization Signal (NSSS), are transmitted in subframes 5 and 9 to synchronize UE and eNB in time and frequency. The first subframe is the Narrowband Physical Broadcast Channel (NPBCH), which is used to exchange critical system information such as deployment mode. The remaining subframes are occupied by the other two channels: Narrowband Physical Downlink Control Channel (NPDCCH) and Narrowband Physical Downlink Shared Channel (NPDSCH). The control channel contains information on uplink and downlink resource scheduling, allowing the UE to know when to receive or send messages. In the shared channel, downlink data and other system

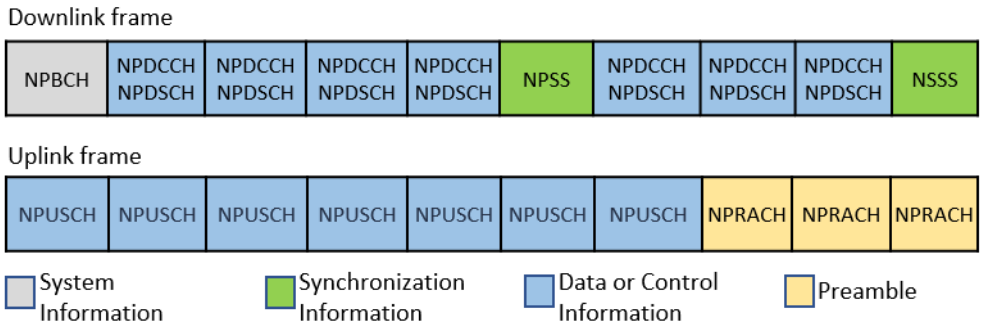

Figure 1.7: Downlink and uplink frames of NB-IoT

messages are exchanged. Note that control and shared channels may occupy several subframes, depending on the size of the message, the number of repetitions, etc.

Two different channels are defined for uplink transmission. The first connection attempt (Random access preamble) of the UE to the eNB is transmitted in Narrowband Physical Random Access Channel (NPRACH), where the collision happens. The uplink data is transmitted in Narrowband Physical Uplink Shared Channel (NPUSCH). Those resources are allocated by the upper layer, avoiding a-priori any collision. Therefore, this channel is also known as a non-contention channel. Finally, NB-IoT supports two transmission modes: Multiton and Singleton. Singleton uplink messages occupy only one subcarrier, while Multiton uplink messages occupy multiple (3, 6, 12) subcarriers. So, multiple UEs can occupy the same channel, allowing more users to be connected simultaneously.

The UE of the NB-IoT must synchronize with the eNB by receiving the synchronization signals before connecting with the eNB. For LoRa, only Class B enables the synchronization between the ED and the gateway using beacons.

When a UE is covered by more than one eNB simultaneously, it measures the received power and then selects the one with the best available coverage (best signal quality). In LoRa, the ED transmits to any gateways in its coverage range. It is up to the LNS to select the best gateway for sending back downlink traffic. Moreover, while in LoRaWAN, the ED receives the configuration parameters from the LNS, in an NB-IoT network, the UE itself determines the Coverage Enhancement (CE) level according to its distance from the eNB and thus, chooses the number of repetitions of a message (2-1024 times). The higher the CE level (0-2), the higher the power consumption of the data transmission [Harwahyu 2021].

When an NB-IoT UE needs to send or receive data through the Internet, it first needs to get synchronized with an eNB in its vicinity [Kanj 2020]. The UE starts a cell search procedure after waking up and waits for NPSS and NSSS signals, as shown in Fig. 1.8. The NPSS is crucial for achieving time and frequency synchronization with the eNB, while the NSSS is used to determine the frame position. Once these synchronization steps are completed, the UE can then receive additional system information, specifically the Master Information Block (MIB) and System

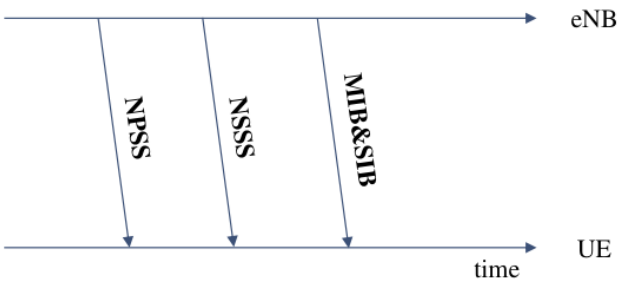

Figure 1.8: The downlink synchronization flow of NB-IoT

Information Blocks (SIBs). The MIB provides essential information for network access, and the SIBs contain detailed configuration parameters necessary for various network operations and services.

The random access process will begin once the UE completes the synchronization with the eNB, as shown in figure 1.9.

Initially, the UE sends a random access preamble to the eNB using the random access channel (Msg1). Upon sending this preamble, the UE starts a timer and waits for a random access response (Msg2) from the eNB.

If no response (Msg2) is received within the allocated time, the UE will attempt the process again by sending a new preamble. Once the UE successfully receives Msg2, it proceeds to send Msg3 to the eNB. Msg3 contains important control information, such as the radio resources allocated to the UE, the data volume that needs to be transmitted, and any reconfiguration requests. The successful transmission of Msg3 depends on the proper alignment and timing established by the TA value provided in Msg2. Finally, Msg4, the connection setup and contention resolution message, is sent from the eNB to the UE. This message indicates that the eNB has successfully identified and resolved any contention, confirming the establishment of the connection with the UE. However, because the temporary ID in Msg2 is calculated based on the subcarrier number, all UEs that selected the same subcarrier will perceive Msg2 as being addressed to them, leading them to send Msg3. This simultaneous transmission can cause collisions as multiple UEs attempt to access the network simultaneously using the same resources. This part will be discussed in Chapter 4. After receiving Msg4, which includes its real ID, the UE will enter the connected state from the idle state. Then, the eNB and UE exchange messages for authentication and AS security configuration (Msg6-9). After that, UE sends its uplink data and receives downlink data. Finally, the eNB releases the connection if it detects inactivity from the UE (Msg10).

NB-IoT defines two optimization methods for data transmission to reduce message exchange: the User Plane (UP) and the Control Plane (CP) optimization.

It must be noticed that for sending and receiving a few bytes of data, the signaling overhead consumed by the UE from the idle state to the connected state is much more significant than the data load. Two optimization schemes have been proposed to make data transmission more efficient: CP and UP optimization. The

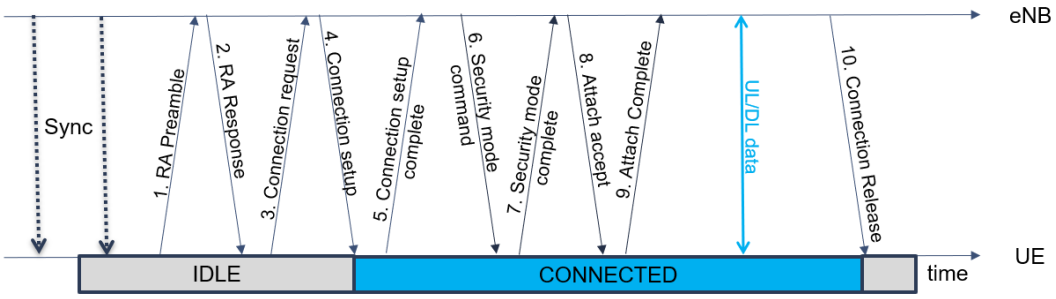

Figure 1.9: NB-IoT Workflow

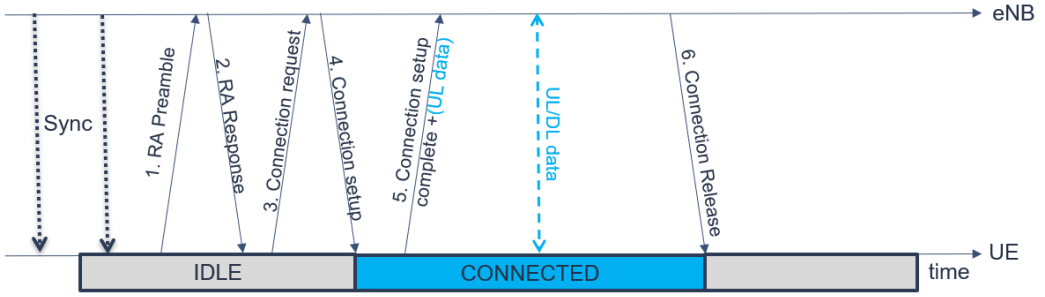

Figure 1.10: NB-IoT CP optimization

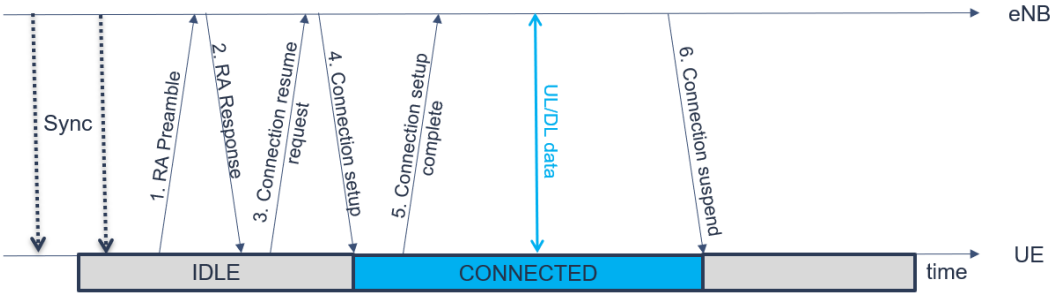

Figure 1.11: NB-IoT UP optimization

CP carries the signaling responsible for accessing the UE, allocating resources (e.g., messages exchanged after random access), etc.; the UP carries the user data. With the CP optimization (Fig. 1.10), small packets can be added to the control message (Msg5) and bypass the security configurations to improve the speed for transferring small data. This mode is insecure compared to other modes.

The UP optimization (Fig. 1.11) allows idle users to transfer data quickly through the *suspend and resume* process. After establishing the first connection, the user's information can be stored in the eNB. No Connection Release message is transmitted. When new data is transferred, the UE can recover the connection without re-establishing the security information.

In Release 15, 3GPP defined the *Early Data Transmission* (EDT) mode to

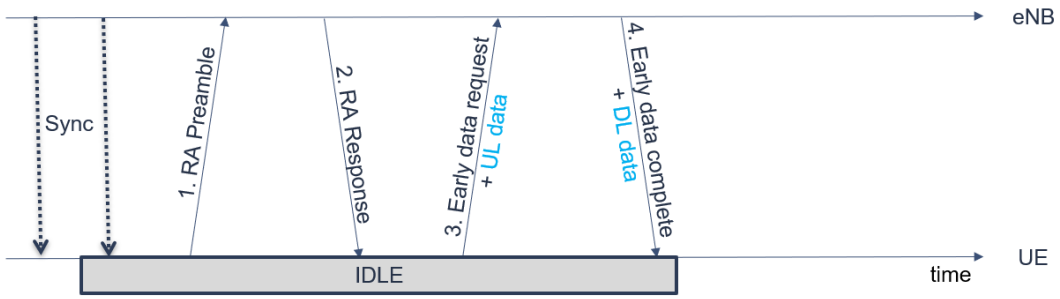

Figure 1.12: NB-IoT Early Data Transmission

reduce UE energy consumption and message latency by reducing the number of transmissions [Hoglund 2018]. Specified for both UP and CP optimization, the EDT can be used when the UE is in idle mode and has less than the maximum broadcast uplink data to send.

In this mode, only four messages between the eNB and the UE are required to complete the data transmission because the data is sent during the random access procedure. As shown in Figure 1.12, the data is included in Msg3. The method of encapsulating and transmitting uplink data is like the optimization of the CP. If the UE receives Msg4 indicating that the procedure is terminated, it can go to the sleep state or stay in the idle state.

Thanks to more complex synchronization and resource allocation techniques, NB-IoT can offer higher reliability than LoRa. This is paid with (i) longer transmission delays, which can be reduced using CP, UP optimization, and EDT; and (ii) higher energy consumption for the IoT device. LoRa, while being more energy-efficient, suffers from high collision probability due to the random access mechanism. Both reliability and throughput can be improved using resource allocation schemes, like TDMA approaches [Piyare 2018].

Table 1.1: Comparative Matrix: NB-IoT vs LoRaWAN

Feature	LoRaWAN	NB-IoT
Specifications	Non-3GPP	3GPP
Uplink Modulation	CSS	SC-FDMA
Downlink Modulation	CSS	OFDM
Frequency Band	ISM unlicensed band	Cellular licensed band
Bandwidth	125/250/500 kHz	180 kHz
Maximum Data Rate	50 kbps	200 kbps
Coverage Range	5-20km [Oliveira 2017]	1-10km
Security	AES 128 bit	3GPP(128-256 bit)

A very high-level summary comparison is provided in Table 1.1. LoRaWAN is ideal for loss-tolerant applications due to its ALOHA-based protocol, which allows devices to transmit data directly without prior connection setup. Operating in the

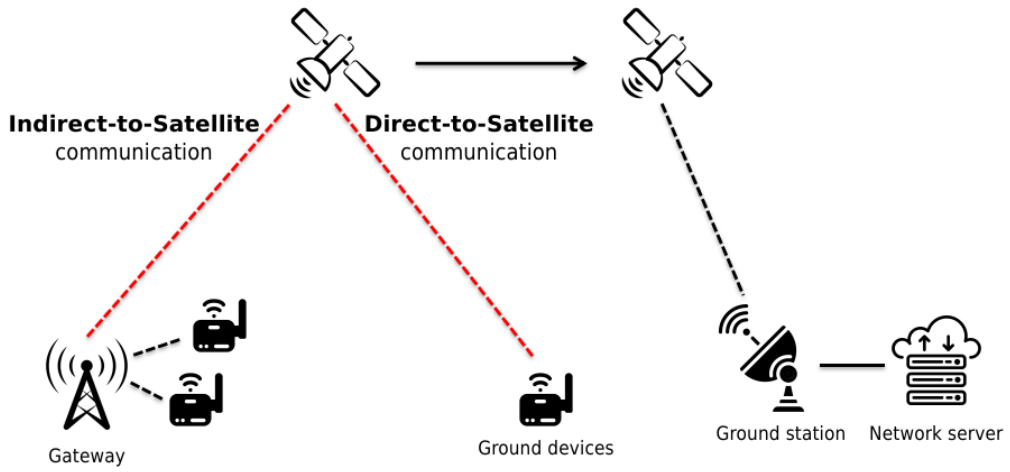

Figure 1.13: Architecture of satellite IoT networks

ISM unlicensed band, LoRaWAN provides flexibility but comes with lower data rates and potential duty cycle restrictions. In contrast, NB-IoT is better suited for delay-sensitive applications. It requires more access procedures, including connection establishment (random access), authentication, and resource allocation before data transmission, which ensures high reliability and security. NB-IoT operates in the licensed spectrum, offers enhanced security with 3GPP standards (128 to 256-bit encryption), and has no duty cycle limitations, allowing continuous data transmission.

1.3 Direct-to-Satellite IoT

For traditional ground-based LPWAN networks, the gateway (eNB) is fixed and has a stable power supply to ensure continuous reception of all data from devices within their coverage area. However, as the variety of applications increases, despite the convenience of long-distance transmission for gateway deployment, there may be significant difficulties in deploying gateways in certain areas, such as mountains and marine regions. Moreover, in natural disasters, wars, and other critical situations, the gateway on the ground or the connection between the gateway and the server can easily be disrupted. Facing these challenges, using satellites as intermediaries to connect ground devices with network servers has emerged as a widely recognized solution [Palattella 2021, Qu 2017, Fang 2021]. Besides extended coverage, the combination of satellites and LPWAN also allows for increasing reliability and network capacity. Satellites may be the only communication medium available when terrestrial networks are unavailable or non-operational.

Moreover, there are two main architectures for satellite communication in IoT networks: Direct-to-Satellite (DtS) [Fraire 2019] and Indirect-to-Satellite, as shown in Fig. 1.13. The direct and indirect architectures differ primarily in how data is

transmitted from low-power *ground devices* to the network. In the indirect architecture, data from end devices is first sent to a ground-based *gateway*, which then relays the information to satellites. Finally, using traditional satellite protocol, the satellite can communicate with the *network server* through *ground station*. However, the Indirect-to-Satellite architecture can still be limited by the availability and deployment of these gateways. In contrast, the DtS architecture allows ground devices to communicate directly with satellites, eliminating the need for ground-based gateways and making them more suitable for remote or challenging environments, which will be the basic architecture for the rest of this thesis. Furthermore, as previously mentioned, in the communication between satellites and ground stations, the ground stations typically have stable power supplies and higher transmission power, allowing them to utilize traditional satellite communication protocols effectively. Consequently, this thesis will primarily focus on the communication between satellites and ground devices. Among all the different orbits of satellites, LEO satellites can be considered the most suitable option for integrating LPWAN because of their lower latency and reduced power requirements for communication. The detailed comparison of different types of satellites will be discussed in Sec. 1.3.1. However, even though LEO satellites are the most suitable choice, they still face several challenges. Since traditional satellite communication protocols are not feasible for low-power devices, and terrestrial LPWANs are not designed to adapt to long-distance satellite communications. Therefore, it is necessary to adapt existing LPWAN protocols to facilitate effective communication between low-power devices and satellites. These adaptations and the specific challenges they address will be discussed in detail in Sec. 1.3.2.

1.3.1 Low Earth Orbit Satellite for DtS IoT

LEO satellites are satellites that orbit the Earth at altitudes ranging from approximately 500 to 1500 kilometers. LEO satellites have significantly lower latency due to their proximity to the Earth, which is crucial for real-time applications, such as voice and video communication, and for time-sensitive data transmissions required by many IoT applications. The shorter distance between the satellite and the Earth means less path loss, resulting in stronger signals and more reliable communication links. This is beneficial for maintaining connectivity with IoT devices, especially those with low-power transmitters. Their high mobility, traveling at speeds that complete an orbit roughly every 90 to 120 minutes, results in rapidly changing coverage areas and requires complex tracking and handover mechanisms to maintain the connectivity with ground devices. Additionally, LEO satellites have limited onboard power resources, constraining operational capabilities and lifespan. To prolong the service life of LEO satellite constellations, efficient power management and energy-saving technologies are needed.

In contrast, GEO satellites orbit at an altitude of approximately 35786 kilometers, remaining fixed relative to a point on the Earth's surface. While GEO satellites provide consistent coverage over large areas and are ideal for applications

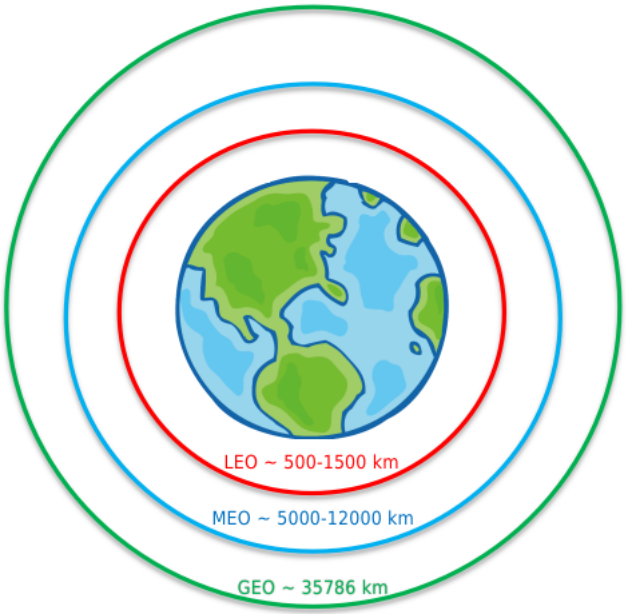

Figure 1.14: Different orbits of satellite

Table 1.2: Comparative Matrix: LEO vs MEO vs GEO Satellites

Feature	LEO	MEO	GEO
Altitude	500-1500 km	5000-12000 km	35786 km
Coverage Area	Small	Medium	Large
Propagation Delay	2-5 ms	17-40 ms	120 ms
Satellites Required	High (many)	Medium	Low (few)
Launch Cost	Low	Medium	High
Lifespan	5-7 years	10-15 years	15-20 years
Handoffs	Frequent	Less frequent	None

like television broadcasting and weather monitoring, they suffer from high latency due to their significant distance from the Earth. This latency makes GEO satellites less suitable for real-time communications and time-sensitive IoT applications. MEO satellites orbit at altitudes between 2,000 and 35,786 kilometers, offering a compromise between LEO and GEO satellites. MEO satellites provide better latency than GEO but still cannot match the low latency offered by LEO satellites. MEO satellites are often used for navigation systems like GPS, where moderate latency is acceptable, and large coverage areas are needed [Vatalaro 1995].

A summary comparison is provided in Table 1.2. Choosing LEO satellites over GEO and MEO satellites for IoT applications hinges on their ability to provide low-latency, high-reliability communication links, essential for real-time and remote applications. LEO satellites' cost-effective deployment and scalability make them a suitable solution for overcoming the limitations of traditional terrestrial networks.

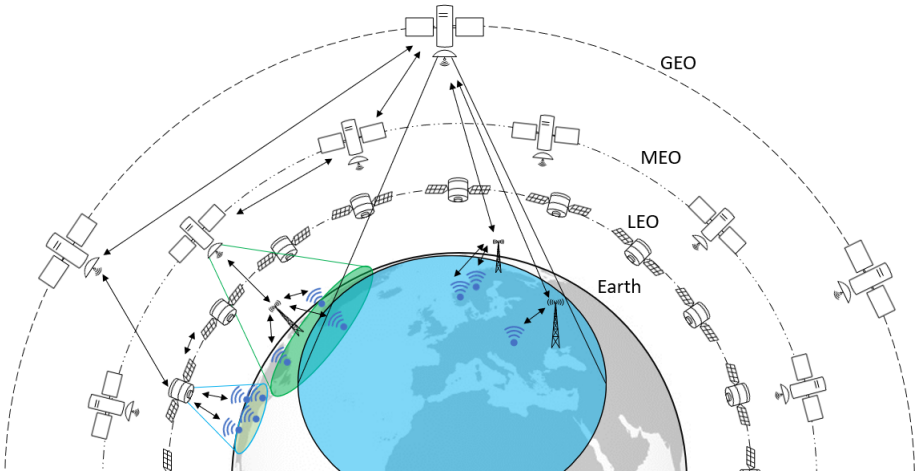

Figure 1.15: Satellites on different orbits

However, integrating with IoT still requires addressing the challenges associated with high mobility, Doppler effects, frequent handoffs, and limited power resources. These challenges will be detailed in the next section.

1.3.2 Research challenges for DtS IoT

Even though LEO satellites are the most appealing for IoT applications due to the shorter round-trip propagation delay that they introduce compared to GEO satellites, their intrinsic orbital properties imply limited visibility time (around 2 minutes per visit). This issue can be overcome by using large constellations of LEO satellites, which are able to provide almost continuous coverage. This problem will be further solved in future systems with relay networks from LEO to GEO satellites and inter-satellite links (ISL). The foreseen scenario is illustrated in Fig. 1.15.

Clearly, connecting IoT devices directly to LEO satellites opens many new opportunities. Besides that, many challenges exist to overcome the smooth integration and interoperability of satellites and LPWAN terrestrial networks [Guidotti 2019, Centenaro 2021a]. This section overviews the challenges, while the following one will discuss their impact on the KPIs introduced in Sec. 1.4.1.

LEO satellites have large relative velocities to the IoT device on the ground, which results in a significant **Doppler effect**. For a LEO-600 km satellite, the maximum Doppler effect is up to ±48 kHz [Conti 2020], which is much larger than the bandwidth of one NB-IoT sub-carrier, equal to only 15 kHz. Moreover, the large distance between the IoT device on the ground and the LEO satellites (500 - 2000 km) introduces a higher **propagation delay**. In NB-IoT networks, UE and eNB must be synchronized in time and frequency. To this aim, several messages are exchanged between the UE and eNB (at least four in EDT mode) before the actual data transmission. Complete the synchronization and resource allocation phase within the limited visibility time of the satellite is a big challenge for NB-IoT. Due

to the Doppler effect and long propagation delay, NB-IoT could easily fail to accomplish the message transmission. [Guidotti 2017, Conti 2020, Liberg 2020] assume that each UE is equipped with a GNSS receiver [Jin 2022] and uses the captured positioning together with the Two-Line Element (TLE) to determine the relative position of the LEO satellite and use this information to predict the frequency and time offset. However, the need for GNSS receivers plays against the two objectives of energy efficiency and cost-effectiveness. While LoRa does not request synchronization between the ED and the gateway prior to the data transmission, the Doppler effect still impacts the LoRa PHY protocol since CSS signals are extremely sensitive to time and frequency offsets. In [Doroshkin 2019], the authors demonstrated that SF 12 is more immune against the Doppler effect when EDs communicate with satellite gateways at a height above 500 Km. Recently, a modification of the LoRa PHY, namely the differential CSS was proposed in [Ben Temim 2022]. Differential CSS allows demodulating the signals without the need to perform a complete frequency synchronization and by tolerating some timing synchronization errors, such as those introduced by the Doppler shift, variable in time.

Satellite communication is remarkable for its long transmission distance, significantly attenuated electromagnetic waves, and high transmission loss. They all together determine the **link budget**, which impacts the energy consumption of the ground equipment, as well the KPIs of the entire system. For NB-IoT, lower spectral efficiency will affect the transmission of resource allocation information. It follows that the UE cannot transmit uplink data on time, which will result in decreased throughput and increased delay [Kodheli 2019, Conti 2020]. The link budget from the LoRa ground sensor to the satellite gateway has been computed empirically in literature [Fernandez 2020], confirming the feasibility of the communication. Both LoRa PHY with SF 12 and LR-FHSS protocol allow increasing network capacity and collision robustness against link budget constraints [Boquet 2021].

As distance increases, ground devices must consume more power than what is needed in terrestrial systems to send or receive messages. This translates into a shorter battery lifetime for the NB-IoT UEs [Kodheli 2019]. The same applies to LoRa EDs. In [Gomez 2021], the authors evaluated the performance of a satellite LoRaWAN using Iridium Satellites: they proved that EDs with a battery of 2400 mAh could operate $\sim$ 1 year, transmitting every 100 minutes. To increase the battery lifetime, the transmission rate should be decreased, which translates into reduced throughput.

A large constellation of LEO satellites with inter-satellite links (as illustrated in Figure 1.15) can provide full and continuous coverage to IoT devices on the heart. Such seamless connectivity comes with increased cost and complexity of the network. A more feasible solution consists of **discontinuous communication** (Fig. 1.16) with a small constellation of few LEO satellites [Tondo 2021]. In such a scenario with intermittent connectivity, to save energy, the IoT devices must wake up and transmit only when the satellite is available. Following the NB-IoT specifications, the synchronization signal must be received before the data transmission. In Release 17 [3GPP 2018], 3GPP proposed using the GNSS signal for the UE to

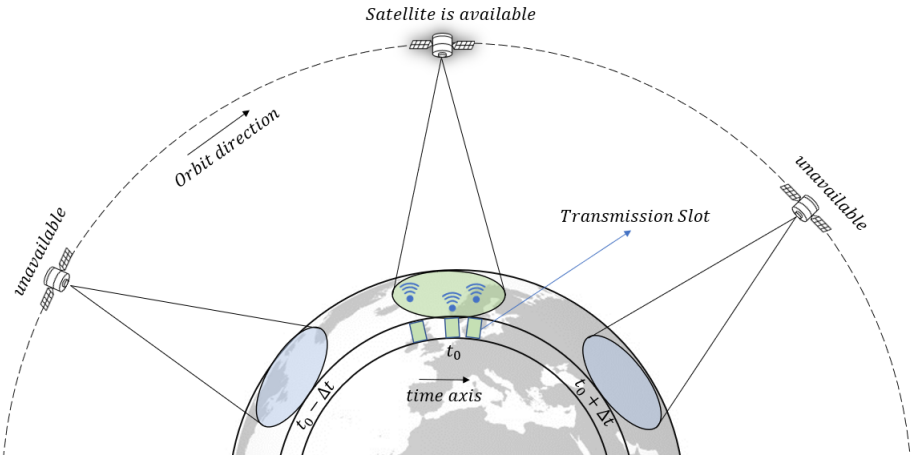

Figure 1.16: LEO satellite coverage

compute the satellites' and their own positions. This information can be used to pre-compensate the Doppler effect, the frequency and time offset caused by the long distance. Those advantages come at the price of high energy consumption. Another solution proposed in literature [Chougrani 2021] makes use of the synchronization signal transmitted in each NB-IoT downlink radio frame to inform on time the ground UEs about the arrival time of the satellite. Even though LoRa, unlike NB-IoT, does not request any synchronization prior to the data transmission, the EDs must be aware of the satellite passes to avoid wasting energy in unsuccessful transmissions. To this aim, the EDs must have access to the TLE data of the satellite. The TLE provides a set of algebraic information, the satellite orbital elements, which allows predicting the satellite's trajectory over time [Guidotti 2017]. Due to deviations from its initial orbit, the TLE data must be updated periodically [Guidotti 2017]. Current satellite LoRaWAN solutions available on the market make use of the TLE data [5]. Due to the considerable number of EDs that could be in the satellite coverage (i.e., within the satellite footprint), knowing the satellite passes is not enough to ensure good network performance. In fact, the probability of collision, already high in LoRaWAN terrestrial networks [Bankov 2019], could only get worse in such a hybrid scenario. It follows the need to adopt scheduling techniques [Afhamisis 2022b] to avoid collisions. In addition, *bulk data transmission* [Zorbas 2021] could be used in combination with TDMA approaches to ensure efficient use of the limited satellite resources (2-3 times visibility per day, for approximately 4 minutes.).

The unavailability of the satellite does not affect only the access network. The communication between the satellite and the network server can be discontinuous too. To ensure end-to-end communication over the entire network and avoid packet drops, the satellite gateway or satellite eNB must be able to store messages and forward them when passing through the ground satellite gateway. The lack

[5]Lacuna Space: https://lacuna.space/

of connectivity between the satellite and the LNS can also hamper the exchange of LoRa-confirmed uplink messages. Even if the packet is correctly received at the LNS, in the absence of ACK (not forwarded at all by the gateway because it is not available, either not transmitted on time or within the receiving windows), the ED will retry the transmission. This results in the wasting of resources: ED's energy, channel resources with contention, and possible collision with other concurrent transmissions. Overall, this deteriorates network performance in terms of reliability, throughput, and energy efficiency.

Discontinuous communication can also cause network authentication problems. In the NB-IoT network, network authentication is unfeasible when the UE and the ground base station are not in the same satellite coverage at the same time. Discontinuous communication makes the handshake between the UE and the core network impossible, which challenges the reliability of the satellite IoT. Like NB-IoT, the LoRaWAN OTAA join procedure would fail when EDs and LNS are not at the same time under the coverage of the satellite gateway [Afhamisis 2022a]. Moreover, stable connectivity is needed to support downlink multicast traffic. Prior to the multicast data exchange, several uplink and downlink unicast messages must be exchanged between the EDs and the LNS (multicast session set-up). Intermittent links would cause the expiration of multicast session timeouts and would thus prevent multicast transmission.

Finally, due to the larger coverage area of satellites, the **higher number of attempts** also presents challenges. For LoRaWAN, collisions can occur when multiple devices attempt to transmit simultaneously within the same frequency channels. For NB-IoT, even if there is a resource allocation strategy in place so that collisions do not occur when transmitting data, collisions may still occur during the random access procedure, where multiple UEs attempt to access the network simultaneously. This leads to increased contention and potential delays in establishing connections.

1.4 Key Performance Indicators for DtS IoT

Interestingly, both LoRa and NB-IoT are highly configurable protocols that allow users to choose among multiple link-layer communication schemes to tackle different reliability requirements. Higher reliability is usually achieved at the price of larger latency. Notably, this trade-off between reliability and latency is highly susceptible to the amount of offered traffic, making the network throughput an additional element to be taken into account when designing the network. As a matter of fact, reliability, latency, and throughput are the three main Key Performance Indicators (KPIs) for any communication network [Soret 2014]. Remarkably, the subset of IoT networks is featured by an additional KPI, i.e., energy efficiency. Indeed, a typical IoT network includes numerous cheap smart devices equipped with batteries, whose most energy-expensive activity is related to the radio module. Hence, IoT communication protocols should be designed to prolong the battery lifetime without requiring frequent substitutions or recharges. All in all, trading off reliability,

Table 1.3: Comparison of the models and their KPI

KPI	NB-IoT	LoRaWAN
Reliability	[Li 2018] [Barbau 2021b] [Cruz 2019]	[Bankov 2019] [Markkula 2019] [Mahmood 2019] [Beltramelli 2018] [Croce 2018] [Sørensen 2017]
Latency	[Migabo 2018] [Li 2018] [Andres-Maldonado 2019] [Azari 2020]	[Bankov 2019] [Sørensen 2017]
Throughput	[Sun 2018] [Migabo 2018] [Cruz 2019]	[Bankov 2019] [Beltramelli 2018] [Markkula 2019]
Energy Efficiency	[Migabo 2018] [Andres-Maldonado 2019] [Azari 2020] [Barbau 2021a]	[Philip 2021] [Nurgaliyev 2020]

latency, throughput, and energy efficiency is the only approach capable of tackling the needs of any application. This section also describes a methodological approach for designing the network, selecting the configuration parameters and traffic patterns, and determining the best trade-off between reliability, latency, throughput, and energy efficiency, considering the challenges introduced by satellites.

1.4.1 Methodological Approach for Performance Evaluation

Before resolving the challenges proposed in Sec. 1.3.2, it is worth designing a basic framework to evaluate the performances of NB-IoT and LoRaWAN, which is the very first step to effectively comparing their modes of operation. Then, the best communication protocol can be selected to fit the target application's requirements, which are expressed as a set of KPIs. In this section, only these four most critical KPIs (**Reliability**, **Latency**, **Throughput**, and **Energy Efficiency**) for LPWAN will be discussed and analyzed. The importance of evaluating all these aspects to choose the most fitting network technology can be intuitively understood as follows. NB-IoT is designed to be a reliable, delay-tolerant protocol on the licensed spectrum, while LoRa is a loss-tolerant protocol. Hence, they provide different link-layer solutions for different needs, making choosing between reliable and delay-constrained protocols possible. With the goal of deeply understanding which parameters affect the identified KPIs, this section focuses on the analysis of the LPWAN terrestrial network. At the same time, an extension to ground-to-satellite communications will be discussed in the following sections.

The most recent works on LPWAN modeling that drove the identification of the

KPIs are listed in Table 1.3.

First of all, a communication protocol is reliable if the transmitter can be notified through an acknowledgment (ACK) about the correct delivery of data frames from the receiver. The lack of any ACK mechanism makes the communication protocol unreliable. This is the case of unconfirmed Class A LoRaWAN frame transmissions. Instead, the portion of acknowledged transmissions provides a measure of the **Reliability** of the communication protocol [Guo 2010]. Such a KPI can be evaluated for LoRaWAN confirmed-based communications and for NB-IoT. When the analyzed protocol enables re-transmission of unacknowledged frames up to a maximum of M times, then the reliability R of the protocol is

$$R = 1 - PLR^M, \tag{1.1}$$

where PLR is the measured Packet Loss Ratio. Clearly, being the PLR a positive real number lower than 1, a higher value for M translates into increased communication reliability [Li 2018]. At the same time, a higher PLR negatively impacts such a KPI. As a consequence, the communication reliability can be kept over a given threshold value by properly tuning either the maximum number of retransmissions M or the PLR. While M can be quickly configured as a parameter setting within the device firmware or via a remote MAC command, the PLR is not a directly configurable parameter since it depends on several variables, as follows:

$$PLR = f(MAC, PHY, g, d), \tag{1.2}$$

As a matter of fact, it is worth noticing that the PLR depends on both MAC and PHY layer configurations. More specifically, a collision-free MAC strategy makes the PLR only dependent on the Signal Noise Ratio (SNR) [Cruz 2019]. Contrariwise, when the MAC layer is contention-based, frames are correctly delivered if they do not incur collisions. Moreover, the PHY layer configuration, such as LoRa's SF value [Beltramelli 2018, Croce 2018] and NB-IoT's CE level, will also affect the PLR. With a higher SF value or CE level, the maximum distance between EDs (UEs) and gateway (eNB) increases. Therefore, the PLR also increases with distance [Markkula 2019]. On the other hand, a broader coverage area corresponds to a higher network load, which in turn increases the collision probability [Bankov 2019]. In addition, the traffic generation rate g of each device and the density of devices d also determine the network load. The collision can happen in both the join and data transmission phase in the LoRaWAN [Bankov 2019, Mahmood 2019, Sørensen 2017] by using the same SF at the same time in the specific channel. But for NB-IoT, the packet loss caused by collision only occurs in the random access phase. By increasing the network load, allocating the limited network resources would be the main issue in the NB-IoT. The resource allocation time (service time) may be too long in the data transmission phase, also resulting in packet loss [Barbau 2021b]. It has to be noticed that the number of retransmissions can also be increased by the unavailability of the

network [Afhamisis 2022a]. This is the case, for instance, of a satellite LoRa gateway: the device may try to deliver several times the message to a network that it is not available.

Then, the time elapsed from the generation of the data frame to its correct delivery (through a variable number of retransmissions) is the **Latency** of the network. It can be described as

$$L = f(MAC, t_p, \tilde{m}) \tag{1.3}$$

Without considering retransmissions, the different modes of the MAC protocol, such as EDT mode for NB-IoT and Class B for LoRa, have different message exchange strategies, thus giving various network latencies. Furthermore, differences in the distance between the device and the gateway (eNB) result in different propagation times t_p [Nurgaliyev 2020], which are usually negligible for terrestrial networks (but considerable for satellite networks). In fact, in the case of retransmissions caused by packet loss, an extra delay will be added to the network, which depends on the average number of retransmissions $\tilde{m}$. PLR directly determines the expected number of retransmissions required to transmit a packet successfully, and M provides an upper limit for this number. So the average number of retransmissions is

$$\tilde{m} = f(PLR, M). \tag{1.4}$$

Obviously, the parameters that affect the PLR also affect the latency, such as the number of connected devices, CE level [Andres-Maldonado 2019, Azari 2020], SF [Bankov 2019, Sørensen 2017], low SNR [Migabo 2018], etc. As introduced in the previous part, when the PLR is high, increasing the maximum number of retransmissions is a better way to maintain network reliability. But as the maximum number of retransmissions increases, the network latency also increases [Li 2018], so a trade-off strategy is needed based on the specific application requirements.

The **Throughput** is the rate of successful packet delivery. The value of throughput is impacted by the traffic generated by each device, the network density, and PLR, as shown in equation 1.5. Obviously, the network with more density will have more generated traffic, which also increases the PLR. Note that the ideal throughput is the generated traffic when PLR is equal to 0.

$$T = f(g, d, PLR) \tag{1.5}$$

For LoRa, several factors such as Inter-SF and Intra-SF [Markkula 2019] impact the throughput by generating collisions due to orthogonality issues of the SFs. These factors will reduce the throughput, especially in networks with high node density, co-existing with other networks, or with a large distance between the EDs and the gateway [Beltramelli 2018]. In this situation, a higher value of g will imply less throughput by increasing more ToA and collision probability. Same for NB-IoT, the model of network throughput can be built on the basis of PLR analysis [Cruz 2019]. The parameters such as the number of UEs and traffic generation

rate [Migabo 2018] are also critical factors that affect the throughput. On the other hand, as the generated traffic increases, the system throughput will increase, but the probability of collision will also increase, which has a negative impact on the system throughput [Sun 2018]. Therefore, an optimum scheduling technique can reach the maximum available throughput by efficiently allocating the network resources [Bankov 2019].

The **Energy efficiency** describes the number of transmission bits obtained when the system consumes a unit of energy and presents the utilization efficiency of energy by the system [Björnson 2018]. Thus, the energy efficiency can be described as

$$EE = \frac{g_s}{E} = \frac{T}{N \times E}, \tag{1.6}$$

where g_s is the rate of successful transmissions for each device. In other words, its value is equal to the network throughput T divided by the total number of devices N in the network. Also the average energy consumption E depends on several parameters

$$E = f(PHY, MAC, \tilde{m}). \tag{1.7}$$

Like other KPIs, the number of retransmissions caused by high PLR directly impacts the energy consumption rate, which requires extra energy to transmit fewer packets per unit of time [Migabo 2018]. For NB-IoT, with the different CE levels based on link quality, battery lifetime can be from 3 years to 23 years [Andres-Maldonado 2019]. In the LoRaWAN, the energy consumption is different based on the SF selection [Nurgaliyev 2020]. The lifetime of an ED battery will be less than two years for the transmission interval of 60 s with $SF = 7$, while it would be about 3 months for $SF = 12$ [Philip 2021]. The main goal of the NB-IoT EDT mode is to simplify the transmission process, reducing energy consumption. The model proposed in [Barbau 2021a] focused on the energy consumption of the UE when working in EDT mode. The results show a significant improvement in the performance. In the LoRaWAN, different classes have different energy consumption behaviors: Class A is the efficient, Class C is the thirsty, and Class B is the middle energy consumer. Also, other variants were proposed in the literature. For instance, Class S was introduced in [Chasserat 2020] to improve the performance of Class B in throughput and, respectively, energy efficiency by wisely enlarging the slots of Class B. Based on Class S, TREMA [Chasserat 2021] presented a scheduling technique to leverage from its energy efficiency and higher throughput.

Clearly, the best performance cannot be achieved for all the KPIs at the same time. Therefore, a trade-off must be considered based on the needs of the specific application. When considering a satellite LPWAN, the KPIs are affected by the several challenges introduced by the LEO satellite. In what follows, the challenges and their impact on the KPIs are discussed.

1.4.2 Qualitative Performance Analysis of DtS IoT

In Section 1.4.1, some KPIs for the performance evaluation of terrestrial LPWAN networks were analyzed. However, when integrating LPWAN with LEO satellites, the challenges presented in the previous section must be taken into account to model and estimate the KPIs of the combined network. In this section, the analysis presented refers to the availability of a single satellite equipped either with a LoRa gateway or a NB-IoT eNB. This represents the worst-case scenario. Instead, LEO constellations will be considered in future works to feature the scalability of such network architecture.

First, it has to be noticed that the **reliability** of the satellite LPWAN network would be highly affected by the LEO satellite and its visibility time. In fact, a major source of packet losses is caused by the frequent unavailability of the LoRa gateway (eNB). Let a_S be the satellite availability. Then, the reliability of the satellite LPWAN R_s is

$$R_s = R \times a_S. \tag{1.8}$$

Clearly, R_s as R is mainly a function of the PLR. The latter can still be formulated as in equation 1.2. Thus, it is dependent on PHY and MAC parameters, traffic generation rate per node, and node density. Thanks to its large footprint, the LEO satellite can provide wide coverage, resulting in a large number of IoT devices being in the satellite visibility at the same time. The higher value of the node density increases the PLR and thus deteriorates the reliability. When considering a constellation of LEO satellites offering continuous coverage, it results in $a_S \to 1$, and thus, $R_s \to R$.

The **Latency** of the network, as expressed in Equation 1.3, is affected by the MAC schemes, together with the propagation time and the average number of retransmissions. In more detail, Latency is the combination of different delays due to the initial synchronization, the following data processing and propagation, and finally, the data delivery to the application server over the satellite backhaul. In a simplified manner, the Latency L_s can be formulated as:

$$L_s = t_{sync} + m \times (t_{pr} + t_p) + t_{sb} \tag{1.9}$$

with m representing the total number of packets exchanged, including retransmissions. A device takes t_{pr} to generate a packet, which will propagate for t_p to be received by the gateway. Compared to the terrestrial network, ground-to-satellite links make the propagation delay t_p much bigger, and also variable based on the satellite movement. Meanwhile, the packet takes t_{sb} to be delivered from the satellite gateway to the remote server. In the case of a LEO satellite constellation, t_{sb} includes the ISL link delay. When the number of ISL increases, then the latency in the network will increase respectively. For LoRa unconfirmed messages, the Equation 1.9 is simplified, with $m = 1$ and $t_{sync} = 0$. For NB-IoT, the synchronization delay is a relevant component of the satellite network latency. Moreover,

m varies according to the different NB-IoT optimization modes (UP, CP, EDT). In case of higher PLR, the value of m will increase, resulting in higher latency. Being the confirmed messages acknowledged directly by the eNB, no additional delay is introduced by the satellite backhaul.

As the reliability, also the **Throughput** is affected by the satellite availability time and large coverage range. So it can be described by equation 1.10. The unavailability of the satellite causes more packet losses and, therefore, less throughput. Similarly, having many devices (with higher density d) in the satellite's coverage range translates into higher PLR due to data packet collisions in LoRa and congestion during NB-IoT synchronization. As a consequence of increased PLR, the throughput of the satellite LPWAN decreases.

$$T_s = T \times a_S \tag{1.10}$$

The communication with a satellite gateway strongly impacts the energy consumption of the IoT device on the ground. The long distance between the device and the satellite asks for more power consumption, both in transmission and E_{TX}, and reception mode E_{RX}. Instead, the energy required for processing the message, E_{pr} remains the same as in fully terrestrial networks. Thus, the energy consumption can be described as

$$E_{total} = E_{sync} + m_1 \times (E_{pr} + E_{TX}) + m_2 \times (E_{pr} + E_{RX}), \tag{1.11}$$

where m_1 and m_2 represent the number of uplink and downlink packets, respectively.

For unconfirmed LoRa message, the equation 1.11 is simplified, by considering $m_1 = 1$, $m_2 = 0$ and $E_{sync} = 0$. In the case of LoRa confirmed messages, then $m_1 = m_2$ and m_1 represent the number of retransmissions, $m - 1$. In a NB-IoT network, the value of m_1 and m_2 change based on the different optimization method adopted. Moreover, the energy spent during the synchronization phase E_{sync} represents a relevant component of the whole energy consumption of the IoT device.

As mentioned in the previous section, one LEO satellite suffers from long unavailability times during a specific time period. Such behavior makes satellite LPWAN unsuitable for applications that require higher reliability (e.g., mission-critical, Tactile Internet, etc.). Since the satellite has a broader coverage area, more devices will try to connect to it at the same time, increasing the probability of collision. As a result, applications requiring high throughput cannot be satisfied. Therefore, to increase network throughput, the network size (i.e., the number of served devices) should be reduced. Finally, satellites cause the network to have longer delays and, thus, longer latency compared to terrestrial networks. This makes them not a good fit for ultra-low latency applications. While the goal of any network is to support higher scalability, then increasing the number of LEO satellites and providing full coverage will help support the applications that need higher reliability and throughput.

NB-IoT and LoRaWAN are among the LPWAN technologies that have fostered a widespread deployment of IoT networks, thanks to their low power, low cost, and long-distance communications. These features have recently been explored for ground-to-satellite communications, enabling a truly pervasive and ubiquitous IoT availability. Such a network architecture is clearly expected to trigger the growth of novel IoT applications unimaginable before. Indeed, the success of future satellite IoT will depend on its ability to meet the needs of specific use cases. Timely, this section pictures a methodological approach finalized to the correct choice of the LPWAN technology and the best communication pattern fitting the needs of *any* satellite IoT application. To do that, reliability, latency, throughput, and energy efficiency have been identified as KPIs to be used for comparing different protocols. Importantly, their inner dependency on configurable settings, e.g., the maximum number of retransmissions in contention-based medium access schemes, has also been properly investigated. Such an analysis will be leveraged in future research to design novel medium access schemes and efficient algorithms able to autonomously adapt the communication protocol to time-varying traffic conditions and grant a sufficient level of quality of service. In addition, such an analysis will be extended to tackle the availability of LEO satellite constellations, thus targeting highly available and scalable LPWANs backhauled by LEO satellites.

1.5 Concluding remarks

This chapter introduced two LPWAN protocols, NB-IoT and LoRa, and discussed the challenges of integrating these protocols with satellite communication. A methodological approach for designing the network was proposed, focusing on optimizing KPIs such as Reliability, Latency, Throughput, and Energy Efficiency. The KPIs introduced in this chapter serve as a framework for future work, especially in comparing and optimizing different LPWAN technologies like NB-IoT and LoRaWAN in satellite communication scenarios.

While both protocols have their strengths, NB-IoT is chosen for the remaining chapters due to its reliability over LoRa, thanks to features like acknowledgments and resource allocation, despite its challenges in complexity, synchronization, and extensive message exchanges. Furthermore, the high energy consumption, increased costs, and potential interference in GNSS-based solutions make exploring alternative approaches that can achieve reliable communication without relying on GNSS or extensive satellite constellations imperative. This aligns with the emerging trends in the "new space" era, where energy efficiency, cost-effectiveness, and innovative solutions are becoming more important.

In the context of 3GPP standards and existing market solutions, this thesis explores how NB-IoT can be optimized for satellite communication. Chapter 2 will delve into the challenge of downlink synchronization, proposing a novel approach that eliminates the need for GNSS while reducing energy consumption and costs. Chapter 3 will introduce a wake-up strategy designed to enhance energy ef-

ficiency, particularly in scenarios with sparse LEO satellite constellations. Finally, Chapter 4 will focus on the early detection of random access collisions, proposing methods to improve the success rate of random access attempts in NB-IoT satellite communication. The following chapters aim to present comprehensive solutions and optimizations that address these key challenges and enhance the performance and feasibility of NB-IoT in satellite IoT networks.

Chapter 2

Energy-efficient synchronization for DtS NB-IoT

Ce chapitre aborde les défis liés à l'intégration du NB-IoT dans les communications par satellite, en particulier le problème de synchronisation causé par l'effet Doppler dû à la haute vitesse des satellites LEO. Une méthode innovante est proposée pour prédire et compenser le décalage Doppler sans utiliser de capacités GNSS, en observant les signaux de liaison descendante du NB-IoT. Cette approche permet aux UEs de fonctionner de manière transparente dans les réseaux NB-IoT terrestres et les liaisons sol-satellite. Les routines nécessaires sont implémentées dans le firmware des UEs et sont déclenchées uniquement lorsque les signaux de synchronisation présentent un décalage de fréquence. La faisabilité de ce système est évaluée par des simulations, qui examinent les erreurs potentielles dans l'estimation de la courbe Doppler. Les résultats de ces simulations montrent que cette méthode est prometteuse pour améliorer les communications NB-IoT avec les satellites LEO. En particulier, les simulations ont révélé que la réception de 10 signaux en une seconde suffit pour accomplir la synchronisation. Le chapitre se termine par une revue des travaux connexes, la description détaillée de la méthodologie, les résultats de l'analyse basée sur les simulations et des conclusions qui envisagent des travaux futurs pour affiner et améliorer cette solution.

Contents

Unlike LoRaWAN, the first and foremost challenge in effectively integrating NB-IoT with satellite communication is the synchronization issue. As a matter of fact, this is the most basic requirement to establish communication. In the case of NB-IoT, an eNB embedded in an LEO satellite acts as a gateway. However, using NB-IoT for ground-to-satellite communications is not cheap and is not energy efficient because the presence of some technical barriers hinders its worldwide adoption. Due to the high-speed motion of LEO satellites, communications are affected by the

Doppler effect, with a measured frequency offset of ±40 kHz for satellites elevated 600 km above the ground [Wang 2019]. As a result, the signal can be significantly degraded, and link layer frames can be lost. Moreover, NB-IoT transmission delays typically range from hundreds of milliseconds to almost 12 seconds [Hoglund 2018], depending on factors like data size, network load, and link quality. During this period, the frequency shift caused by the Doppler effect may vary from tens to several kilohertz, so the Doppler frequency shift cannot be calculated through the initial synchronization of NB-IoT. Therefore, a varying Doppler shift is the biggest challenge for the massive adoption of NB-IoT between ground UEs and eNBs mounted on LEO satellites. Similarly, if the UE cannot pre-compensate the Doppler shift, the LEO satellite's listening frequency band will be larger and consume more power. In the same way, UE should listen to a larger frequency band for the following interactions. In this sense, starting from Release 17 [3GPP 2018], 3GPP has been specifying how NB-IoT/eMTC (enhanced Machine Type Communication) can support non-terrestrial networking and the case scenario pictured above: each UE must be equipped with a GNSS receiver and must be configured with the ephemeris of the satellite using the TLE to pre-compensate the Doppler shift and propagation delay. However, the need for a GNSS receiver implies extra power consumption and an increased cost of UEs.

In this context, a new approach is proposed to predict the Doppler effect by estimating the satellite's trajectory in the sky without GNSS capabilities. This is done through the observation of NB-IoT downlink signals. The computed prediction is used to pre-compensate the Doppler shift. The related routines implemented in the firmware of any ground UE are meant to be triggered only if the synchronization signals are detected to be frequency-shifted. Otherwise, the UE works according to default terrestrial NB-IoT policies. Thus, this solution makes transparent the use of any firmware-updated UE in both terrestrial NB-IoT networks and ground-to-satellite NB-IoT links.

The feasibility of such a system over ground-to-satellite links is studied by simulating the unpredictability of the errors that may happen in estimating the Doppler curve, and the results presented hereafter encourage such an investigation. In detail, Section 2.1 presents a review of the related works, while Section 2.2 pictures the proposed idea. Then, Section 2.3 presents the results of a simulation-based analysis. Finally, Section 2.4 draws conclusions and envisages future works.

2.1 Related works

As discussed in the introduction, the default configuration for an NB-IoT DtS architecture requires that ground devices be equipped with GNSS capabilities. With a different approach, [Kodheli 2018] proposes a Doppler precompensation of NB-IoT beacon signals that does not require any change on the configuration of UEs: they do not need either to be equipped with GNSS or to listen to a wider spectrum to cope with Doppler effect. This strategy is energy-efficient for UEs but requires

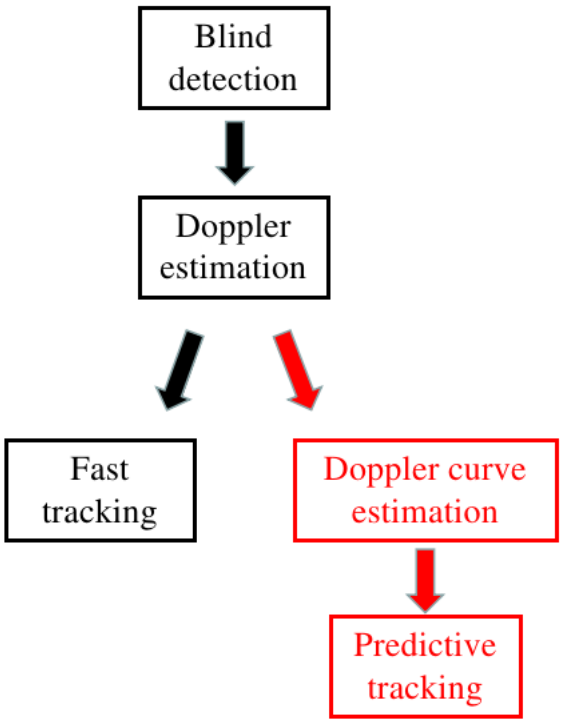

Figure 2.1: Different ways of synchronization

significant changes to the hardware and software of the eNB-equipped satellite. In fact, from the software point of view, the eNB uses a centralized resource allocation scheme based on the partition of the entire coverage area into multiple small regions: the differential Doppler shift is reduced on a per-region basis, thus improving the quality and reliability of the communication link. From the hardware point of view, a multi-beam satellite is required to work properly on a specific channel with each region. Finally, since the UE does not pre-compensate the frequency shift, the satellite must listen to a wider bandwidth to catch any frame arriving on a frequency shifted according to the Doppler effect. Instead, [Chougrani 2022] proposed to modify the NB-IoT physical layer about what concerns the preamble structure and the synchronization procedure to achieve uplink synchronization. In addition, there is no pre-compensation, thus requiring the UE to keep receiving the synchronization signals until sending the first uplink signal. Both these solutions require significant changes either to the NB-IoT protocol or to the hardware.

For the sake of a clear positioning, it is worth mentioning other works not related to NB-IoT yet dealing with downlink synchronization between a ground terminal and a LEO satellite. To achieve such synchronization, the influence of the Doppler frequency shift must be eliminated. As shown in Fig. 2.1, first of all, two main research lines have been identified [You 2022]: (i) *Doppler estimation*, i.e., how to measure the Doppler shift in a received signal and determine the relative speed of the transmitter; (ii) *Doppler compensation*, i.e., how to correct the transmitting

frequency to cope with the Doppler shift in a signal. In regard to Doppler characterization, the studies of [Neinavaie 2021, Pan 2020, Huang 2021] demonstrate that the Doppler shift can be estimated by low-power devices, thus making this approach applicable to IoT devices. Instead, with regard to Doppler compensation, a standard strategy is to use "Fast-tracking," i.e., a terminal on the ground should keep receiving downlink beacon signals to calculate the real-time Doppler offset [Li 2016, Wang 2019, Huang 2021, An 2020]. However, this approach requires high processing units and constant communication capabilities, thus not fitting the desired behavior of low-power duty-cycled IoT devices. Instead, the "predictive tracking" strategy is to estimate the Doppler curve during the satellite's passage from the Doppler-shifted frequency of several consecutive downlink synchronization signals. Once the Doppler curve is understood, the expected trajectory is also known, thus requiring no further estimation of the frequency shift. [Rouzegar 2019] uses the received signal combined with satellite position information from TLE to plot a Doppler curve, allowing for prediction of the Doppler shift at each moment throughout the process. Using a mathematical model, the authors of [Ali 1998] proposed a method to figure out the Doppler curve through two downlink signals. However, neither of these papers considered the impact of the downlink signal measurement error on the drawing of the Doppler curve.

2.2 Proposed approach

In order to gently introduce the core idea of this chapter, it is first worth giving some more details about how an NB-IoT communication is set up as introduced in Sec. 1.2.2. When a UE wakes up (or it is bootstrapped), the first step is to perform a cell search to obtain key information about the network. This is done by waiting for a NPSS received from an eNB in the scope. The NPSS is a 1ms-long signal periodically broadcast by any eNB every 10 ms. Once synchronized, the UE waits for the NSSS to obtain the cell ID. After this downlink synchronization process is finished, NB-IoT will receive network system information through other downlink messages, i.e., the MIB and SIB. At this point, the UE is able to send uplink messages and complete the setup of reliable bidirectional communication.

The synchronization process described so far is not directly applicable to non-terrestrial communications without some trick. A LEO satellite equipped with an eNB is responsible for forwarding messages transmitted between the UE and the ground base station. Unlike traditional NB-IoT networks, the UE needs to receive several NPSS to draw the Doppler curve and get synchronized to the network. Understanding the Doppler curve is functional for the UE to pre-compensate the frequency used to transmit (or receive) link layer frames during the visibility time of the eNB. For this reason, the next subsection describes how to link a Doppler curve with a given satellite trajectory, while Section 2.2.2 details the model used to identify a Doppler curve based on NPSS noisy receptions.

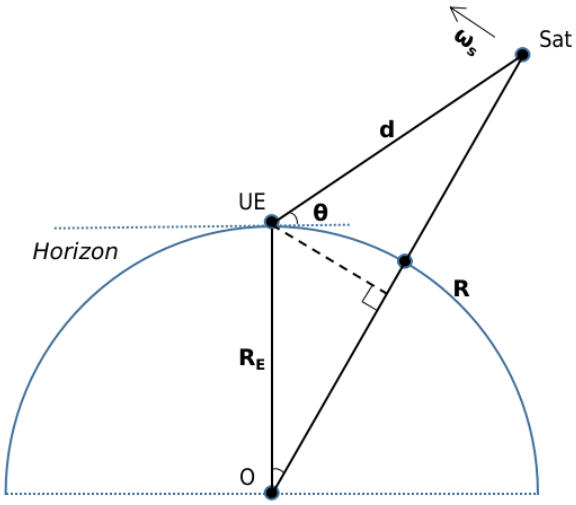

Figure 2.2: LEO satellite and UE.

2.2.1 Doppler Curve

The Doppler effect deals with a perceived frequency shift due to the relative motion between a transmitter and a receiver. In detail, the frequency f_r observed by the receiver is

$$f_r = \left(1 + \frac{\Delta v}{c}\right) f_0 = f_0 + \Delta f, \tag{2.1}$$

where f_0 is a known emitted frequency used by the transmitter to propagate the signal, Δv is the relative speed between transmitter and receiver, and c is the speed of light. Finally, Δf is the Doppler frequency shift.

As explained in [Ali 1998], obtaining the relative speed change between the satellite and the UE is necessary. For the sake of readability, the topological scenario used in this chapter is pictured in Fig. 2.2. In that, R_E is the Earth radius, and R is the radius of the satellite orbit, while ω_s is the angular velocity of the satellite. Even if ω_s varies with latitude due to the Earth's rotation, such a variation is negligible for low to medium orbit altitudes [Ali 1998], so it is assumed constant hereafter.

Then, θ is the elevation angle between the horizon and the line of sight of the receiver. Due to a series of physical reasons (including the antenna, the altitude, etc.), communication can happen only if the elevation angle is bigger than a minimum value $\theta_{\min}$. In the rest of the chapter, the assumed value of $\theta_{\min}$ is 30° [Fadilah 2022]. Furthermore, the trajectory of a LEO satellite passing through the communication scope of a UE is featured by a maximum elevation angle θ^*. In other words, for a given satellite pass, θ^* is the elevation angle achieved when the satellite is the closest to the UE. Clearly, the range of θ^* lies in the following interval $[\theta_{\min}, 90°]$. When the satellite passes directly above the UE, $\theta^* = 90°$ (Fig. 2.3). Another angle of interest is the one between R and R_E when when $\theta = \theta^*$, namely

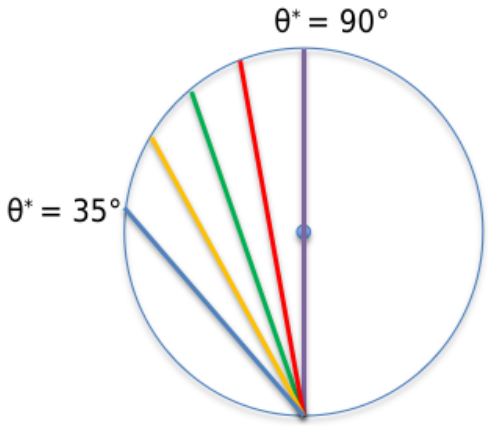

Figure 2.3: Example of different maximum elevation angles corresponding to different trajectories.

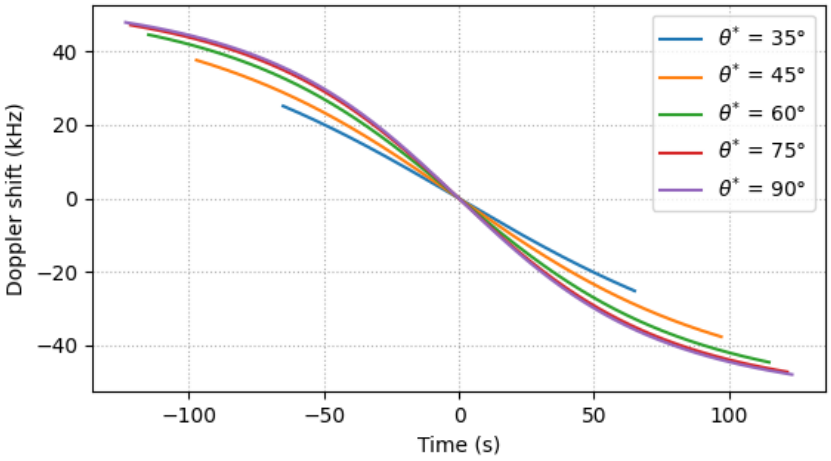

Figure 2.4: Example of Doppler effect with a 600-km LEO Satellite with different maximum elevation angles.

α_0:

$$\alpha_0 = \arccos\left(\frac{R_E}{R}\cos\theta^*\right) - \theta^*. \tag{2.2}$$

Under [Ali 1998], during a satellite pass, the origin $t = 0$ on the timeline corresponds to the instant when the elevation angle is $\theta = \theta^*$. The relative distance $d(t)$ between the UE and the satellite at a given instant t during a satellite pass is then

$$d(t) = \sqrt{R_E^2 + R^2 - 2RR_E\cos(\omega_s t)\cos(\alpha_0)}, \tag{2.3}$$

and the relative speed between UE and the LEO satellite is

$$\dot{d(t)} = \frac{RR_E\omega_s \sin(\omega_s t)\cos\alpha_0}{d(t)} = -\Delta v. \tag{2.4}$$

Combining (2.1) with (2.4) and (2.3), the frequency shift formulation depending on t, R, R_E, ω_s, and α_0 is

$$\Delta f = -\frac{f_0}{c}\frac{RR_E\omega_s \sin(\omega_s t)\cos(\alpha_0)}{\sqrt{R_E^2 + R^2 - 2RR_E\cos(\omega_s t)\cos(\alpha_0)}}. \tag{2.5}$$

Fig. 2.4 and 2.3 shows the Doppler curves related to a 600 km elevated LEO satellite with several values of θ^*. The carrier frequency used here and for the rest of the chapter is 2.4 GHz, the S-band spectrum. The S-band is commonly used for satellite communications due to its favorable propagation characteristics, including good penetration through atmospheric conditions and a balance between bandwidth availability and coverage.

2.2.2 Estimation of the Doppler curve

In reality, the measured Doppler shift will always be affected by an error. The assumption made throughout this contribution is that such an error can be modeled as an Additive White Gaussian Noise (AWGN), with zero mean ($\mu = 0$) and a variance value σ^2 that can be properly tuned to mimic different noise levels. Such an assumption comes from the consideration that the Gaussian distribution well approximates randomness in many natural phenomena and engineering problems. More specifically, it is possible to relate the measured Doppler shift, $\Delta\hat{f}$, to the actual one, Δf, as

$$\Delta\hat{f} = \Delta f + \varepsilon, \tag{2.6}$$

where ε is the measurement error.

However, the actual Doppler shift Δf is unknown. Indeed, its formulation, given by (2.5), depends on the time instant t, which is unknown. According to the model presented so far, t represents the instant when a beacon NPSS signal was sent by satellite within the portion of its trajectory within the scope of the UE receiving that signal. At the same time, t can be always expressed as the sum of the unknown instant when the very first NPSS was received at the UE, t_0, and the known interval Δt, that could be expressed as multiple of the time between 2 consecutive NPSS transmissions, i.e., 10 ms. Substituting $t = t_0 + \Delta t$ in (2.5), the supposed model for Δf is $D(\Delta t)$ and depends on the known independent variable Δt:

$$D(\Delta t) = -\frac{f_0}{c}\frac{RR_E\omega_s \sin(\omega_s(t_0+\Delta t))\cos(\alpha_0)}{\sqrt{R_E^2 + R^2 - 2RR_E\cos(\omega_s(t_0+\Delta t))\cos(\alpha_0)}} \tag{2.7}$$

with t_0 and θ^* being unknown parameters to be determined (θ^* does not appear directly in the formulation of (2.7), because it is embedded within α_0).

More specifically, assuming to receive m signals, the method of least squares can be used to determine such parameters. In that, the vector of measured data is

$$\boldsymbol{\Delta}\hat{\mathbf{f}} = \left[\Delta\hat{f}_1, \ldots, \Delta\hat{f}_m\right], \tag{2.8}$$

so that the vector of the residuals, $\mathbf{r}(\beta) = [r_1, \ldots, r_m]$, is composed by the following elements

$$r_i = \Delta\hat{f}_i - D(\beta; \Delta t_i) \qquad \text{with} \quad i = 1, \ldots, m \tag{2.9}$$

where $\beta = [\theta^* \;\; t_0]^T$ is the vector of unknown parameters and Δt_i is the time interval between t_0 and the i-th NPSS signal. The resulting loss function

$$L(\beta) = \mathbf{r}(\beta) \cdot \mathbf{r}(\beta)^{\mathbf{T}} \tag{2.10}$$

can be minimized through the Gauss-Newton method.

The optimal solution for the two parameters can be found by iterating the following algorithm

$$\beta_{k+1} = \beta_k - (J^T J)^{-1} J^T \mathbf{r}(\beta), \tag{2.11}$$

where J is the Jacobian matrix of the residual and k is the iteration number.

2.3 Simulation Results

In this section, some results are presented based on the simulation of the proposed method for estimating the Doppler curve. First, each NPSS signal is generated together with the corresponding Doppler effect. Then, this value is incremented (or decremented) according to a random value drawn according to a normal distribution with zero mean and variance equal to σ^2 in order to mimic the AWGN-like measurement noise. Next, these values are meant to represent the measured NPSS signals and are used within the model in Section 2.2.2 to estimate the Doppler curve. Finally, the estimated Doppler curve is compared against the actual one to evaluate the model's performance. The index used to measure such a performance is the maximum communication time, i.e., how long the estimated Doppler curve can be used in subsequent interactions between the UE and the eNB-equipped LEO satellite to pre-compensate the transmission and reception frequencies on the UE. In detail, such a performance index is defined as the time interval during which the error between the estimated Doppler curve and the real one stays below a given threshold value. As a narrowband communication technology, NB-IoT usually has a small maximum allowed frequency error (950 Hz) [Kodheli 2018]. To provide reliable results, a conservative approach has been adopted, and the threshold value for determining the maximum communication time was set to 500 Hz.

To help in appreciating the performance evaluation, Fig. 2.5 shows an example of how to interpret the simulation results. The figure compares the original Doppler curve and the estimated one calculated through the mathematical model. Herein, the standard deviation σ of the simulated AWGN-like source of errors is set to 20

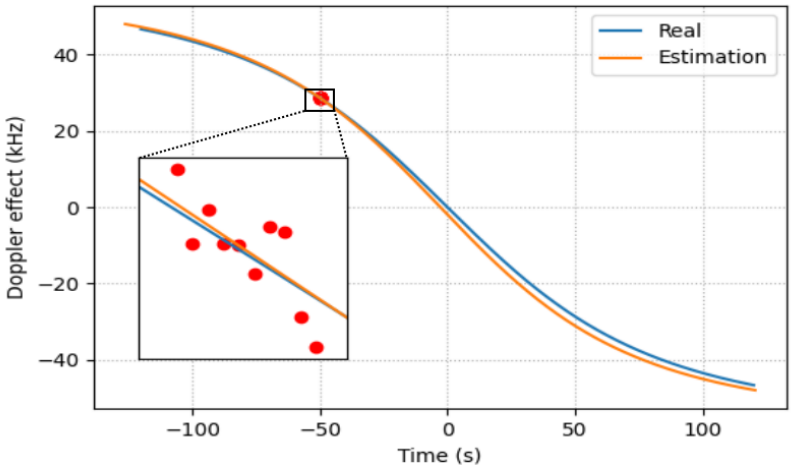

Figure 2.5: Example of a sample simulation result with $\sigma = 20$.

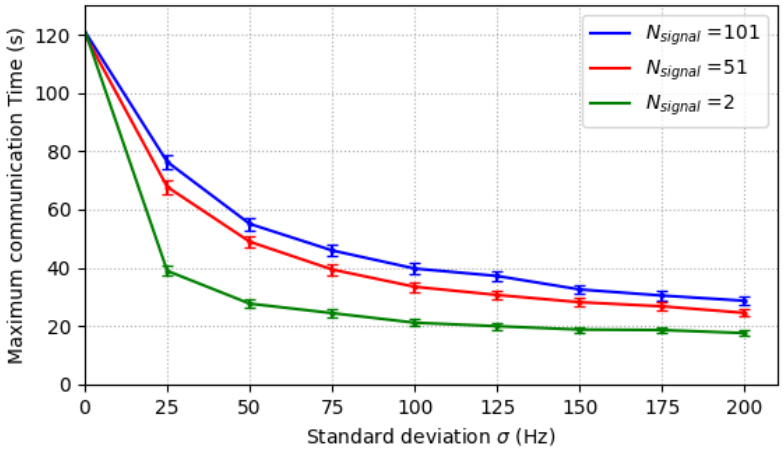

Figure 2.6: Maximum communication time ($T_{\text{measure}} = 1$ s).

Hz, and the UE needs to receive 10 NPSS beacons in order to derive the estimation of the Doppler curve. Zooming on the evaluated time interval (see Fig. 2.5), it can be noticed that each signal is affected by a random error, and the final fitting result is very close to the original Doppler curve, which shows that the mathematical model is feasible.

Furthermore, each point on the following plots represents an average of 3000 measures in simulated scenarios. Each scenario is obtained by randomly choosing the time for the first NPSS reception in the visibility time related to the chosen maximum elevation angle. 95% confidence intervals are also shown for the sake of statistical significance.

First, the impact of different amounts of NPSS used for the Doppler curve

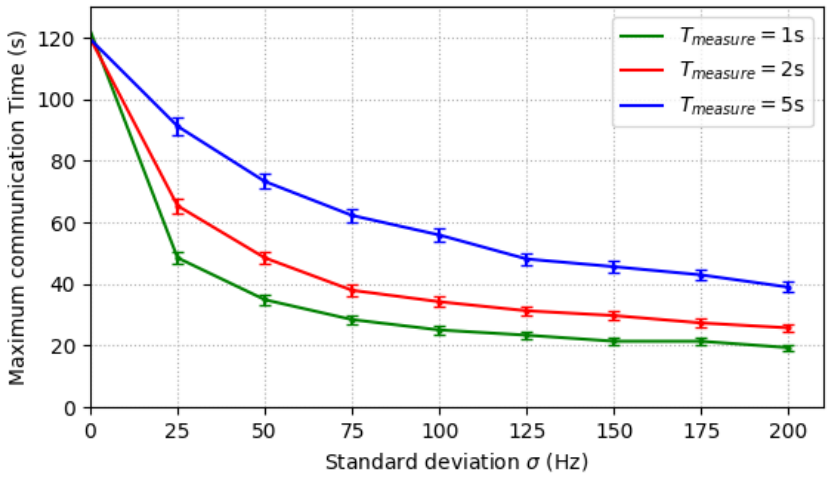

Figure 2.7: Maximum communication time ($N_{\text{signals}} = 11$).

prediction was studied. The maximum elevation angle θ^* was fixed to 70° for all simulations, while the measurement time was limited to 1 second. The NPSS used for estimating the Doppler curve are taken uniformly over the measurement time. For instance, when the number of used NPSS is 51, the time interval between two consecutive NPSS used for the estimation is 20 milliseconds. As shown in Fig. 2.6, the prediction accuracy increases with the amount of NPSS used for predicting the Doppler curve. Yet, it also comes with a higher energy consumption. Therefore, there is a need to find a trade-off between prediction accuracy and energy efficiency.

Pushing forward the analysis, Fig. 2.7 plots simulation results obtained when the number of used NPSS ($N_{signals}$) in the Doppler curve prediction is fixed to 11, while the measurement time T_{measure} is varied among $1, 2, 5$ s. The considered NPSS are taken uniformly in time over the measurement interval. Results show that the wider the intervals, the more accurate the prediction. This is because a larger measurement interval allows for a difference in Doppler shift between consecutive measurements, which is greater than the measurement error: larger measurement intervals produce more accurate predictions. However, due to the short pass time, prolonging such an interval can lead to potential interference from other causes, which can negatively affect the accuracy of the predictions.

Another step ahead in the analysis can be done by considering a non-uniform sampling of the received NPSS. Here, the measurement time T_{measure} is set to 1 second. The non-uniform sampling strategy involves concentrated measurements at the beginning and at the end of the measurement period, resulting in uneven time intervals. For example, if 11 NPSS are used in total over a measurement time of 1 s, the first 5 considered NPSS are those transmitted at the very beginning of such interval (each of them is sent every 10 ms), while the remaining 6 NPSS are those received at the very end of the same measurement interval (each of them is

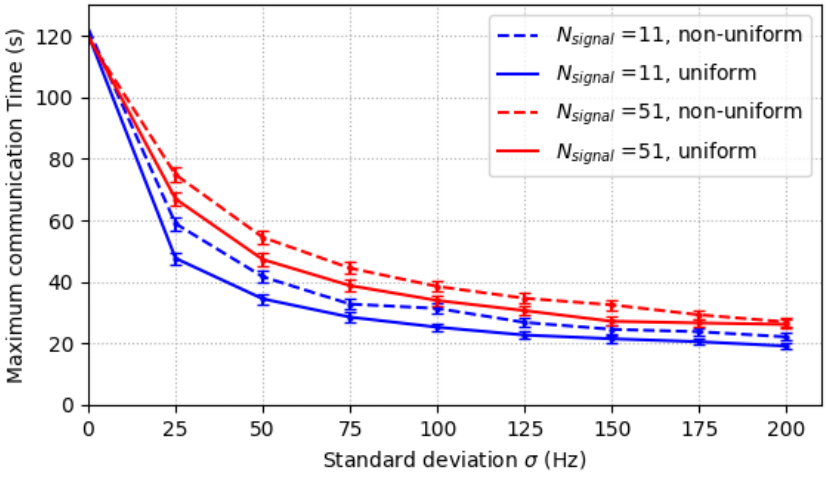

Figure 2.8: Maximum communication time with different sampling strategies.

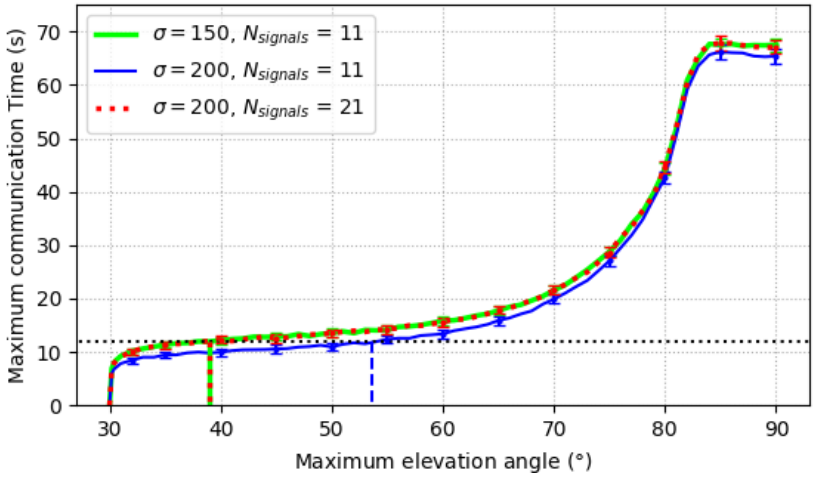

Figure 2.9: Maximum communication time with different θ^* ($T_{\text{measure}} = 1$ s).

also sent every 10 ms). The results related to this approach are those pictured with dashed lines in Fig. 2.8. Comparing the two sampling strategies, it can be seen that with the same number of used NPSS, the highest sampling frequency used in the non-uniform strategy produces a more accurate prediction for the Doppler curve, as already proved in Fig. 2.6. This approach takes advantage of the non-linear characteristics of Doppler shifts, which are less informative in the middle of the pass, where the change in relative velocity is more gradual.

All results presented so far show how the sampling strategy can affect the prediction accuracy of the Doppler curve in NB-IoT communications to LEO satellites. All in all, it was found that increasing the number of received signals and using non-

uniform time or larger intervals between measurements can improve the accuracy of predictions. Considering the energy consumption and limited communication time, these factors must be balanced according to the measurement error.

For the sake of generality, the impact of the maximum elevation angle θ^* was also studied by varying it between 30° and 90° (see Fig. 2.9). Considering that the maximum value of the time required for an NB-IoT session must be handled in the architecture analyzed so far (i.e., 12 seconds [Hoglund 2018], see the horizontal dotted line in Fig. 2.9), results show that for a noisy environment featured by $\sigma = 150$, the reception of 11 NPSS beacons within 1 second is sufficient to accommodate the communication requirements for most of the UEs in the scope of the eNB-equipped LEO satellite: if $\theta^* \geq 40°$, then the NB-IoT session can happen, otherwise the UE should not start the NB-IoT session and wait for another pass (see the green line). If the noise is featured by a higher noise, i.e., $\sigma = 200$, then the UE able to handle an NB-IoT session are those having $\theta^* \geq 55°$ (see the blue line). However, in the same noisy scenario, if UEs collect 21 NPSS (see the red dotted line), then they can be able to handle an NB-IoT session for $\theta^* \geq 40°$, as in the case of $\sigma = 150$ and 11 NPSS collected. In other words, when the noise increases, the possibility of handling an NB-IoT session can be ensured by collecting more NPSS to predict the Doppler curve, thus trading off energy efficiency for better communication ability.

2.4 Concluding remarks

This chapter introduced a lightweight method for ground NB-IoT UEs to compute the Doppler curve based on the reception of several synchronization signals from eNB mounted on LEO satellites. Such a curve predicts the Doppler shift and pre-compensates the transmission and reception frequency in the following interaction during the satellite pass. Based on a simulation campaign, it is demonstrated that the proposed method effectively synchronizes the frequency of NB-IoT downlink signals for LEO satellite communication systems by utilizing the NPSS even in the presence of measurement errors. Compared with other methods, the proposed method requires a lower level of complexity and can be implemented with simple equipment on satellites and ground terminals. The simulations also show that the method can achieve high synchronization accuracy and reliability under various operating factors, making it suitable for practical use in LEO satellite communication systems. The proposed method will be compared against other synchronization strategies available in the literature to fully demonstrate its inherent effectiveness. In addition, periodic wake-up schemes for UEs will be investigated to save the energy stored in the feeding batteries while preserving the accuracy of the Doppler curve estimation. However, it is essential to note that this method's effectiveness assumes that the UEs are within the satellite's coverage area during the synchronization process. Building on these results, the next chapter will explore how the accurate Doppler curve estimation achieved here can be utilized in designing periodic wake-up schemes for UEs to avoid wasting energy when no satellite exists.

Chapter 3

A wake-up strategy for GNSS-free DtS NB-IoT

Ce chapitre propose une nouvelle stratégie de réveil permettant aux UEs sans GNSS de configurer des communications NB-IoT avec des constellations clairsemées de satellites LEO, même dans le scénario le plus difficile avec un seul satellite disponible. Cette stratégie maintient l'efficacité énergétique tout en assurant une communication fiable entre les UEs et les satellites LEO. Au lieu de s'appuyer sur les signaux GNSS, l'UE utilise une stratégie de réveil intermittent pour rechercher le signal de synchronisation descendant du satellite. En recevant plusieurs signaux descendants, l'UE peut se synchroniser avec le satellite sans transmissions supplémentaires en amont, préservant ainsi le débit et l'évolutivité du réseau. Grâce aux passages répétés des satellites, l'UE estime sa position en se basant sur ces signaux, permettant finalement une communication normale. Les expériences de simulation ont vérifié que cette stratégie proposée peut réduire considérablement la consommation d'énergie des UEs à long terme par rapport à l'utilisation du GNSS, sans nécessiter de changements matériels importants pour satellites LEO et UEs. Cette optimisation se concentre sur la réduction de la complexité et de la consommation d'énergie des UEs.

Contents

The study of DtS NB-IoT networks conducted so far has been based on the assumption that a satellite is always in range. In this context, the previous chapter explored the integration of NB-IoT with satellite communication, focusing on the synchronization challenges posed by the high-speed motion of LEO satellites and the resulting Doppler effect. However, this analysis assumes that a satellite is always within range. If global coverage is unavailable, an additional challenge is ensuring that ground devices wake up when a satellite passes by and remain in sleep mode when no satellite is in reach. This chapter examines the critical aspect of the wake-up strategy for UEs in scenarios with sparse LEO satellite constellations to further address another issue associated with providing NB-IoT coverage through LEO satellites. Unlike traditional ground NB-IoT networks, UEs wake up from a sleep state only when they need to transmit some data. In ground-to-satellite communications, sparse LEO satellites ensure discontinuous coverage [Capez 2022], and UEs may wake up without any satellite in their reach. To cope with this issue, the most straightforward solution is to achieve global coverage through dense satellite constellations. Even though the price of LEO satellites is getting lower and lower, to achieve global coverage and maintain continuous communications between ground devices and satellites, at least dozens to hundreds of satellites are needed [Su 2019, Tuzi 2023]. Herein, 3GPP has included the possibility for UEs to use GNSS together with broadcast satellite information to make communication run under discontinuous coverage. The standard assumes that during a satellite pass, a UE is informed by an eNB-equipped satellite passing through its range about next satellite passes. The way how a satellite can produce such information is not specified. For example, this could be done by letting each satellite gather such data from a central constellation supervisor. In any case, the knowledge of a limited number of next satellite passes does not ease the scalability of the system.

Herein, the core idea of this chapter is to picture and analyze a new wake-up strategy that allows a GNSS-free UE to set up NB-IoT communications with sparse constellations of LEO satellites of any size, even the most challenging scenario with a single satellite available. The study focuses on the communication between UEs and LEO satellites. This strategy retains its energy efficiency advantage even in the most challenging scenarios, such as when only a single satellite is available. In the absence of its own location and ephemeris information, the UE uses an intermittent wake-up strategy to attempt to search for the satellite's downlink synchronization signal. Then, instead of receiving GNSS signals before each communication, multiple downlink signals should be received to synchronize UE and satellite. The method is based on the work of Chapter 2, which includes an analysis of measurement errors to demonstrate the method's reliability. Notably, this strategy achieves these goals using only downlink messages, avoiding additional uplink transmissions that could affect network throughput and scalability. Meanwhile, each time the satellite passes by, UE will estimate its position based on these signals. After multiple estimations, the UE will determine its approximate position, and finally, it

can perform normal communication as needed. After simulation experiments, it has been verified that the strategy proposed in this chapter can significantly reduce device energy consumption in the long term compared to using GNSS without particular changes to the hardware. In short, it is optimized from the perspective of device complexity and energy consumption.

The rest of the chapter is organized as follows. Sec. 3.1 reviews related works, while Sec. 3.2 introduces the technical background of the presented proposal. Next, Sec. 3.3 pictures the core idea of this wake-up strategy. Then, Sec. 3.4 presents the results of a simulation-based analysis. Finally, Sec. 3.5 concludes and envisages future works.

3.1 Related works

To face the challenge of discontinuous coverage, 3GPP standards [3GPP 2021] bases the correct functioning of NB-IoT on the availability of GNSS on UEs. Herein, the specification recognizes that GNSS is energy expensive thus the evaluation of energy consumption related to some implementations is also detailed. Calculating and pre-compensating frequency shifts and delays through GNSS and TLE data is undoubtedly an accurate solution. Still, as this chapter will show, GNSS-enabled devices are not the best choice for IoT applications. From a practical point of view, GNSS draws more current than needed, adds complexity to the circuit design, and eventually increases the cost of low-power devices. Furthermore, from a technical perspective, linking NB-IoT for LEO DtS communications to the availability of GNSS makes such an architecture neither resilient to outages nor viable in GNSS-denied environments.

As a matter of fact, the need for GNSS-free DtS solutions has been recognized in the scientific literature. In [Kodheli 2018], the authors proposed a method to reduce the impact of the Doppler effect from the satellite's perspective without using GNSS. This approach uses multi-beam satellites to divide the ground into smaller regions, providing different channels for each area. By doing so, ground devices can communicate with the satellite using Time Division Multiple Access (TDMA) or Frequency Division Multiple Access (FDMA) methods. However, allocating additional frequency and time domain resources to different regions requires additional frequency and time domain resources. Moreover, implementing multi-beam technology significantly increases the complexity of satellite design. Smaller satellites, like CubeSat, typically cannot support multi-beam technology due to their limited size, power, and payload capacity.

With a different GNSS-free approach, the circuitry of eNB remains unchanged, while ground UE devices must be able to measure Doppler shifts. In [Zhang 2022], a frequency offset independent timing synchronization method is proposed to measure the significant Doppler shift accurately. However, since the frequency shift and delay constantly change, simply measuring the Doppler frequency shift is insufficient to complete synchronization. [Wang 2019] proposed a tracking method that continues

after initial synchronization. This approach allows ground devices to continuously track downlink signals for real-time updates of frequency shift changes. However, considering the low energy consumption goal of IoT devices, such a high processing capacity is not suitable. In [Ali 1998], the author first proposed a method to draw the Doppler curve based on the measured frequency shift of only two downlink signals to achieve pre-compensation without considering the measurement errors.

In the last chapter, a least squares method was proposed as a means to achieve and maintain downlink synchronization for a sufficiently long time to permit NB-IoT uplink data transmissions and downlink data receptions in such a research landscape. This was done by estimating the Doppler curve based on the measurements related to several NB-IoT beacon signals, i.e., the so-called NPSS. Different detection strategies were also proposed to deal with measurement errors of varying sizes and application requirements. With the same approach in mind, the research developments introduced by this contribution represent an attempt to set up a GNSS-free scheme that makes UEs capable of (i) estimating the trajectory of LEO satellites through the maximum elevation angle, (ii) their own locations, and, through these two pieces of information, (iii) the next satellite passes in its own communication scope. The goal of such a computation is to let the device save energy by waking up when a DtS communication can happen, i.e., when a LEO satellite is in its transmission range.

In this sense, after collecting the satellite's orbital data transmitted by an eNB-equipped LEO satellite through downlink messages, a UE can calculate the trajectory of that satellite using algorithms like the Simplified General Perturbations Model 4 (SGP4) [Morales 2019]. Indeed, given TLE sets, the SGP4 algorithm can calculate a satellite's position and velocity vector at a specific time point. Its high efficiency and accuracy make it a suitable choice for IoT devices.

As for the UE's position, some methods for locating IoT devices, including terrestrial-based LPWAN techniques, novel GNSS solutions, and innovative positioning techniques leveraging LEO satellite constellations, have been summarized and compared in [Janssen 2023]. Focusing on solutions for LEO satellites, there are two possible methods: some satellites collect uplink signals sent by the same ground UE, or the ground UE collects downlink signals. In both cases, a common aspect is measuring the Doppler frequency shift. On the one hand, the first method requires the participation of ground stations to integrate the uplink signals received by each satellite, which adds complexity to discontinuous systems and results in devices being unable to obtain their location. On the other hand, both methods require the simultaneous presence of multiple satellites sending or receiving the same copy of the signals. As mentioned earlier, these approaches are not feasible in scenarios with only a single satellite or a limited number of satellites. Similarly, an IoT-over-satellite-based framework [Mohamad Hashim 2023] was proposed as a means to achieve localization by using the angle of arrival (AoA) and Doppler shift by multiple satellites.

As said before, when the UE's location on the ground and the satellite orbit information are known, the most accurate way to predict the next satellite pass is to

use the SGP4 algorithm to calculate both the satellite's position within a certain period in the future and its relative position to the UE. However, this method requires a certain amount of computational effort, which can pose a challenge for resource-constrained IoT devices. In [Luo 2017], the authors proposed a novel method to calculate the revisit time of LEO satellites and applied it to the optimal design of remote sensing satellites. Yet, this method focuses on repeated ground track orbits [Jafari-Nadoushan 2015], thus applying to a very specific subset of LEO orbits. To provide a more general solution, [Crisp 2018] proposed a semi-analytical method for calculating revisit times for the Walker constellation with discontinuous coverage. However, only the maximum and average revisit time are discussed.

Finally, many studies have focused on the energy consumption of NB-IoT or LTE, such as [Andres-Maldonado 2019, Vomhoff 2023, Sørensen 2022]. These works provide valuable insights into the battery life optimization of ground NB-IoT networks. At the same time, the 3GPP technical report [3GPP 2021] offers crucial information on energy consumption in DtS scenarios.

Overall, with respect to the literature reviewed so far, this chapter contributes the following: (i) an energy-efficient initial search method for downlink signals instead of methods combining GNSS with satellite ephemeris; (ii) a GNSS-independent technique able to estimate the UE's potential locations and predict future satellite passes based on the downlink synchronization method pictured in a previous contribution; (iii) an iterative algorithm able to refine the UE's estimated position and make it totally aware of next communication windows; (iv) simulation results proving that this strategy is more energy-efficient than GNSS-based methods.

3.2 Technological background

This chapter pictures a wake-up strategy for NB-IoT UE communicating over DtS links with constellations of LEO satellites. Then, its performance is deeply analyzed, as well as compared with the current mandatory 3GPP GNSS-based solution. Such a comparison is based on the expected energy consumption of getting and keeping synchronization. Before discussing the details of such an algorithm and its performances, it is worth gently introducing the system information of NB-IoT, LEO constellations, and energy-consumption models used throughout this chapter.

3.2.1 System information required

The process of how NB-IoT achieves downlink synchronization has been introduced in the previous two chapters. Here, the focus will be on the critical system information received after downlink synchronization, specifically SIB and MIB. A MIB contains basic system information required by all devices and scheduling information for SIB. MIB fragments are sent every 10 ms, and a complete MIB takes 640 ms, including repetition. Different devices will receive different SIBs according to their needs, including resource scheduling information and network information.

The scheduling of SIBs is not fixed and can be adjusted based on the operator or applications. According to Huawei's technical report [3GPP 2021], the time for receiving MIB and SIBs during one communication is 60 ms and 24 ms, respectively.

Among all SIBs defined in the 3GPP release [3GPP 2023], SIB31 and SIB32 address the need for NTN, i.e., infrastructures able to make communications happen between UE on the ground and eNB on board of satellites or any aerial platform. Together with SIB16, they are of utmost importance in this chapter since they provide all necessary information to UEs willing to communicate with eNB-equipped LEO satellites. For the sake of clarity, it is worth sketching their definition and behavior to infer better how the system described below builds up on top of them. In detail, SIB16 encodes the Coordinated Universal Time (UTC) with an accuracy of 10 ms. Instead, SIB31 provides some information related to the serving satellite. More specifically, it includes orbital parameters in either ephemerides or instantaneous values of the satellite state vectors. It also includes some timing information related to the setup of the next communication phases, and that is not further used alongside this contribution. Then, SIB32 is meant to broadcast information about the next satellite passes in case of discontinuous coverage by LEO constellations. The UE can obtain the trajectory of satellites using this SIB. It is shaped as a list, with each entry related to the satellite pass. The parameters disclosed for each satellite pass are the TLE-formed ephemerides and the footprint shape. However, this SIB does not provide information about the geometry of the whole LEO constellation. Finally, it is worth mentioning that the content, size, and scheduling of SIBs can be adjusted according to application scenarios, operators, and other factors. After the broadcast of SIBs, the UE can start transmitting random access messages to complete uplink synchronization and access the cell. However, as said before, the focus of this chapter is on the steps preceding this phase.

3.2.2 Walker constellations of LEO satellites

In Sec 1.3.1, different types of satellites are introduced. Since satellites have limited coverage, they usually work in constellations to cover as many areas as possible at the same time. Satellite constellations are a collection of satellites that are launched into orbit and cooperate to perform some functions. Among many types of geometrical scenarios, the Walker Constellation is the most commonly used type for handling LEO satellites [Wang 1993]. In this configuration, all satellites have the same orbital inclination and are evenly distributed across multiple orbital planes. This uniform distribution ensures a balanced coverage of the Earth's surface, making the Walker Constellation an efficient choice for various applications. Any Walker Constellation is indicated with the notation $i : T/P/F$, where i represents the inclination angle, T is the total number of satellites, P is the number of orbital planes, and F the relative phasing between satellites in adjacent planes. The angular difference for equivalent satellites in neighboring planes equals $F * 360/T$ degrees.

In the context of the present contribution, three different discontinuous coverage situations are considered, all of them being represented as Walker Constellations.

Table 3.1: Energy consumption before communication

	Energy consumption [mJ]
GNSS cold start	1110.00
GNSS warm start	185.00
GNSS hot start	37.00
100 NPSS	11.70
50 NPSS	7.35
20 NPSS	4.74

In the worst case, the "Single satellite" case offers a very sporadic coverage, limiting the visibility of the satellite on any spot of the Earth to around 20 minutes per day, with an average of 2 passes per day [Fraire 2019]. The second case is "Single orbit," which involves multiple satellites organized into a single orbit. Finally, the "Multiple orbits" scenario is meant to represent a generic sparse Walker constellation, with multiple orbits and a number of satellites per orbit. It has to be noted that only circular orbits have been used for simplicity, with the satellite's altitude fixed to a typical value of 600 km. The inclination angle is set to 85° to allow a fair coverage of the poles (note that if the inclination angle was set to 90°, a satellite would pass through the poles for each orbit period, thus providing an unbalanced coverage for unpopulated areas).

3.2.3 Energy consumption for synchronization

This subsection is meant to list the values related to energy consumption for synchronization purposes. In that, the 3GPP release mandated the availability of a GNSS receiver on UEs. In order to compare the presented GNSS-free wake-up strategy against the mandatory implementations, it is of core importance to provide the benchmark energy consumption due to GNSS here.

According to [3GPP 2021], ground devices equipped with GNSS should initiate the GNSS receiver for positioning before each communication. Depending on the situation, the start of a GNSS receiver can be referred to as "cold start", "warm start", or "hot start" [Paonni 2010]. A "cold start" occurs when the receiver is used for the first time or after a long period of inactivity. During a cold start, the receiver must obtain the satellite's data to calculate its current position, and the total duration of the process is 30 seconds. Instead, a "warm start" occurs when the receiver has not received GNSS signals for over 2 hours. In that case, the receiver needs to update certain information, which takes 5 seconds. Then, a "hot start" occurs when the receiver has all the necessary up-to-date information to lock onto the satellite quickly. Such a mode of operation lasts 1 second. Furthermore, from a hardware perspective, there are two ways to link a GNSS receiver on devices, i.e., either a separated GNSS module or an integrated one [3GPP 2021]. Huawei and CATT utilize separate GNSS modules in their devices, which offer flexibility

and upgradability. However, a separate module is featured by both a higher power consumption (100 or 216 mW) and an increased cost. On the contrary, Ericsson, MediaTek, and Nokia chose an integrated module that allows for better optimization of power consumption, i.e., 37 mW. From the energy consumption perspective, this chapter will compare the presented strategy against the solution that consumes the lowest energy, i.e., the one with integrated GNSS modules.

Contrariwise, the GNSS-free strategy introduced later requires that UEs receive several NPSS signals to achieve and keep synchronization. This process can be completed in 1 second. Recalling that NPSS signals are transmitted for 1 ms every 10 ms by eNBs, UE can listen up to 100 NPSS during 1 second. However, the NPSS collection strategy on the UE can be implemented in a way to listen to less than 100 NPSS within the 1 second observation time, with the interval between two consecutive NPSS receptions being higher than 10 ms. In all cases, the chosen value of power consumed for listening to incoming downlink signals (i.e., NPSS, NSSS, MIB, and SIBs) is 90 mW, and this is the highest setting presented in [3GPP 2021]. Such a conservative choice has been made to compare the best GNSS-based solution with the worst-case GNSS-free settings. According to [3GPP 2021], the power consumption value for idle state between consecutive NPSS receptions has been set to be 3 mW. The power consumption during idle state is significantly higher than 0.015 mW consumed during sleep mode. A UE goes into this state after a completed communication until it wakes up again to listen to NPSS.

Table 3.1 compares the described approaches in terms of energy consumed by a UE to get synchronized. The comparison focuses only on this part because the energy consumption in subsequent exchanges does not differ for any approach. In particular, it can be seen that the GNSS-free approach based on the reception of up to 100 NPSS signals consumes less than 33% of the least energy-intensive GNSS hot start process. This also means that a GNSS-free solution is the best choice in the case of capillary coverage ensured by a dense constellation of LEO satellites. However, such a scenario is not further analyzed since the focus is on the most challenging scenario of discontinuous coverage. Indeed, due to the lack of precise location information, a GNSS-free UE consumes additional energy for accurate self-positioning, thus making non-trivial comparisons with GNSS-enabled solutions.

3.3 Proposed approach

The rationale of the wake-up strategy introduced by this chapter can be summarized as an “ask, learn, go” process. Indeed, the “ask” part is represented by a *Network Search* phase. Ground UEs intermittently wake up and poll the radio for beacon signals, i.e., NPSS NB-IoT signals. Once an NPSS signal is detected, a *Synchronization to LEO satellites* phase can be started, and the wake-up strategy enters into its “learn” part. During this phase, the UE tries to predict when a LEO satellite will be within its range and builds up a list of next satellite passes. The UE wakes up at each expected satellite pass to check whether the prediction was

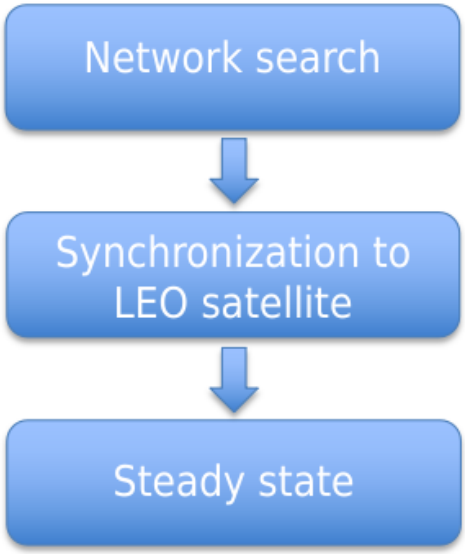

Figure 3.1: The procedures of wake-up strategy

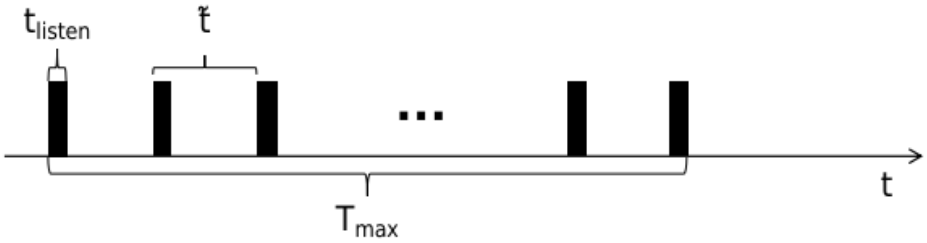

Figure 3.2: Search for NPSS signal.

correct and to continuously update the list. Once the UE verifies that its prediction is converging to stability, the wake-up strategy enters into the *Steady State* phase, i.e., the "go" part of the strategy. With this organization in mind, this section is organized as follows. Sec. 3.3.1 pictures the actions taken during *Network Search* phase. Then, Sec. 3.3.2 describes the operations to be done during the *Synchronization to LEO satellites* phase. Finally, Sec. 3.3.3 provides details about how a UE can pass from the *Synchronization to LEO satellites* phase to the *Steady State* one.

3.3.1 Phase 1: Network Search

The *Network Search* phase represents Phase 1 (Algorithm 1) of the wake-up strategy presented hereafter and refers to the period of time going from the UE's initial wake-up through the reception of the first NPSS from the eNB-equipped satellite. Since the UE does not have any information about the position of LEO satellites at

Algorithm 1 Wake-up Strategy: Network Search

Input:
    Wake-up interval $\tilde{t}$
    Maximum waiting time T_{max}
    Current time t
Initialization: $t = 0$, $flag = False$
while $t < T_{max}$ **and** $!flag$ **do**
    UE wakes up
    Attempt to receive NPSS
    if NPSS received **then**
        $flag = True$
    else
        UE goes to sleep mode
        Wait for time $\tilde{t}$
        $t = t + \tilde{t}$
    end if
end while
if $flag$ **then**
    Perform synchronization operation
else
    Output "Synchronization failed within the given time."
end if

bootstrap, it can only attempt continuous signal monitoring. However, considering the worst-case network scenario with a single satellite, its next pass into the UE's range could take up to several hours, and uninterrupted listening would quickly deplete a large portion of the stored energy. Therefore, an intermittent listening strategy may be used to reduce the UE's energy consumption.

As shown in Fig.3.2, the device wakes up at regular intervals $\tilde{t}$ and starts listening to the possible transmission of NPSS signals for a time interval t_{listen}. When t_{listen} is elapsed, the UE goes back to sleep mode. If an NPSS has been received, the UE is ready for Phase 2 (described in Sec. 3.3.2). Given that NPSS signals are transmitted every 10 ms and that each transmission lasts 1 ms, setting $t_{listen} = 11$ ms ensures that if a satellite is in the range of the UE for the duration t_{listen}, at least one NPSS signal will be received. Note that the propagation delay does not need to be considered in the t_{listen} because the synchronization signals are continuous. The interval between signal arrivals remains constant, irrespective of the propagation delay. In this configured access scheme, the length of the interval $\tilde{t}$ defines the duty cycle. The longer $\tilde{t}$, the smaller the duty cycle. If $\tilde{t}$ is too short, the UE will consume more energy. Contrariwise, if $\tilde{t}$ is too long, the satellite's arrival may be missed. Therefore, the setting of $\tilde{t}$ is of core importance for finding a tradeoff between energy consumption and protocol reactivity. Such a setting will be discussed in Sec. 3.4 on the basis of some simulation results related to various satellite constellations. To anticipate possible hardware issues or other sort of problems, the maximum duration

T_{max} of Phase 1 can be properly set to a limited value. When T_{max} elapses, the UE stops searching for NPSS signals. In this chapter, for evaluation purposes, T_{max} is set to be infinity for Phase 1.

3.3.2 Phase 2: Synchronization to LEO satellites

Building upon the reception of the first NPSS signal, Phase 2 of the proposed strategy is meant to let a UE achieve and keep *Synchronization to LEO satellites*. During such a phase, the UE repeatedly performs estimations and makes predictions. In detail, if a LEO satellite is within the communication reach, a UE tries to estimate the satellite's trajectory through the algorithm described in the last chapter and quickly reviewed in Sec. 3.3.2.1. The knowledge of the satellite's trajectory is useful for two reasons: (i) it allows the UE to pre-compensate in time and frequency the reception of the subsequent SIBs; (ii) the associated maximum elevation angle is used to estimate two potential positions of the UE on the Earth. The latest estimation takes as input also timing and orbital information included in the received SIBs, and it is described in Sec. 3.3.2.2. Through the estimation of the UE positions, the UE can attempt the prediction of next satellite passes, as described in Sec. 3.3.2.3. Thanks to such a prediction, the UE can go back to the sleep state after a satellite pass and wake up again just before the next one. The wake-up strategy is then described in Sec. 3.3.2.4.

3.3.2.1 Estimation of Maximum Elevation Angle

As described in Chapter 2, by measuring the Doppler shift associated with the reception of multiple downlink NPSS signals, it is possible to figure out the relative position of the satellite trajectory with respect to the UE. Alongside this chapter, the model of (2.5) is used to estimate the values of α_0 and t_0. To illustrate the performance evaluation, Fig. 2.5 in Chapter 2 compares the original Doppler curve with the estimated one calculated through (2.5). In this simulation, the standard deviation of the simulated AWGN error source is 20 Hz, and the UE needs to receive 10 NPSS signals to estimate the Doppler curve. The zoomed-in view shows that while each signal has random errors, the final fitting is very close to the original Doppler curve, demonstrating the model's feasibility. The results show that even with a significant measurement error standard deviation (200 Hz), this method can keep the estimated Doppler curve within an acceptable range of the original curve for tens of seconds to more than a minute. This ensures that receiving multiple NPSS signals supports a complete NB-IoT communication session (uplink and downlink synchronization).

Considering the computational constraints of IoT devices, performing trigonometric or root calculations could be challenging. Current approaches, such as linear approximations or look-up tables [Lygouras 2000], can simplify the calculations required with low memory. These approaches can efficiently address the complexities involved in computations like Doppler curve estimation and the rest of this section,

making them more suitable for IoT devices. The evaluation of the actual impact of such approximations on the overall system performances is out of the scope of this chapter and will be tackled in future investigations.

3.3.2.2 Positions of UE

The previously estimated α_0 and t_0, combined with some data broadcast by the satellite within SIB16 and SIB31 (as anticipated in Sec. 3.2.1), can be utilized to estimate 2 approximate positions of the UE. One of these 2 locations is the actual position of the UE. The other location is exactly the mirrored point of the actual position with respect to the projection of the satellite trajectory on Earth. A method to identify the actual position is later proposed in Sec. 3.3.3. To calculate the UE position, a reference point needs to be selected first. Herein, such a point is the projection on the Earth of the satellite in the instant when it is closest to the UE, i.e., when $\theta = \theta^*$. The UTC time T^* of this instant can be computed as:

$$T^* = T_r - (t_0 + \tau_{sib}), \tag{3.1}$$

where T_r is the UTC time communicated within SIB16. For a satellite traveling at the height of 600 km on the ground level, SIB16 is usually received with a delay of 2 to 4 ms, but since the time accuracy of T_r is 10 ms, this delay can be neglected. Instead, τ_{sib} is the time interval duration between the reception of the first NPSS signal and the reception of SIB16. This chapter assumes a worst-case scenario where this interval is 4 seconds long. Then, the coordinates of the satellite's projection on the Earth when closest to the UE are calculated through the SGP4 algorithm [Morales 2019] using as input T^* and the vector of ephemerides orbital data $\mathbf{E}$ sent in SIB31:

$$(\phi_s, \lambda_s, \mathbf{v_s}) = SGP4(T^*, \mathbf{E}). \tag{3.2}$$

In such an equation, ϕ_s is the latitude of the satellite, λ_s is its longitude, and $\mathbf{v}$ is the speed of the satellite expressed in the associated Cartesian coordinates (v_s^x, v_s^y, v_s^z).

Based on the joint knowledge of the satellite coordinates $(\phi_s, \lambda_s, \mathbf{v_s})$, of the ephemerides $\mathbf{E}$, and of the angle α_0 between the UE and the satellite when they are closest, the UE can compute the two possible locations $U_1(\phi_1, \lambda_1)$ and $U_2(\phi_2, \lambda_2)$ for its own position on the Earth. For the sake of readability, Fig. 3.3 plots the system model that will be used in the following discussion, with the Earth's center placed at O. In detail, the great orange circle represents the projection of the satellite's trajectory on the ground. Such a trajectory intersects the equator (i.e., the black great circle) in 2 points. One of them is indicated with A in the figure, while the other point is located at the antipodes of A and not shown in the figure. Of these 2 intersection points, A is the closest to the actual UE position U_1, and it will be the only one considered in the next discussion. The closest satellite position to U_1 is S, while the mirrored location is U_2. The points U_1, S, and U_2 are all aligned on the great circle plotted with a dotted line and intersecting the equator at D. Such a great circle is orthogonal to the orange projection of the satellite trajectory.

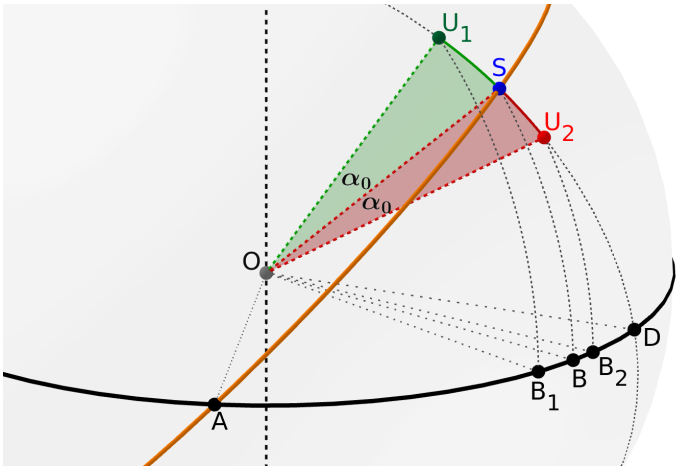

Figure 3.3: System model.

In such a scenario, the latitudes of U_1 and U_2 can be calculated considering the spherical triangles U_1B_1D and U_2B_2D, noting that $\angle U_1DB_1 = \angle U_2DB_2 = \angle SDB$, and using the spherical law of sines $\sin(\phi_{1/2}) = \sin(\angle SDB)\sin(\angle SOD \pm \alpha_0)$, with the 2 angles $\angle SDB$ and $\angle SOD$ still being unknown. Focusing on the spherical triangle SBD and according to the spherical law of sines, $\angle SOD = \arcsin[\sin(\phi_s)/\sin(\angle SDB)]$. Hence, the remaining unknown is $\angle SDB$. So, considering the spherical triangle ASD, and using the second spherical law of cosines, $\angle SDB = \arccos[sin(i)cos(\angle AOS)]$. Finally, using the law of sines on the triangle ASB, it is possible to evaluate $\angle AOS = \arcsin[\sin(\phi_s)/\sin(i)]$. Putting all together, the latitudes of U_1 and U_2 are

$$\phi_{1/2} = \arcsin[\sin(\phi_s)\cos(\alpha_0) \pm \cos(i)\sin(\alpha_0)]. \tag{3.3}$$

Then, to compute the longitudes of U_1 and U_2, note that the unit vector $\hat{\mathbf{u}}$ placed at O and pointing to any of such positions forms an angle α_0 with the unit vector $\hat{\mathbf{s}}$ still placed at O and pointing to S. This corresponds to let the scalar product $\hat{\mathbf{u}} \cdot \hat{\mathbf{s}}$ be equal to $\cos(\alpha_0)$. After some calculations, the following equation can be found:

$$\cos(\lambda_{1/2} - \lambda_s) = \frac{\cos(\alpha_0) - \sin(\phi_{1/2})\sin(\phi_s)}{\cos(\phi_{1/2})\cos(\phi_s)}. \tag{3.4}$$

Solving (3.4) for a specific latitude ϕ, it is possible to find 2 points with longitudes λ^w and λ^e forming an angle α_0 with the satellite projection S. Specifically, going from West to East λ^w precedes λ_s, and λ_s precedes λ^e. In total, there are: (i) 2 possible longitudes associated to ϕ_1, i.e., λ_1^w and λ_1^e; (ii) 2 possible longitudes associated to ϕ_2, i.e., λ_2^w and λ_2^e. However, only one longitude for each latitude is the correct one. It can be quickly recognized that if the satellite is ascending, the correct longitude associated with ϕ_1 is λ_1^w, while the correct longitude associated with ϕ_2 is λ_2^e. Instead, if the satellite is descending, the correct longitude associated with ϕ_1 is λ_1^e, while the correct longitude associated with ϕ_2 is λ_2^w. Given that a

satellite is ascending (descending) if the component v_s^z of its speed along the z axis is positive (negative), and indicating with $\text{sgn}(\cdot)$ the sign function, the longitudes of U_1 and U_2 can be evaluated as:

$$\lambda_{1/2} = \lambda_s \mp \text{sgn}(v_s^z) \arccos\left[\frac{\cos(\alpha_0) - \sin(\phi_{1/2})\sin(\phi_s)}{\cos(\phi_{1/2})\cos(\phi_s)}\right]. \tag{3.5}$$

3.3.2.3 Prediction of next passes

To predict the next satellite passes in case of discontinuous coverage, the current 3GPP specification [3GPP 2023] defines SIB32 as a means used by an eNB-equipped satellite to broadcast the orbital parameters related to 4 satellites at most (see the definition of the parameter `maxSat-r17`). While it is understandable the reason for such a small number of satellites, i.e., the cumulative orbital data related to each satellite within a constellation would make the transmission of a too-long SIB32 unfeasible in practice, in this chapter, it is argued that SIB32 can be forged in a different way. In fact, it must provide a few constellation parameters so that the receiving UE can compute the next passes related to all the satellites belonging to the constellation. This choice has some advantages: (i) there is no need for the satellite and/or the network to make a selection of the `maxSat-r17` satellites advertised in a given spot of the Earth because SIB32 is designed to provide general constellation parameters instead of specific orbital parameters for a limited number of satellites, thus increasing the scalability of the system; (ii) the knowledge of the whole constellation would allow all UEs to exactly compute what is the very next pass by any satellite in the constellation, thus increasing the communication chances; (iii) The SIB length would be much shorter, thus reducing the energy consumption and resources required by both LEO satellites and UEs. Additionally, the UEs only need to receive this SIB32 once during initial communication with the satellite. It can be almost ignored over the long term. Therefore, in the simulations later, the energy variations due to receiving SIB32 are not considered significant enough to affect the outcomes. In Release 18, 3GPP also introduces SIB33, which provides satellite assistance for neighboring cells. However, the strategy discussed in this chapter does not require this additional information. Therefore, SIB33 is not considered in the analysis.

More specifically, the parameters of a Walker constellation to be broadcast in SIB32 are the values T, P, and F introduced in Sec. 3.2. Note that the inclination angle i is implicitly understood through SIB31 and is related to the serving satellite. The total number of satellites T can be encoded with 1 byte to allow up to 255 satellites. As well, P and F can be encoded each with 1 byte. As further detail, F is set to be 0 when there is only a single orbital plane, i.e., when $P = 1$. Theoretically, there are no absolute maximum values for the parameters T, P, and F in satellite constellation configurations, as they depend on the specific requirements and design considerations of particular missions. The size of these parameters can be adjusted according to different applications. Assuming to represent each of those 3 values

with 2 bytes, a Walker constellation with a maximum size of 65535 satellites would be able to capillary cover the whole Earth surface with satellites, each featured by a 100 km wide footprint. Hence, a SIB32 long 6 bytes is more than sufficient to allow all constellations targeting a discontinuous coverage.

By combining the estimated UE's coordinates (see Sec. 3.3.2.2) and the trajectory of all satellites in a Walker-like constellation, it is possible to fill up a sorted list with all next passes of satellites in the considered constellation up to a given time T_{lim}. First, for each of the 2 possible locations of the UE position, it is possible to build a time-sorted list by adding at each step the pair $(time, longitude)$ associated with the next satellite belonging to the constellation and passing at the same latitude associated to the considered location. This list is continuously filled with next passes at the same latitude until T_{lim}. Then, the passes with "non-compliant" longitudes will be discarded. Finally, the 2 lists are merged to create a single time-sorted list containing the next feasible passes through the UE possible locations.

In more detail, it must be observed that during a nodal period P_N (i.e., the time taken by a satellite to complete an entire orbit around the Earth and pass by the same latitude with the same direction), the Earth rotates for exactly the difference in longitude

$$\Delta\lambda = P_N(\dot{\Omega} - \omega_E), \tag{3.6}$$

where ω_E is the angular velocity of the Earth and $\dot{\Omega}$ is the nodal regression rate of the satellite orbit [Zong 2019]. However, given the first estimated longitude $\lambda_1^{u/d}$, for the objective of the proposed approach, it is more important to find the longitude of the next pass $\lambda_1^{d/u}$ through the same latitude ϕ and opposite direction (the "u" means upside, the "d" means downside):

$$\lambda_1^{d/u} = \lambda_1^{u/d} + \pi \mp 2\arcsin\left(\frac{\tan(\phi)}{\tan(i)}\right) + \left(0.5 \pm \frac{1}{\pi}\arcsin\left(\frac{\sin(\phi)}{\sin(i)}\right)\right)\Delta\lambda. \tag{3.7}$$

In general, the set of all longitudes associated with passing through the same latitude is:

$$\left\{\lambda_j^{u/d} | \lambda_j^{u/d} = \lambda_1^{u/d} + (j-1)\Delta\lambda, \text{ for } j = 1, 2, ... \left\| \frac{T_{lim}}{P_N} \right\| \right\} \tag{3.8}$$

Referring to Walker Constellation (see Sec. 3.2), the longitudes in different planes are [Crisp 2018]

$$\left\{\lambda_{j,k}^{u/d} | \lambda_{j,k}^{u/d} = \lambda_j^{u/d} + 2\pi(k-1)\left(\frac{1}{P} + \frac{F}{T}\right), \text{ for } k = 1, 2, ..., P\right\}. \tag{3.9}$$

Finally, the complete set of longitudes for the constellation is:

$$\left\{\lambda_{j,k,o}^{u/d} | \lambda_{j,k,o}^{u/d} = \lambda_{j,k}^{u/d} + \frac{(o-1)P}{T}\Delta\lambda, \text{ for } o = 1, 2, ..., \frac{T}{P}\right\}. \tag{3.10}$$

with the longitude of the reference point being $\lambda_{1,1,1}^{u/d}$, and its time instant indicated as $T_{1,1,1}^{u/d}$.

Now that the list of longitudes where each satellite passes through the same latitude of the UE within a certain period of time is built, it is necessary to determine which longitudes are within the communication range of the UE and find the elapsed time since the time instant $T_{1,1,1}^{u/d}$ associated to reference point, so that the revisit time for longitude $\lambda_{j,k,o}^{u/d}$ is

$$T_{k,o,j}^{u/d} = T_{1,1,1}^{u/d} + (j-1)P_N + \frac{(k-1)F}{T}P_N + \frac{(o-1)P}{T}P_N \tag{3.11}$$

Recalling that the area covered by a traveling satellite is called swath [Hayes 1988], it is worth defining Λ as the width of the satellite swath at the latitude ϕ of the UE. In other words, when a satellite passes through latitude ϕ, if the satellite's longitude $\lambda_{j,k,o}^{u/d} \in [\lambda - \frac{\Lambda}{2}, \lambda + \frac{\Lambda}{2}]$, the device can communicate with this satellite. Considering also α_0 and the UE's latitude, the swath can be calculated as follows:

$$\Lambda = \cos^{-1}\left(\frac{\sin(\phi)\cos(i) - \sin(\alpha_0)}{\sin(i)\cos(\phi)}\right) - \cos^{-1}\left(\frac{\sin(\phi)\cos(i) + \sin(\alpha_0)}{\sin(i)\cos(\phi)}\right). \tag{3.12}$$

A larger swath Λ' is required to predict the next pass, depending on the error margin. This also means the device can move within a certain range within the maximum error distance. This value can also be adjusted according to different applications. The formula to calculate Λ', taking into account the acceptable distance error, is as follows:

$$\Lambda' = \Lambda + 2 * \frac{D_{error}}{R_E * \cos(\phi)} \tag{3.13}$$

3.3.2.4 Wake up on predicted satellite pass

Once a UE has caught the first NPSS signal (see Sec. 3.3.1), estimated the maximum elevation angle of satellite's trajectory (see Sec. 3.3.2.1), computed 2 possible locations for its own position (see Sec. 3.3.2.2), and predicted the associated next satellite passes (see Sec. 3.3.2.3), it can communicate with the satellite. After that, it can turn its radio off and stay in sleep mode.

Thanks to the knowledge of the next passes, the UE can wake up exactly again around the estimated revisit time T_{next} associated with the first item on the list. The same listening strategy pictured in Fig. 3.2 is used. It is important to notice that since the prediction is based on 2 potential locations, it is possible that the first item on the list is associated with the wrong location. As well, even if the first item is associated to the correct location, there could be an error in the predicted revisit time. Given that the maximum visibility time τ_v of the satellite is around 4 minutes for a 600 km LEO satellite. If no NPSS has been captured before $T_{next} + \tau_v$, then it is reasonable to assume that the next pass was associated with the wrong location. It also seems reasonable to let the UE start listening not before $T_{next} - \tau_v$. As a matter of fact, the uncertainty on the start of the visibility time is assumed to be bounded to τ_v before and after the computed revisit time. In this way, the

search time T_{max} is set to twice the maximum visibility time of the satellite, so around 8 minutes for the targeted scenario. If no NPSS has been received, the UE will go to sleep and start the same procedure around the next revisit time in the list of future satellite passes. Additionally, since the value of T_{max} during this phase is quite short if compared with the *Network Search* phase, the interval $\tilde{t}$ between 2 consecutive polls can be shortened to 30 seconds to capture with more precision the start of the visibility time and have more time to communicate.

3.3.3 Getting to Phase3: Steady State

The *Synchronization to LEO satellites* phase pictured above in Sec. 3.3.2 requires that a UE always wakes up for the next satellite pass present in the built sorted list of predicted passes. This is done in order to perform a position estimate and update the list of next passes. A UE will also wake up if the next pass is associated with a mirrored position, thus wasting energy. In this sense, a UE should combine the subsequent position estimations in order to select just the actual position and narrow down the associated error. The algorithm pictured below is meant to refine the UE's estimated position through multiple satellite passes. The stopping condition for this algorithm is given by the number of estimation N_e, whose value will be discovered through simulation-based analysis in Sec. 3.4.2. It is worth noting that the algorithm behavior differs among (i) the very first satellite pass (the one triggering the switch from *Network Search* to *Synchronization to LEO satellites*), (ii) the second pass, and (iii) the following ones up to N_e. The details of the algorithm are shown in Algorithm 2.

As a matter of fact, after the first satellite pass, the UE will discover 2 locations for the UE position, namely U_1^1 and U_2^1. These 2 locations and the location S^1 of the satellite projection on the ground closest to the UE are stored and used for the next algorithm run. Based on the computed list of time-sorted next passes, the UE will wake up for the next pass. If no NPSS is received, the UE goes to sleep and wakes up again for the following pass in the list. This process continues until the UE wakes up and finds out that a satellite pass is happening.

At this stage, the second run of the algorithm can be executed. In detail, the satellite estimates the satellite position when it is closest, S^2, and the 2 possible locations for its own position U_1^2 and U_2^2. In addition, it computes a reference point $R^2 = (S^1 + S^2)/2$. Then, it selects between the location found during the first pass, U_1^1 and U_2^1, the one which is the closest to R^2, namely U_C^1; it also selects between the location found during the second pass, U_1^2 and U_2^2, the one which is the closest to R^2, namely U_C^2. It can now estimate its own position as $V^2 = (U_C^1 + U_C^2)/2$.

The third and following runs of the algorithm are executed when a satellite pass is detected during the next wake-up according to the updated list of satellite passes. Specifically, at run n, the satellite location S^n and the 2 locations for the UE U_1^n and U_2^n are estimated. Based on these, the reference point $R^n = (S^1 + S^2 + \cdots + S^n)/n$ is computed. Then, the UE selects between U_1^n and U_2^n the closest location U_C^n to R^n, and can compute the estimate of its own position $V^n = (U_C^1 + U_C^2 + \cdots + U_C^n)/n$.

Algorithm 2 Wake-up strategy: Determination of UE's Position

Input:
  Minimum number of estimations N_{est}
Initialization: $n = 0, V^n = None, R^n = 0$
while $n < N_{est}$ and NPSS received **do**
  $n = n + 1$
  Obtain Satellite information (Ephemeris) from SIB
  Calculate two potential UE positions: U_1^n and U_2^n
  Store Satellite's current position S^n
  if $n == 1$ **then**
    $V^n = [U_1^n, U_2^n]$
  else if $n == 2$ **then**
    Calculate reference point $R^2 = (S^1 + S^2)/2$
    U_C^1 = Closer point to R^2 among U_1^1 and U_2^1
    U_C^2 = Closer point to R^2 among U_1^2 and U_2^2
    $V^n = (U_C^1 + U_C^2)/2$
  else
    Calculate reference point $R^n = (S^1 + S^2 + \cdots + S^n)/n$
    U_C^n = Closer point to R^n among U_1^n and U_2^n
    $V^n = (U_C^1 + U_C^2 + \cdots + U_C^n)/n$
  end if
  Update next pass list based on V^n
end while
Output: Estimated Position V^n

After the N_e run, the UE can wake up just when it needs to transmit IoT data through the LEO constellation. To do that, the list of next passes used is based only on the estimate V_{N_e} found at the end of the N_e-th run.

3.4 Simulation Results

In this section, some results are presented based on the simulation of the proposed strategy. The simulation environment can work with various types of satellite constellations and mimic random UE deployments on the ground. The simulation environment is built in Python and leverages the Skyfield library [Rhodes 2023] to generate satellite trajectories accurately. Skyfield is a powerful tool for astronomical computations, enabling the precise modeling of satellite orbits based on real-world orbital parameters such as altitude, inclination, and eccentricity. Each NPSS signal received by a UE is affected by the Doppler effect. Additionally, as discussed in the previous section, the accuracy of the measured signal frequency and the following calculations cannot be perfect due to hardware limitations. To represent the measurement noise more realistically, each signal is affected by Additive White Gaussian Noise (AWGN). This is achieved by incrementing (or decrementing) the original value of the Doppler shift by means of a random value drawn from

Table 3.2: Parameters of the Simulations

Parameters	Value
Power of GNSS	37 mW
Power of RX NPSS/NSSS	90 mW
Power of RX MIB/SIB-satellite	90 mW
Power of Idle	3 mW
Power of Sleep	0.015 mW
GNSS cold start duration	30 s
GNSS warm start duration	5 s
GNSS hot start duration	1 s
RX SIB-satellite duration	24 ms
RX MIB duration	60 ms
Search for NPSS duration	11 ms

a zero-mean normal distribution with configurable standard deviation σ. The value of σ has been varied in the interval $[0, 300]$ Hz to feature different noisy environments. Finally, all the NB-IoT settings presented in Sec. 3.2 and based on the 3GPP technical report [3GPP 2021] as shown in Table 3.2 have been used to set up simulations.

In detail, this section provides some rules of thumb to configure the wake-up strategy presented in Sec. 3.3 with the proper settings and evaluates the energy consumption due to it in the long term. Sec. 3.4.1 discusses how to set the wake-up interval $\tilde{t}$ introduced in Sec. 3.3.1, while Sec. 3.4.2 shows how to set up the algorithm that lets the strategy enter the Steady State phase. Finally, Sec. 3.4.3 provides an evaluation of the energy consumed by the presented GNSS-free wake-up strategy and compares it with the standard GNSS-enabled configuration.

3.4.1 Optimal wake-up interval during Network Search

As introduced in Sec. 3.3.1, when a UE is switched on (or in general when it is bootstrapped), it must first join the NB-IoT network. To do so, it starts a polling procedure where it intermittently wakes up for very short time intervals, i.e., 11 ms, and listens to the radio for possible incoming NPSS signals. The challenge inherent to this approach is to find a suitable wake-up interval between 2 consecutive polls in order to maximize energy efficiency while preserving the reactivity of the joining protocol (see Fig. 3.2).

The results of the simulation-based analysis conducted to address this issue are shown in Fig. 3.4 and 3.5. In detail, Fig. 3.4a, 3.4b, and 3.4c show the average energy consumed by a UE implementing the Network Search procedure as a function of the configured wake-up interval $\tilde{t}$. Instead, Fig. 3.5a, 3.5b, and 3.5c picture the average time elapsed before the first NPSS signal is received, and such a value is plotted as a function of the configured wake-up interval $\tilde{t}$ as well. Then, Fig. 3.4a and 3.5a refer to the scenario with a single satellite, while Fig. 3.4b and 3.5b consider the

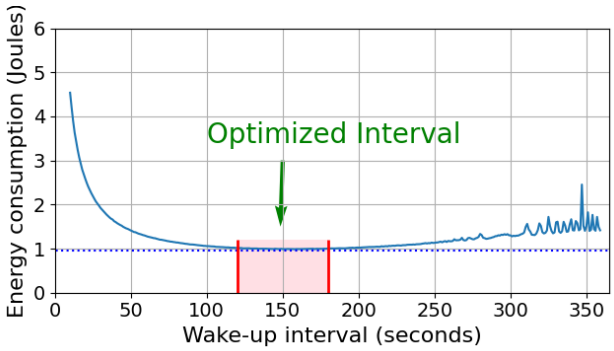

(a) Energy consumption for Single satellite.

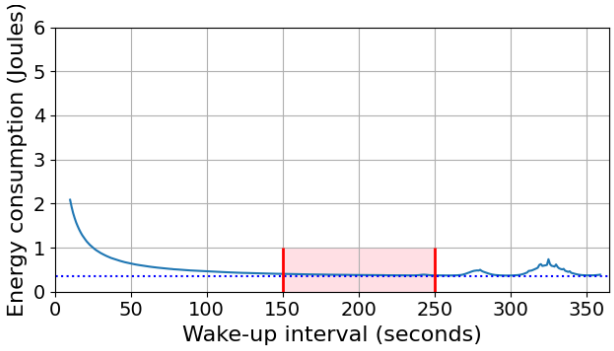

(b) Energy consumption for Single orbit with 4 satellites.

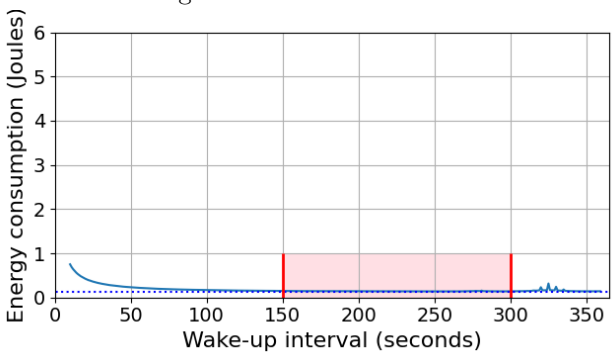

(c) Energy consumption for Walker constellation: 12/3/1.

Figure 3.4: Performance evaluation of Network Search (Energy consumption).

single orbit configuration, and Fig. 3.4c and 3.5c deal with a Walker constellation 12/3/1. In all figures, the value $\tilde{t}$ has been varied from 10 seconds to 6 minutes, with an incremental step of 1 second. For any given value of $\tilde{t}$, 400 random locations on the Earth have been selected. For each location, 1000 random instants of time have been chosen to mimic different bootstrap times with respect to the current positions of satellites in the sky. Hence, each point in the plots of Fig. 3.4 and 3.5

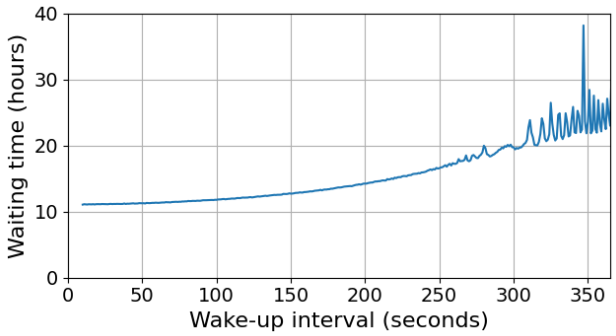

(a) Latency for
Single satellite.

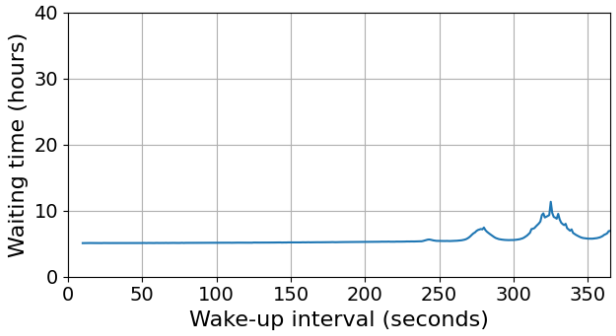

(b) Latency for
Single orbit with 4 satellites.

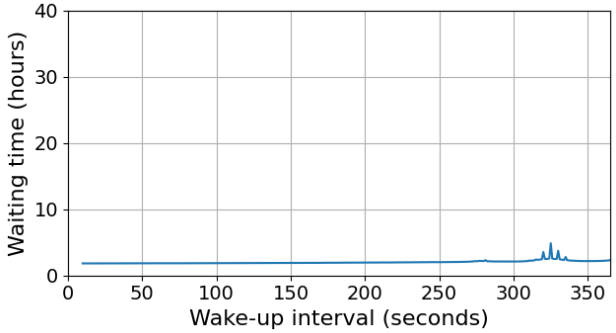

(c) Latency for
Walker constellation: 12/3/1.

Figure 3.5: Performance evaluation of Network Search (Waiting time).

represents the average of 0.4×10^6 simulations.

Starting from the analysis of the energy consumption due to the very first Network Search, as it can be seen in Fig. 3.4a, 3.4b, and 3.4c, the length of the interval $\tilde{t}$ has a significant impact on it. Indeed, if $\tilde{t}$ is too short, UEs wake up to check for downlink NPSS signals more frequently than needed. Given that the time interval between satellite passes over a given spot on the Earth can range from several

Table 3.3: Network Search energy consumption comparison

Constellation types	GNSS implemented	No GNSS
Single satellite	3.6 J	0.99 J
Single Orbit (4 satellites)	3.27 J	0.37 J
Walker constellation (12/3/1)	3.11 J	0.14 J

minutes to over 10 hours, depending on the constellations, frequent wake-ups lead to a significant waste of energy. On the other hand, if $\tilde{t}$ is too long, the UE can miss satellite passes more frequently, resulting in the inability to join the NB-IoT network for a very long time. In general, it may be noticed that the lowest values of energy consumption can be achieved for values of $\tilde{t}$ close to the average time of a LEO satellite pass over any spot on the Earth: if a UE wakes up frequently enough not to miss a satellite pass, the chance of saving energy is higher. In addition, due to the approximate periodicity of satellite passes, some specific wake-up frequencies may cause the UE to miss multiple satellite passes in a row. Although energy consumption is lower in sleep mode, sleeping too long can still result in a significant cumulative energy consumption. Considering the need for UEs to transmit uplink IoT data, the prolonged inability to get connected to the network translates into big amounts of cached data, which in turn may affect the communication efficiency and result in delayed or failed data transmission.

Furthermore, comparing the single satellite scenario (see Fig. 3.4a) with the single orbit one (see Fig. 3.4b), the increased number of satellites lets the interval between satellite passes decrease, thus leading to a decreased waiting time for a UE to join a DtS NB-IoT network and a reduced energy consumption. This is even more evident by inspecting the scenario with a Walker constellation Fig. 3.4c). One final remark on the energy consumption can be made by observing that the availability of more satellites leads to the expansion of the range of optimal values for $\tilde{t}$. If this interval ranges between 120 and 180 seconds in the single satellite scenario, in the case of multiple satellites in a single orbit, the optimal values of $\tilde{t}$ vary between 150 and 250 seconds. For a Walker constellation, which involves a larger network of satellites distributed over multiple orbits, the wake-up interval can be further expanded to $[150, 300]$ seconds.

With regard to the analysis of the measured latency between the instant when the UE is bootstrapped and the instant when it gets synchronized to the NB-IoT network, Fig. 3.5a, 3.5b, and 3.5c show that it looks like very much similar to the energy consumption. However, for very small values of $\tilde{t}$, the latency is just an increasing function of the wake-up interval. For example, by having a close look at the energy consumption and the measured latency in the single satellite scenario (Fig. 3.4a and 3.5a), it may be noticed that for $\tilde{t}$ becoming smaller and smaller than 100 seconds, the energy consumption increases, but the latency decreases. In other words, waking up more frequently is energy expensive, yet it allows a fast join to the network. Hence, the correct setting of $\tilde{t}$ must be driven by the final

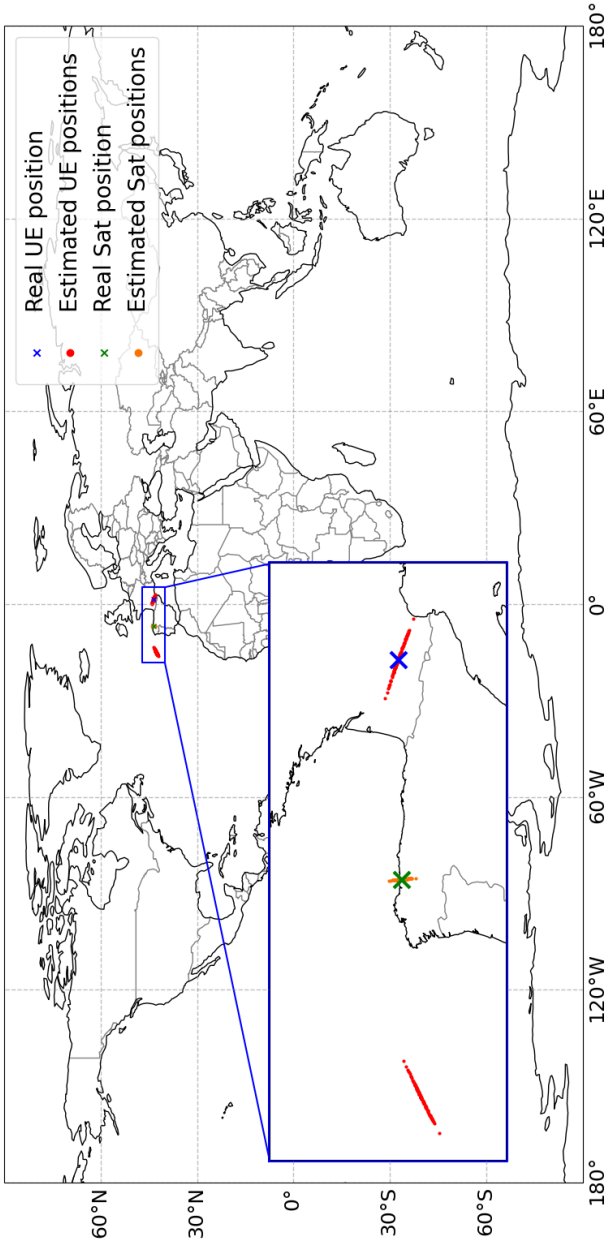

Figure 3.6: Possible estimations of one single pass with $\sigma = 50$.

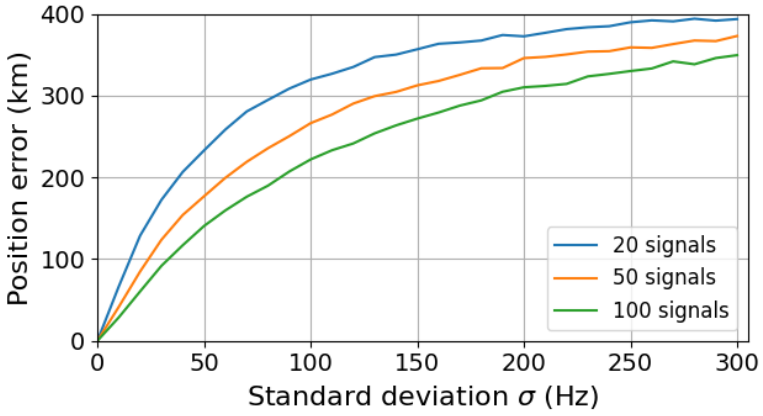

Figure 3.7: Error of estimation.

IoT application: for time-critical data, it may be more convenient to trade off the energy consumption in favor of the fastest Network Search phase. Although the study was limited to using the Walker constellation, the worst-case scenario still involves only one satellite in any constellation configuration. As the number of satellites increases, both energy consumption and latency are expected to decrease, and the wake-up intervals can become longer. Therefore, 150 seconds in wake-up intervals can be applied to any type of constellation, and it will also be used in upcoming simulations. However, this value may require adjustments for different altitudes and orbital inclinations, which will be further investigated in future work and are not covered in this chapter.

Finally, it is worth providing a comparison with the mandatory GNSS-enabled implementation. When a GNSS-enabled UE is bootstrapped, the GNSS receiver must run a "cold start". Assuming that the information about satellite constellations is pre-loaded, a UE only needs to enter sleep mode after startup and remain in such a state until the first expected pass of the satellite. Table 3.3 shows the resulting comparison between GNSS-enabled UE and GNSS-free UE for different satellite constellations. In that, the GNSS-free UE is set with an optimal value of $\tilde{t}$. It can be seen that there is a clear reduction of energy consumption when using the GNSS-free solution, mainly because the cold start of GNSS is very much power-hungry.

3.4.2 Optimal number of estimation runs to get into Steady State

After the very first synchronization based on the reception of several NPSS signals (see Sec. 3.3.2.1), a UE can estimate 2 possible locations for its actual position by using the method introduced in Sec. 3.3.2.2. To help the reader quickly figure out what are the outputs of the position estimation, Fig. 3.6 shows the example of a satellite running across the same path. This corresponds to the orbital plane of the satellite rotating synchronously with the Earth. Even if this is physically

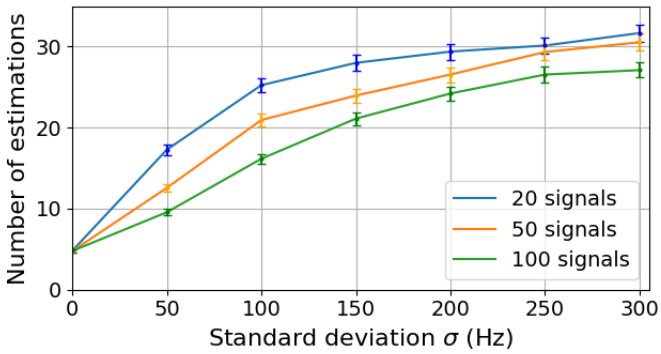

(a) Error less than 50 km.

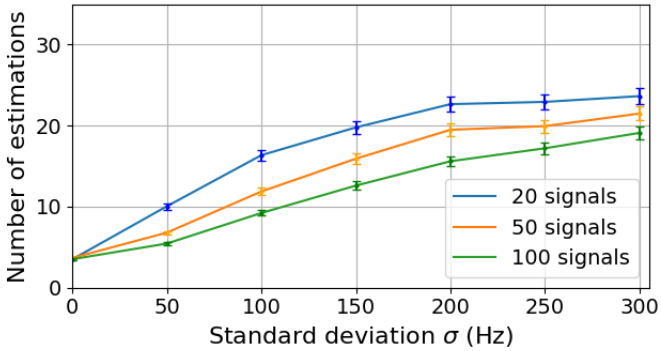

(b) Error less than 75 km.

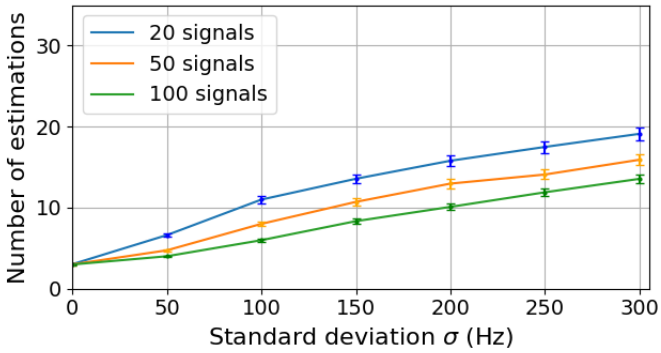

(c) Error less than 100 km.

Figure 3.8: Number of estimations.

impossible in practice, it allows a quick rendering of the estimated locations (in red) with respect to the actual position of the UE (in blue). The inclination angle of the orbit is 85°, and a satellite goes from North to South in the pictured trajectory. The UE wakes up exactly at a specific instant of time, and it is able to uniformly capture 50 NPSS signals (broadcast by that satellite) over a period of 1 second. In this case, the standard deviation of the simulated error distribution on the measured Doppler-

shifted frequency is set to 50 Hz. Based on such measurements, it is possible to estimate both the maximum elevation angle θ^* of the satellite trajectory and the time t_0 when the first NPSS was received. The estimated value t_0 is used by the UE together with SIB information to compute the coordinates of the satellite's projection on the Earth when it is the closest to the UE. As it can be seen in Fig. 3.6, the actual position of the satellite is indicated in green, while the computed values (based on measurements affected by random errors) are pictured in orange. They are aligned along the actual trajectory of the satellite, whose parameters are known through the received SIB. It can be noticed that a UE cannot determine on which side of the satellite it is located since there are exactly 2 trajectories with the same orientation within the UE's communication range and the same maximum elevation angle. For this reason, estimation results are grouped around 2 locations, the actual one and the mirrored version, with respect to the satellite track. In that, the measurement errors affecting the estimation of the NPSS Doppler-shifted frequencies translate into an estimation error on θ^* and on t_0, and thus on the estimated satellite position and on the UE possible locations. Interestingly, the UE location estimations are also aligned. Such an alignment can be explained by the fact that if t_0 is estimated to be earlier than in reality, the UE will compute the position of the satellite projection when closest to the UE to be further north (in the configured scenario) and θ^* to be higher (compare with Fig. 2.4) so that the final UE positions will be thought to be closer to the trajectory than in reality. Contrariwise, if t_0 is estimated to be later than in reality, the UE will compute the position of the satellite to be further south and θ^* to be smaller so that the final UE positions will be thought to be further from the trajectory than in reality.

Pushing further the analysis on the same virtual environment with the orbital plane rotating synchronously with the Earth, Fig. 3.7 plots the position error when the standard deviation of the measurement error on the Doppler-shifted frequency is varied and for 3 different amounts of measured NPSS frequencies (i.e., 20, 50, and 100) used to estimate the maximum elevation angle and, as a consequence, the position of the UE. Each point on the plot results from the average of 8000 random measurements made by a UE placed at the same location of Fig. 3.6. Clearly, a higher standard deviation for the simulated measurement error translates into a bigger positioning error. As well, using more NPSS measurements narrows down the positioning error.

Being the goal of this subsection to study how the number N_e of estimation runs needed to have the UE position converge to a stable value, Fig. 3.8 plots N_e as a function of the standard deviation of the measurement error. 95% confidence intervals are also shown for the sake of statistical significance. It can be seen that to keep the positioning error lower than 50 km (see Fig. 3.8a) around 32 estimation runs have to be performed if the measurement error is particularly intensive (300 Hz of standard deviation) and the UEs cannot treat more than 20 frequency measurements simultaneously. In this worst case scenario, a UE must wake-up 32 times to finally have a small error on its positioning. As it can be expected, a smaller standard deviation for the measurement error, e.g., 100 Hz, permits the convergence to

a positioning error lower than 50 km after $N_e = 26$ runs. Using more NPSS signals to trigger the estimation process, e.g., 100 signals, significantly reduces the number of estimation runs to values going from 6 in the best scenario without measurement errors to 28 when the measurement error is very intensive. It must be noticed that in the considered simulation scenario with the measurement error being null, the UE still needs a number of estimation runs bigger than 2 to converge to a stable positioning value, because with the algorithm presented in Sec. 3.3.3 the UE does not make any assumption on the value of the measurement error, so the stopping condition is not anticipated by the lack of measurement error. It is worth mentioning that the positioning precision can be traded off in favor of a faster convergence of the algorithm, as shown in Fig. 3.8b and 3.8c, showing the same analysis when the acceptable errors are increased to respectively 75 and 100 km.

Finally, note that these results should be implemented in devices before the first wake-up. Once the number of estimations reaches this value, the device can switch to the *Steady State* phase: a UE will wake up based on the application's requirements rather than waking up every time a satellite passes in its transmission range.

3.4.3 Energy consumption on the long term

This subsection analyzes the energy consumption of the proposed strategy and compares it with the currently mandatory GNSS-helped 3GPP solution. To show the importance of the combination of the 3 phases of the proposed strategy, the comparison will show what would happen if a subset of the 3 phases is implemented. Specifically, the *Network Search* phase implemented alone configures UEs to wake up at fixed intervals to search for NPSS signals. Even after the end of the communication, intermittent wake-ups continue to wait for the next satellite passes. Then, if the *Network Search* phase is followed only by the *Synchronization to LEO satellites*, a UE intermittently wakes up, estimates 2 potential positions, thereby building a list for the next passes and entering sleep mode to wait. In this configuration, a UE must wake up at every satellite's pass. For the sake of energy comparison, a simulation also shows what energy is consumed if the UE does nothing.

Furthermore, the comparison is shown for different satellite constellation scenarios, as plotted in Fig. 3.9 and 3.10. Given that a single 600 km satellite typically passes over a given point on Earth 1-2 times per day, the data transmission frequency is set to once per day to fit all types of constellations. Then, the *Network Search* wake-up interval $\tilde{t}$ is set to 150 seconds (see Sec. 3.3.1, and Sec. 3.4.1). Instead, $\tilde{t}$ is set to 30 seconds when a UE wakes up during the *Synchronization to LEO satellites* phase for a predicted satellite pass (see Sec. 3.3.2.4). In detail, Fig. 3.9a, Fig. 3.9b, and Fig. 3.9c show the results for simulations lasting 7 days and related to the case of the standard deviation for the measurement error being equal to 50 Hz. The number of NPSS signals used for the estimation is 100 and they are uniformly captured in a window long 1 second. The maximum tolerated positioning error is fixed at 75 km. By using Fig. 3.8b, the configured N_e value

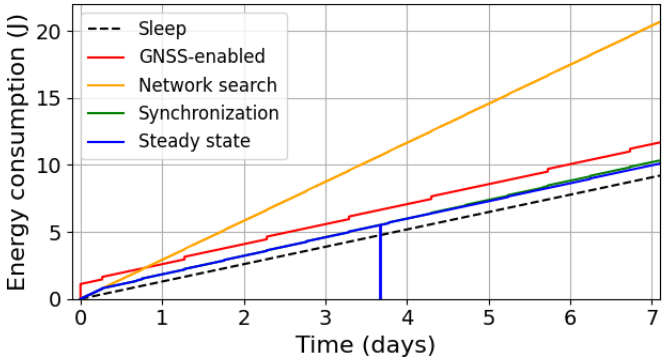

(a) $\sigma = 50$, 100 signals
Single satellite.

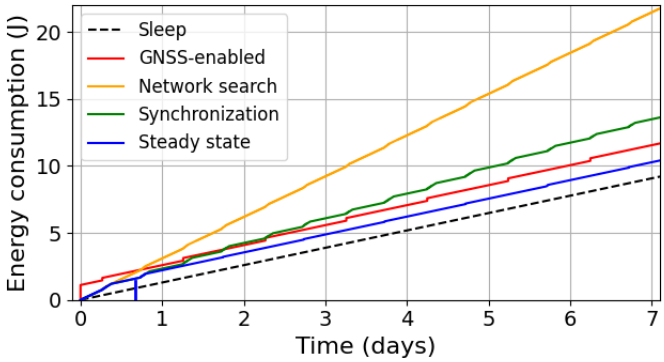

(b) $\sigma = 50$, 100 signals
Single orbit with 4 satellites.

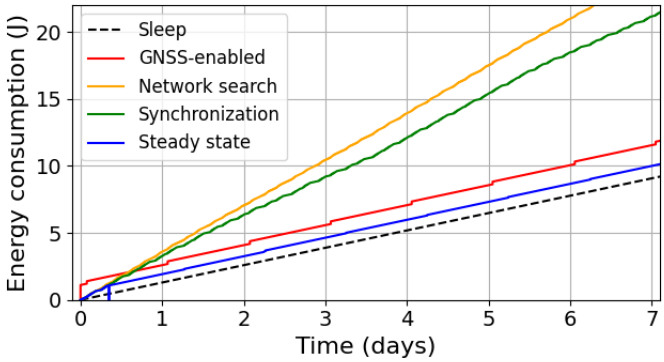

(c) $\sigma = 50$, 100 signals
Walker constellation: 12/3/1.

Figure 3.9: Energy consumption with $\sigma = 50$

is 7. Instead, Fig. 3.10a, Fig. 3.10b, and Fig. 3.10c show the worst-case scenario related to the standard deviation of the measurement error being equal to 300 Hz and the possibility to capture only 20 signals to estimate the position. As shown in Fig. 3.8a, a UE must perform $N_e = 32$ estimation run to determine its position

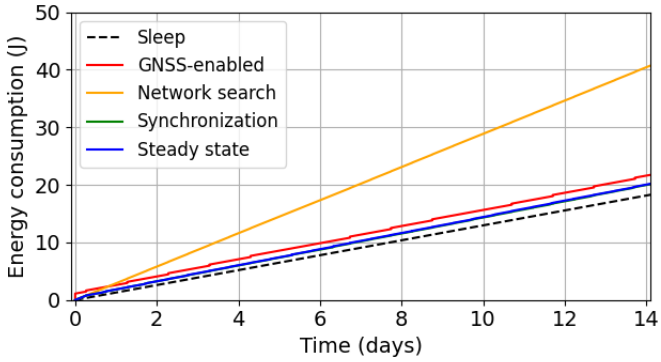

(a) $\sigma = 300$, 20 signals
Single satellite.

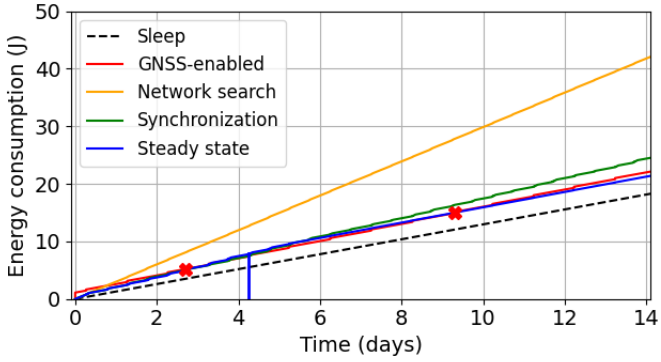

(b) $\sigma = 300$, 20 signals
Single orbit with 4 satellites.

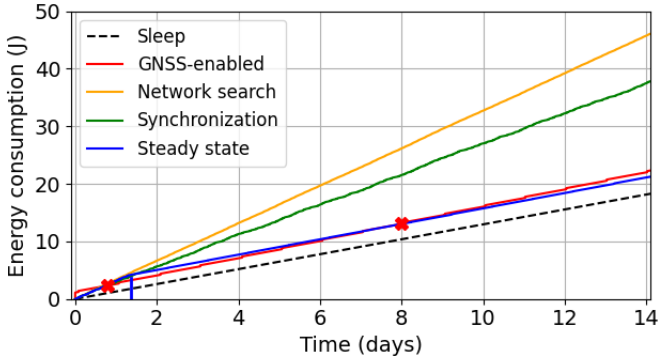

(c) $\sigma = 300$, 20 signals
Walker constellation: 12/3/1.

Figure 3.10: Energy consumption with $\sigma = 300$

with a maximum tolerated error of 50 km. In these cases, the simulations represent the energy consumption in the first 14 days.

First of all, Fig. 3.9a refers to the single satellite scenario and it clearly shows that if a UE only employs *Network Search* phase, its energy consumption is sig-

nificantly higher than any other solution. This is mainly due to the continuous wake-up strategy aimed at constantly searching NPSS signals. However, all the other GNSS-free solutions are more energy efficient than the GNSS-based ones. This is attributed to the reasons previously explained in Sec. 3.2.3: the GNSS cold start process demands the highest energy consumption before starting the very first communication. Note that in the single satellite scenario, the algorithm presented in Sec. 3.3.3 to stop the position estimation process does not improve the energy-saving strategy already enforced by the *Synchronization to LEO satellites* phase. Interestingly, the energy consumption behavior changes when more satellites are coordinated in a LEO constellation, as shown in Fig. 3.9b (single orbit scenario) and Fig. 3.9c (Walker constellation). It can be clearly seen that the energy consumption of UEs not implementing the stopping condition for getting into the *Steady State* phase exceeds that of the GNSS-based solution. This is due to the device needing to wake up at all satellite passes in order to continuously update the list of next passes. As the number of satellites increases, the frequency of satellite passes can reach dozens of times per day, thus implying considerable energy waste. Additionally, since each position estimation results in 2 potential locations, the device also wastes energy waking up when no satellite is passing. In any case, the GNSS-free wake-up strategy presented so far definitely outperforms the GNSS-based solution in terms of energy efficiency. It is worth pointing out that as the number of satellites increases, UEs can enter the *Steady State* phase more quickly since the number of needed passes to narrow down the estimation error will be reached sooner in a denser constellation.

When considering the worst-case scenario (highest standard deviation for the measurement error, smallest required positioning error, smallest number of NPSS signals used for estimation), the energy consumption in the single satellite scenario of Fig. 3.10a does not significantly differ from the corresponding scenario of Fig. 3.9a: as the satellite only passes 1-2 times per day over a given spot, there is no significant change in the energy consumption. However, in the case of one single orbit and the Walker constellation (Fig. 3.10b and 3.10c), due to an increased number N_e of estimation runs, the energy consumption is higher in the short term. As it may be noticed in Fig. 3.10b, the red cross indicates the point at which the energy consumption of both solutions becomes equal. The GNSS-based solution becomes more energy efficient than the complete GNSS-free wake-up strategy proposed within this chapter after 2.5 (first red cross) days. However, after 9.5 (second red cross) days of activity, the GNSS-free solution becomes again and stays even more energy-efficient than the GNSS-based one. This is also visible for the Walker constellation of Fig. 3.10c: on the short term (in the first half day) and on the long term (after 8 days) the GNSS-free solution is the most power efficient.

The final comparison of Fig. 3.11 refers to the employment of a Walker constellation composed by 16 satellites allowing different data transmission frequencies up to 6 per day. The comparison is done between the complete GNSS-free wake-up strategy introduced in this chapter (in red) and the GNSS-based solution (in blue). From Fig. 3.11, it is clear that as the number of data transmissions per day

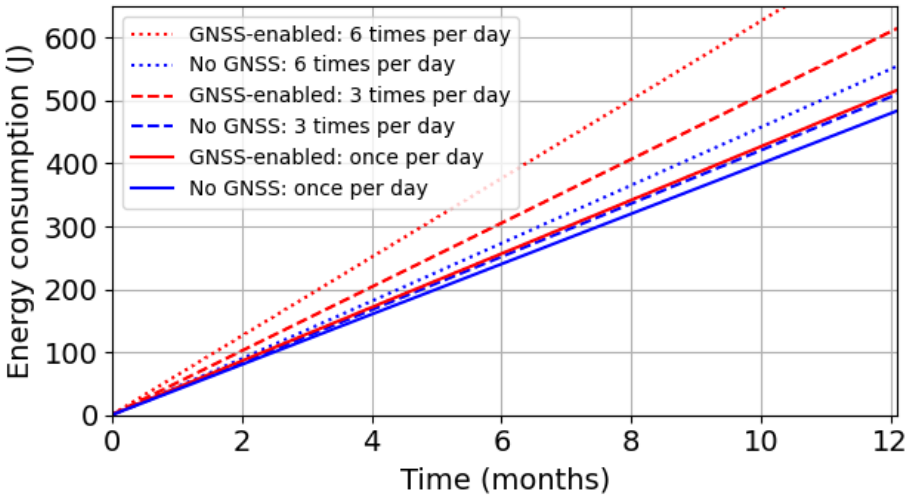

Figure 3.11: Comparison of energy consumption during one year.

increases, the difference in energy consumption becomes increasingly significant in favor of the GNSS-free solution introduced so far.

3.5 Concluding remarks

In this chapter, a GNSS-free wake-up strategy for NB-IoT involving LEO constellation of any size has been proposed and compared against the mandated GNSS-based 3GPP solution. Focusing on discontinuous coverage of LEO satellite constellations, this strategy allows NB-IoT UE to estimate their own position and predict future satellite passes, all without GNSS capabilities based on the method in Chapter 2. Further, the implicit advantage of making DtS NB-IoT architecture non-dependent on GNSS and increasing the network resiliency, with the help of simulation-based analysis, has verified that the introduced strategy can effectively reduce energy consumption due to network synchronization issues. In addition, this strategy does not require any hardware update to the network devices, yet it just requires a firmware update on ground UEs. This makes it an ideal option for applications that do not require precise positioning. The chapter uses the Walker constellation as an example. Still, this strategy can be extended to other constellations to address a broader range of scenarios by adding additional information in SIB.

The first two chapters focused on downlink synchronization signals and the reception of system information, where devices operate independently without directly affecting each other. However, as NB-IoT continues to be integrated with LEO satellite networks, the random access procedure becomes increasingly problematic, particularly in scenarios with a high density of devices. Addressing this issue is critical for ensuring efficient and reliable communication in such environments, which will be the focus of Chapter 4.

Chapter 4

Early detection in random access for DtS NB-IoT

Ce chapitre propose deux méthodes pour améliorer le taux de succès de l'accès aléatoire dans les communications par satellite, en augmentant ainsi le débit global du système. Dans les deux méthodes, les UEs transmettent le Msg1 sans précompensation de retard. En utilisant la position précise du satellite et une estimation approximative de leur propre position (sans recourir au GNSS), les UEs peuvent déterminer leur région dans la couverture satellite grâce à la valeur de Timing Advance renvoyée par le satellite. La Méthode CFM ne nécessite aucune modification de la modulation de Msg1 ni du récepteur au niveau de la couche physique ; le satellite renvoie simplement la valeur TA du premier Msg1 reçu. La Méthode NFM, en revanche, demande un équipement plus complexe pour permettre au satellite de recevoir uniquement un Msg1 d'une seule région avant de renvoyer le Msg2. Les résultats de simulations montrent que ces deux méthodes peuvent augmenter efficacement le taux de succès de l'accès aléatoire et améliorer ainsi le débit du système.

Contents

Chapter 2 and 3 addressed the significant challenge of enabling NB-IoT UEs to function effectively with LEO satellites without relying on the GNSS. The strategies developed, including lightweight synchronization through Doppler effect prediction and energy-efficient wake-up techniques, ensure that NB-IoT UEs maintain reliable communication links with LEO satellites even in scenarios where the GNSS is unavailable. These methods focus on only one among the KPIs introduced in Sec. 1.4, i.e., on energy consumption. In fact, the conducted analysis has focused on the behavior of a single UE since the number of UEs does not impact these methods because only downlink system messages and synchronization signals are

used. However, this chapter aims to shift focus from initial synchronization to investigating how the network manages a large number of UEs during the random access procedure. As discussed in Sec. 1.3.2, satellites have a much larger coverage area than traditional terrestrial networks, which means they accommodate a significantly higher number of UEs, thereby increasing the likelihood of congestion during the random access phase. When a UE communicates with an eNB, the first uplink message sent is the random access preamble (Msg1). It is common for numerous UEs to initiate this process simultaneously, leading to contention for limited network resources and to achieve uplink synchronization, which is when collisions occur. As mentioned in Sec. 1.2.2, the UEs do not immediately detect an incurred collision by inspecting the Random Access response (Msg2). Instead, all UEs receiving the response will send Msg3 on the designated resources. Only when they do not receive Msg4 they do realize a collision has occurred and begin sending the next Msg1 after an inevitable time delay. As the number of UEs increases in the non-terrestrial scenario, more collisions are likely to occur during Msg1 and Msg3, leading to higher energy consumption and longer delays, which reduces the overall throughput.

This issue affects satellite communications and terrestrial networks, prompting research into **early detection** methods to address these challenges. The related works in this domain have focused on utilizing various techniques to detect when an eNB receives Msg1 from different UEs on the same subcarrier, allowing it to avoid sending Msg2. These methods can prevent UEs from proceeding to Msg3 by preventing the transmission of Msg2, reducing unnecessary energy consumption. However, the problem with these approaches is that when multiple Msg1 signals are received simultaneously on the same subcarrier, a collision inevitably occurs, making it impossible to identify which UEs are allowed to transmit Msg3. As a result, even though energy costs associated with Msg3 are avoided, the probability of a successful connection remains low, as only a few UEs can ultimately connect to the eNB. This chapter leverages a unique characteristic of satellite communications: the long transmission distance. Two new early detection methods are proposed that prevent the unnecessary transmission of Msg3 and increase the number of successful transmissions, thereby improving overall system throughput. In both methods, UEs transmit Msg1 by computing, pre-compensating the propagation delay, and applying a controlled shift to the initial moment they start transmitting. Such a shift is related to the computed relative position between the UE and the satellite. Since the UEs are aware of the satellite's precise position and have an approximate understanding of their own location (even without relying on GNSS), the satellite's coverage area can be divided into regions of equal area. Based on the Time Advance value returned by the satellite, UEs can determine whether they are within the area corresponding to that TA value and decide whether to proceed with sending Msg3. It is important to note that in this context, the TA is used with a different behavior compared to the standard one specified by 3GPP. Traditionally, in 3GPP standards, the UE adjusts the timing of transmissions based on the TA value to achieve uplink synchronization between the UE and the eNB. However, in this chapter, the TA

is also used to estimate the UE's location relative to the satellite and determine whether to send Msg3.

The first method, called **Closest First Method (CFM)**, requires no changes from the satellite's (eNB) perspective, as it only needs to return the TA value of the earliest received Msg1 as the standard. In contrast, the second method, called **Non-collided First Method (NFM)**, requires modifications to hardware on eNB so that the satellite can detect different Msg1 from different UEs. It enables the satellite to selectively receive only one Msg1 from a single area before returning Msg2. The choice to present both methods is justified because each serves a different purpose: CFM can be easily implemented on all legacy platforms without requiring significant changes, making it a practical solution for immediate deployment. On the other hand, NFM, which offers more advanced capabilities, can be considered a feature for future platforms where the necessary technological enhancements can support its implementation.

Simulation results demonstrate that both methods effectively increase the random access success rate, thereby improving overall system throughput. In detail, Section 4.1 presents a review of the related works, while Section 4.2 pictures the proposed idea. Then, Section 4.3 presents the results of a simulation-based analysis. Finally, Section 4.4 draws conclusions and envisages future works.

4.1 Related works

The random access procedure is a crucial process in terrestrial and satellite networks that allows UEs to connect with the network. A common challenge in these environments is the high probability of collisions. Several studies have focused on modeling the random access procedure to evaluate the performance. [Sun 2018] models the system throughput of the NB-IoT random access procedure in terrestrial networks, considering factors like retransmission counts and backoff mechanisms using Markov chains. It focuses on the need for UEs to retransmit after Msg1 collisions without considering the collisions in Msg3 and evaluates system throughput in terms of packet generation rate. [Martín 2018] focuses on the ground networks. It proposes a modeling framework to perform the evolution of random access procedures. The model is based on Msg3 and incorporates traffic and radio propagation models using a SINR-based approach in an AWGN channel. As for satellite networks, [Amatetti 2022] models the NB-IoT random access procedure as a multi-channel slotted Aloha system, focusing on collision probabilities and delays under varying satellite parameters. The authors assume that poor channel conditions and collisions cause failure, in which only one UE may succeed while others must retry after a back-off period. [Kodheli 2021] explores the random access procedure across LTE, NB-IoT, and NR technologies, detailing challenges such as RAO mismatches, message scheduling issues, and decoding problems. It proposes solutions like timing advance adjustments using GNSS positioning, timing delay adaptations at the base station, and timer adjustments focusing on power consumption and coverage. A

hardware experiment demonstrated that access time can be reduced to less than 1 second.

As introduced in Sec. 1.2.2, the random access procedure is not only for network access but also relies on the TA value provided in Msg2 to achieve UE uplink synchronization. In the satellite scenario, the greater distance and higher link loss also make estimating the TA value challenging. [Zhu 2024] focuses on TA value estimation in LEO satellite networks within 5G, aiming to achieve accurate uplink synchronization without relying on GNSS. It proposes user-side precompensation using synchronization signals, employing a least-squares method to estimate initial TA, Doppler shift, and frequency offset caused by local oscillators. The study also introduces a cyclic prefix-free preamble format and analyzes inter-preamble interference while neglecting preamble collisions in the analysis. Different from Chapters2 and 3, which address system-level challenges such as synchronization without GNSS and energy-efficient wake-up strategies, this study is more focused on enhancing the physical layer for TA estimation during the random access procedure in 5G. Instead, [Cui 2015] explores Timing Advance Estimation in NTN LTE networks using Symmetric Zadoff-Chu sequences (TAE-SZC) to address the challenges posed by large frequency offsets. This method improves accuracy without requiring additional time or frequency resources.

Finally, studies on early collision detection primarily focus on two approaches: the first requires modifications only on eNB [Xu 2023, Yin 2023], while the second involves modifying the preamble so that the eNB receiver can detect Msg1 from different UEs [Jang 2017, Zhen 2021]. For the first approach, [Xu 2023] proposes an NB-IoT random access scheme without relying on GNSS due to concerns over battery life, positioning performance, and vulnerability to intentional attacks. The method involves designing a receiver-side preprocessing technique featuring a two-stage estimation process based on change point detection and employing an auto-encoder with time-invariant representation (TIRE) for change point detection. And [Yin 2023] explores early preamble collision detection in terrestrial LTE networks using deep learning techniques without altering the existing protocol. Specifically, a Convolutional Neural Network (CNN) is employed on the eNB side to identify collisions based on physical layer features. From a satellite communications perspective, both studies place significant demands on the satellite side, particularly with integrating deep learning techniques. As a result, these approaches may not be suitable for low-cost LEO satellites. [Zhen 2021] introduces an RA preamble design using Single Root Preamble Sequences (SRPS) to enhance early collision detection. The results demonstrate that by detecting collisions early, the eNB can avoid transmitting Msg2, which improves the collision detection performance and boosts preamble detection accuracy.

However, while all existing studies focus on detecting collisions, they do not reduce the probability of collisions. So, this chapter proposes two methods aimed at addressing this issue. CFM does not modify the original random access preamble design or the eNB receiver but instead focuses on early collision detection at the UE side, thereby reducing the probability of collisions. NFM is based on [Zhen 2021] by

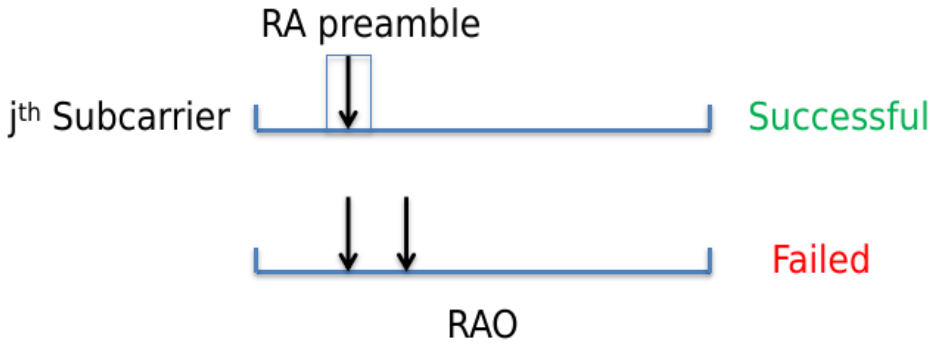

Figure 4.1: Collisions in Standard RA procedure

modifying the preamble and the eNB receiver, enabling the eNB to detect different preambles from different UEs. This further reduces the likelihood of collisions and enhances the success rate of the random access procedure compared to CFM.

4.2 Proposed approach

To address the limitations of current collision detection methods, this section first models the standard random access procedure before introducing two novel approaches to reduce collision probability and improve access success rates. As introduced in Sec. 1.2.2, all UEs choosing the same subcarrier receive a common Msg2 containing the TA value, after which they transmit Msg3. Depending on the signal quality, only one or none of these Msg3 can be successfully received by the eNB. For simplicity, this chapter assumes that if multiple Msg3 messages are sent on the same resource, none of them can be successfully received, as shown in Fig. 4.1.

Based on the Slotted ALOHA formula introduced by [Roberts 1975], the probability of successful transmission in a Slotted ALOHA system is given by

$$S(G) = Ge^{-G}, \tag{4.1}$$

where G represents the average number of transmission attempts per time slot. In the context of the random access procedure of NB-IoT, this success probability can only be applied to individual subcarriers within one Random Access Opportunity (RAO). Herein, by indicating with Γ the average number of transmission attempts within an RAO on any of the m available subcarriers, it turns out that the average number of attempts within an RAO on a specific subcarrier is $G = \Gamma/m$. Additionally, let μ denotes the density of UEs within the coverage area, expressed as the number of UEs per unit area. The coverage area itself is represented by A. The packet generation rate, which indicates how frequently each UE generates packets, is denoted by ρ. Finally, T_{RAO} represents the duration of the RAO period. Taking all these factors into account, Γ can be expressed as:

$$\Gamma = \mu A \cdot \rho T_{RAO}. \tag{4.2}$$

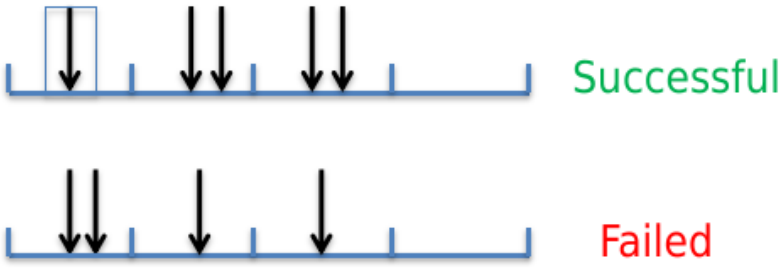

Figure 4.2: Collisions in Closest First Method

However, these parameters are not explicitly considered in subsequent analysis, so the focus remains on the average number of attempts Γ.

Therefore, the probability that exactly one UE's RA attempt is successfully received on a given subcarrier P_{s_0} is thus

$$P_{s_0} = \frac{\Gamma}{m} \cdot e^{-\frac{\Gamma}{m}}. \tag{4.3}$$

This formula represents the throughput on each subcarrier, reflecting the probability of successfully transmitting the preamble when exactly one UE uses that subcarrier. To determine the number of successful random access preambles across all subcarriers, this probability is multiplied by the total number of subcarriers m, so the average number of successful attempts N_{s_0} in standard random access procedure is

$$N_{s_0} = \Gamma \cdot e^{-\frac{\Gamma}{m}}. \tag{4.4}$$

4.2.1 Closest First Method

Building on this foundational understanding of the random access procedure, CFM introduces an approach to reduce collision probabilities by enabling early collision detection at the UE side without changing the random access preamble waveform. The core idea of this method is to utilize the TA value returned in Msg2 to allow UEs to determine whether their Msg1 was successfully received by the satellite. By dividing the satellite's coverage area into regions, each corresponding to a specific TA value, UEs can assess whether their location matches the region from which the successfully received Msg1 originated. If there is a match, the UE proceeds to send Msg3. Otherwise, it detects a potential collision early and does not continue with the transmission. This method includes quantifying the TA to map UEs to specific regions within the satellite's coverage area, ensuring that only UEs within the correct region proceed to the next step in the random access procedure. As shown in Fig. 4.2, assuming that the coverage area is divided into four areas, resulting in 4 time slots for each RAO. Since the eNB cannot distinguish between multipath signals (as discussed in Sec. 1.2.2), it always returns the TA value of the first arriving preamble. Transmission is considered successful if the time slot of the first

arriving preamble is free of other preambles. However, if another UE's preamble is also within the same time slot, both UEs will believe they were successful and send Msg3, leading to a collision.

According to [3GPP 2023], the maximum TA value allowed is 0.8 ms. At the same time, the delay range for a 600 km LEO satellite with a minimum elevation angle of 30° spans from 3 ms to 4.5 ms, a simple removal of delay pre-compensation is insufficient. Instead, the pre-compensated delay $\hat{T}$ must be scaled into the allowable TA range, which can be achieved using the following formula:

$$\hat{T} = \frac{\hat{T}_{\max}}{D_{\max} - D_{\min}} \cdot (\hat{D} - D_{\min}), \tag{4.5}$$

where $\hat{D}$ represents the actual estimated delay that can be calculated using the approach in Chapter. 2, $D_{\min}$ and $D_{\max}$ denote the minimum and maximum delays (3 ms and 4.5 ms, respectively), and $\hat{T}_{\max}$ is the maximum allowed TA value (0.8 ms).

Now, the probability of successful random access can be calculated. Based on (4.1), the parameter G represents the average number of transmission attempts per time slot, and the subcarrier can be defined as $G = \frac{\Gamma}{mn_s}$, where n_s is the number of time slots in each subcarrier per RAO. So the probability of one single preamble transmitted in any time slot of any subcarrier P_1 is given by:

$$P_1 = \frac{\Gamma}{mn_s} \cdot e^{-\frac{\Gamma}{mn_s}}. \tag{4.6}$$

And the probability of no preamble transmitted in any time slot of any subcarrier P_0 is given by:

$$P_0 = e^{-\frac{\Gamma}{mn_s}}. \tag{4.7}$$

Therefore, the probability of successful random access in any subcarrier for CFM, P_C, is given by:

$$P_C = \sum_{i=1}^{n_s} P_0^{i-1} P_1. \tag{4.8}$$

Similarly, by multiplying P_C by the total number of subcarriers m, the expected number of successful random access attempts:

$$N_C = \frac{\Gamma}{n_s} \sum_{i=1}^{n_s} e^{-\frac{i\Gamma}{mn_s}}. \tag{4.9}$$

4.2.2 Non-collided First Method

As introduced in Sec. 4.1, various studies have proposed techniques enabling the eNB to distinguish between preambles from different UEs. Building upon these advancements, this chapter introduces NFM, which imposes higher complexity requirements on the UEs further to enhance the success of the random access procedure. From the UE's perspective, there is no difference between the two methods.

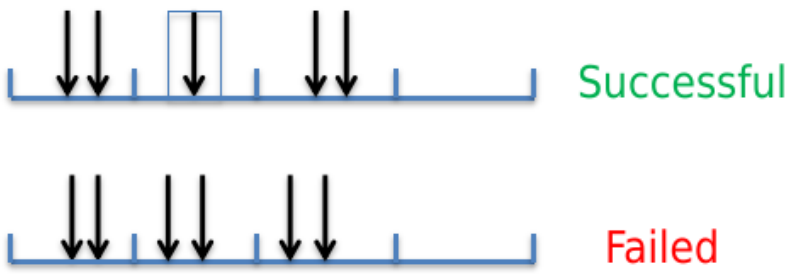

Figure 4.3: Collisions in Non-collided First Method

After adjusting the delay pre-compensation using (4.5), the UE determines whether to send Msg3 based on the TA value received in Msg2. However, from the satellite's perspective, since it can distinguish between different preambles, as shown in Fig 4.3, the satellite can select a time slot that contains only a single preamble and return the corresponding TA value. This ensures that no competitors exist when the UE sends Msg3, effectively preventing collisions. Therefore, if there is at least one time slot within a subcarrier that contains only one single preamble, the random access can be considered successful. The probability of success for NFM, denoted as P_N, is given by:

$$P_N = 1 - (1 - P_1)^{n_s}. \tag{4.10}$$

Similarly, the expected number of successful random access attempts:

$$N_N = m \left[1 - \left(1 - \frac{\Gamma}{mn_s} \cdot e^{-\frac{\Gamma}{mn_s}} \right)^{n_s} \right]. \tag{4.11}$$

However, in practical scenarios, as discussed in Chapter 3, the UE's estimation of its position may have significant errors when GNSS is not used. Therefore, these two methods require further simulation and validation to assess their effectiveness, which will be discussed in the next section.

4.3 Simulation Results

In this section, the effectiveness of the proposed methods is assessed through simulations that consider potential inaccuracies in UE position estimation. In the simulations of this chapter, each RAO includes 48 subcarriers, and for simplicity, all UEs within the coverage area transmit their preamble in the same RAO. The satellite is positioned at an altitude of 600 km, resulting in a coverage radius of approximately 850 km. The UEs are randomly distributed within the satellite's coverage area. As shown in Fig. 4.4, which is an example of 500 UEs, the satellite's coverage area is divided into 4 regions of equal area, each corresponding to one of the 4 time slots of a single subcarrier. In the figure, UEs in different areas are distinguished by different colors.

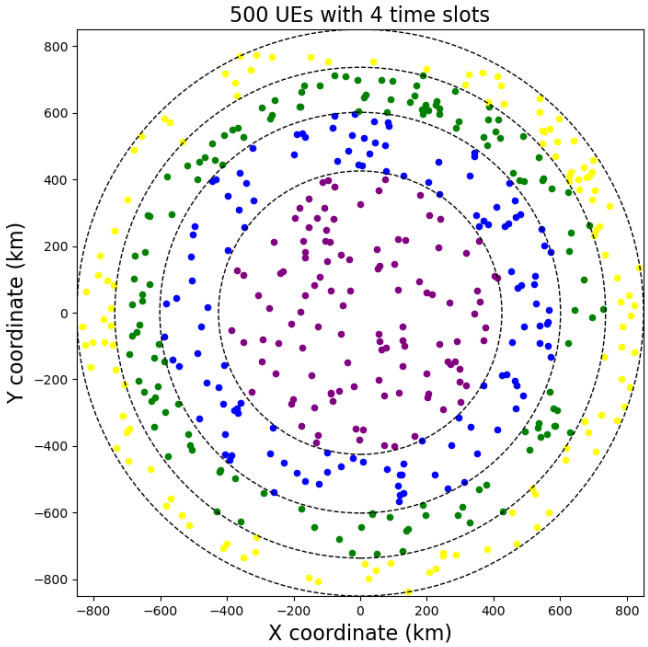

Figure 4.4: Random UEs distributed in different areas

Next, the accuracy of the mathematical models proposed in Sec. 4.2 is validated, as shown in Fig. 4.5a and 4.5b. The figures illustrate the comparison between theoretical and simulation results for different random access methods, with 95% confidence intervals. Each data point represents the average outcome from 200 random deployment simulations. The solid lines represent the results obtained from the theoretical formulas discussed in Sec. 4.2, while the dashed lines correspond to the simulation results. The close alignment between the solid and dashed lines indicates that the simulation results closely match the theoretical predictions, demonstrating the accuracy of the mathematical models. The results also demonstrate that CFM and NFM achieve a significantly higher number of successful random access attempts than the standard method. Furthermore, NFM consistently outperforms CFM, particularly as the number of time slots increases, as shown in Fig. 4.5b.

However, as said in 4.2, errors may occur when the UE estimates its position. This can lead to situations where only one UE initially sends a preamble in a given time slot. Still, due to its position estimation, the UE believes it is in a different area, causing it to miss sending Msg3. Alternatively, a UE in another area may mistakenly think it is in the same area, leading to multiple UEs sending Msg3 simultaneously, resulting in a collision. Both of these situations will lead to a decrease in the random access success rate. This issue becomes particularly significant when there are more areas, as the smaller area of each area increases the likelihood that a UE will mistakenly believe it is in a different area. Therefore, it is

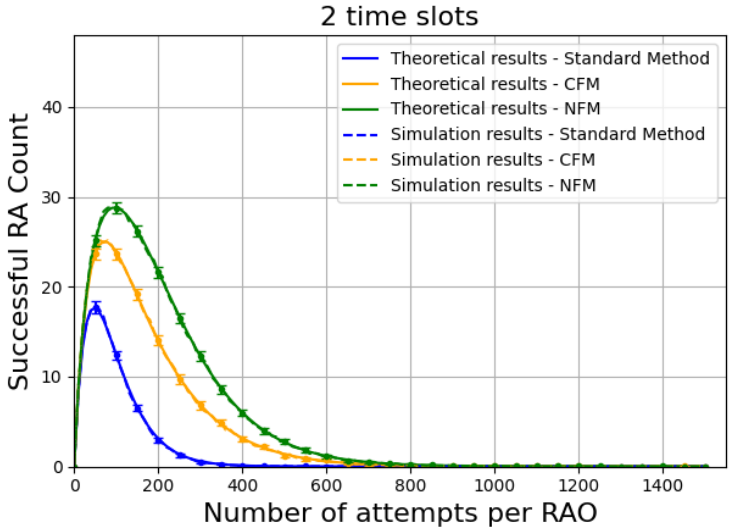

(a) CFM and NFM with 2 time slots.

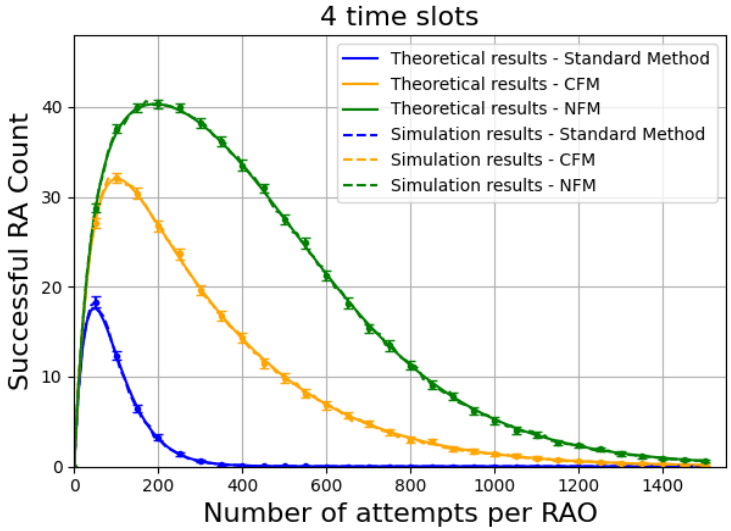

(b) CFM and NFM with 4 time slots.

Figure 4.5: Comparison of simulations with theoretical models.

essential to study the impact of position estimation errors and the number of time slots on the overall results.

Since the position error is minimal and almost negligible when using GNSS, this section's simulations focus on the scenarios discussed in Sec. 3.4.2 (without GNSS), where the position error ranges from 50 to 100 km. Fig. 4.6a and Fig. 4.6b shows the scenario with an average position error of 50 km. It can be observed that for both Closest First Method and NFM, the results show almost no significant difference when there are only 2 time slots. This is because, with only two areas, each with

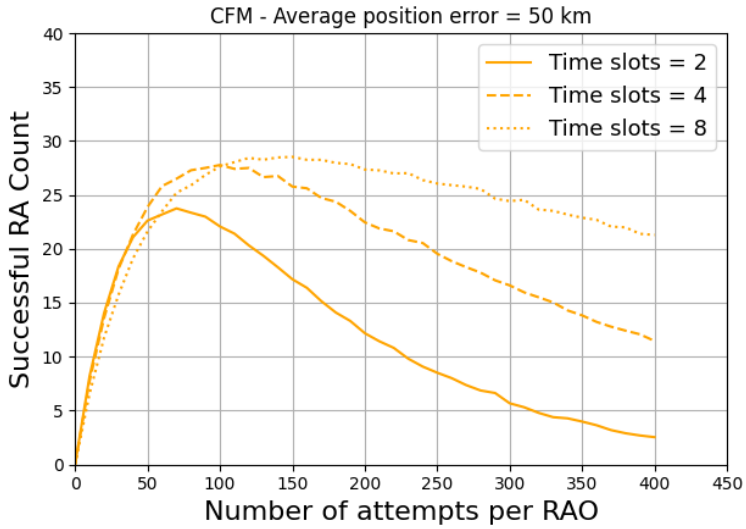

(a) Closest First Method

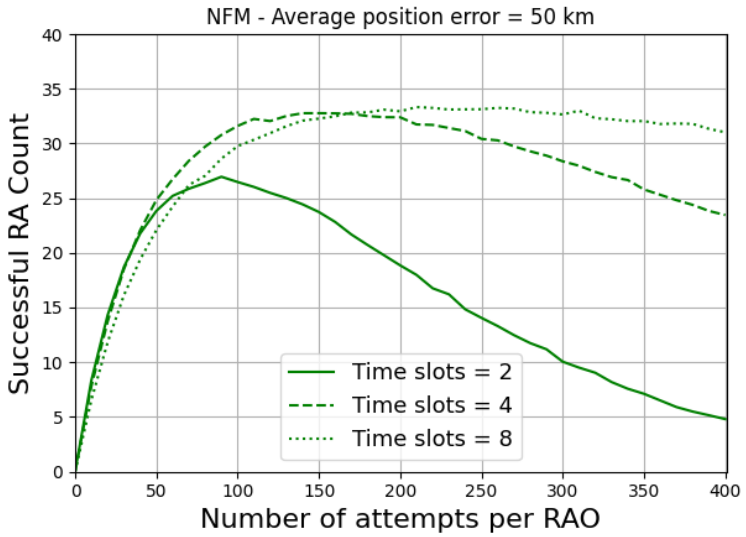

(b) Non-collided First Method

Figure 4.6: Simulation results of CFM and NFM with 50 km of average position estimation error.

a radius of nearly 400 km, the probability of a UE incorrectly identifying its area is very low. As the number of time slots increases, the impact of the position error becomes more significant. Despite this increase, the success rate with 8 time slots is still higher than with 4 or 2 time slots. However, as shown in Fig. 4.7a and Fig. 4.7b, when the position error increases to 100 km, the highest success count for 4 time slots surpasses that of 8 time slots.

In cases of more significant errors, fewer time slots may lead to higher success

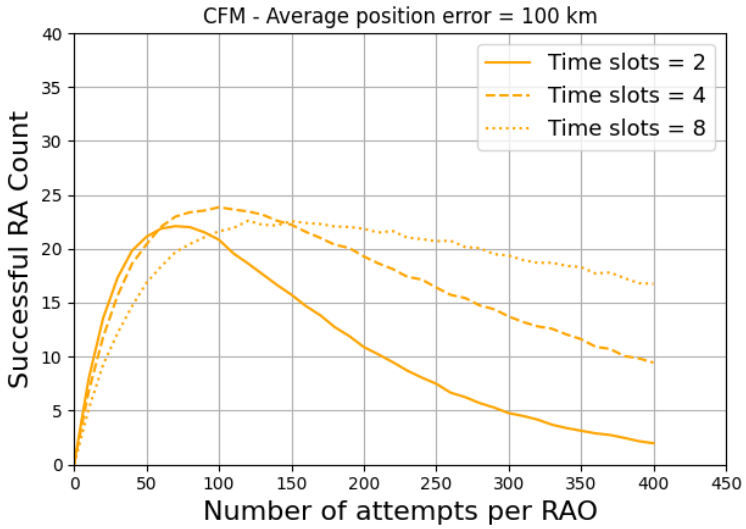

(a) Closest First Method

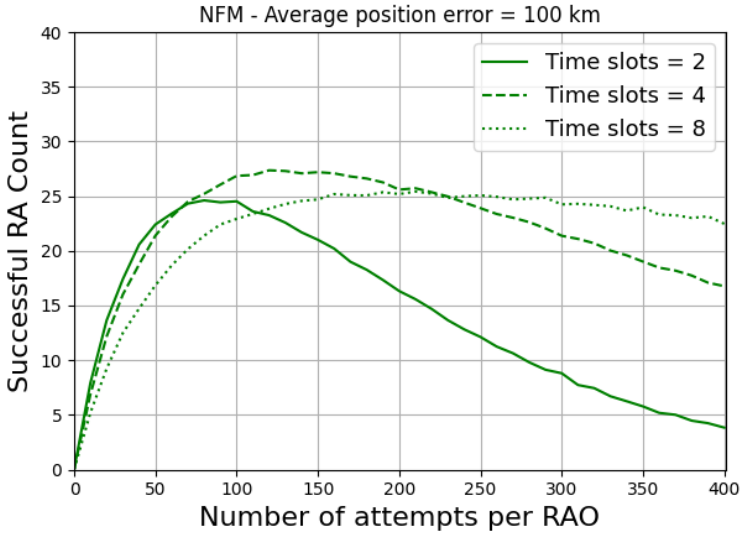

(b) Non-collided First Method

Figure 4.7: Simulation results of CFM and NFM with 100 km of average position estimation error.

rates because the more extensive area reduces the probability of UEs misjudging their area. This indicates that when the position error is significant, the choice of the number of time slots must consider multiple factors, including the average error value, the number of UEs, etc.

4.4 Concluding remarks

This chapter introduced two methods to improve the success rate of random access in NB-IoT satellite communications. The first method reduces collision probabilities through early detection without altering the random access preamble waveform. In contrast, the second method enhances this approach by enabling the satellite to distinguish between different preambles from various UEs. Both methods were validated through simulations that considered errors in UE position estimation. The results showed that while increasing the number of time slots generally improves the success rate, the benefits diminish when position errors are significant. In such cases, fewer time slots can sometimes result in higher success rates, reducing the likelihood of UEs incorrectly identifying their regions.

Chapter 5

Conclusion

Ce manuscrit a fourni une analyse comparative des protocoles NB-IoT et LoRaWAN, proposant un modèle mathématique basé sur quatre indicateurs clés de performance: fiabilité, latence, débit et efficacité énergétique. Une méthode innovante pour prédire et compenser l'effet Doppler sans GNSS a été développée, utilisant les signaux de synchronisation descendante NB-IoT. Une stratégie de réveil intermittent pour les UEs sans GNSS a été proposée, permettant des communications NB-IoT avec des constellations clairsemées de satellites LEO, réduisant ainsi la consommation d'énergie tout en maintenant une communication fiable. Une méthode utilisant le timing advance pour la détection précoce des collisions a été proposée, améliorant le débit du réseau. Les travaux futurs devraient se concentrer sur la mise en œuvre pratique des méthodes proposées pour valider les modèles théoriques et les résultats de simulation. Une évaluation détaillée de la latence et de la fiabilité est cruciale, avec des tests approfondis pour optimiser les communications NB-IoT avec les satellites LEO. Enfin, l'optimisation des stratégies d'allocation des ressources, l'interopérabilité entre NB-IoT et autres technologies IoT, et le renforcement de la sécurité des communications IoT basées sur les satellites sont également essentiels. En abordant ces domaines, les recherches futures pourront s'appuyer sur les bases établies dans ce manuscrit, menant à des solutions plus avancées pour l'intégration du NB-IoT avec les satellites LEO et contribuant au développement de réseaux IoT fiables, efficaces et évolutifs.

Contents

5.1 Contributions

This thesis comprehensively explores integrating NB-IoT with LEO satellites, addressing the unique challenges and opportunities this integration presents.

Chapter 1 offers a comparative analysis of NB-IoT and LoRaWAN and proposes a mathematical model framework based on four KPIs: **Reliability**, **Latency**, **Throughput**, and **Energy efficiency**. This framework sets the stage for evaluating and optimizing the performance of IoT communications via satellite.

Chapter 2 focuses on the challenge of downlink synchronization. Due to the high-speed motion of LEO satellites, the Doppler effect significantly impacts communications, leading to frequency offsets. This chapter introduces an innovative approach that utilizes downlink synchronization signals to estimate the Doppler curve, achieving downlink synchronization without relying on GNSS capabilities. This method not only addresses the synchronization issue but also reduces energy consumption and costs associated with GNSS receivers.

Chapter 3 presents a novel wake-up strategy designed to enhance **Energy efficiency** of synchronization procedure, one of the critical KPIs. In scenarios with sparse LEO satellite constellations, GNSS-free UEs employ an intermittent wake-up strategy to search for downlink signals from the satellite. This strategy allows UEs to establish effective communication even with intermittent satellite coverage. Simulation results validate the strategy's feasibility and demonstrate significant reductions in energy consumption compared to traditional GNSS-based methods while still maintaining reliable communication.

In satellite communication scenarios, the significantly higher number of connected devices increases the probability of random access failures due to collisions. To resolve this, Chapter 4 introduces and validates two innovative methods designed to enhance the success rate of random access by dividing the coverage area into different regions. This allows the UE to determine from Msg2 whether it is in the correct region, enabling collision-free transmissions, thereby increasing the system's **Throughput**.

5.2 Lessons learned

Several key lessons were learned in integrating NB-IoT with LEO satellite networks throughout this research. One significant lesson was the importance of using simulation experiments to model and validate scenarios with many devices, which was essential for verifying the accuracy of mathematical models. Accurate synchronization without GNSS emerged as crucial for reducing energy consumption and system costs, emphasizing the need for robust synchronization strategies in satellite IoT networks. Energy efficiency proved a critical KPI, with GNSS-free wake-up strategies demonstrating substantial energy savings, particularly in scenarios with intermittent satellite coverage. As device density increases, the random access procedure becomes a significant bottleneck, highlighting the need for advanced collision detection methods to maintain network reliability. Furthermore, aligning the research with 3GPP standards ensures that the proposed solutions are practical and ready for real-world implementation, contributing to satellite IoT systems' overall resilience and sustainability.

5.3 Potential future works

This thesis has laid the foundation for integrating NB-IoT with LEO satellites by addressing critical challenges and proposing innovative solutions. However, there are several areas where further research and development can optimize these initial findings and lead to more efficient systems.

5.3.1 Hardware implementation

Future work should focus on the practical implementation of the proposed methods on actual hardware, particularly those introduced in Chapter 2, 3, and 4. In Chapter 2, it is essential to validate the feasibility of the proposed synchronization method, assess whether estimating the Doppler curve increases device complexity, and determine how effectively NPSS signal monitoring performs in real-world environments. Chapter 3's GNSS-free wake-up strategy requires testing on actual devices to measure energy consumption and validate the simulation results. For Chapter 4, the focus should be on studying how other real-world factors affect device access performance, particularly the impact of environmental variables on random access success. Developing and testing prototypes will be crucial for validating the theoretical models and simulation results presented in this thesis, providing insights into the real-world challenges and performance of NB-IoT devices communicating with LEO satellites and enabling further refinements and optimizations.

5.3.2 Latency and reliability evaluation

While this thesis has addressed key performance indicators such as energy efficiency (Chapter 3) and throughput (Chapter 4), a detailed evaluation of latency and reliability in practical scenarios remains crucial. Potential research topics could include optimizing communication protocols to reduce the number of message exchanges, which would decrease latency directly. Additionally, exploring adaptive protocols that adjust to varying satellite trajectories and orbital parameters could enhance latency and reliability. Moreover, assessing the impact of environmental factors, such as atmospheric conditions and interference, on communication performance will be essential for developing robust NB-IoT solutions for satellite networks.

5.3.3 Resource allocation strategy optimization

Another important area for future work is the optimization of resource allocation strategies. While Chapter 4 focused on increasing the number of devices that can successfully perform random access, the challenge of efficiently allocating resources during the data transmission phase remains. Efficient resource management is essential to handle the high density of devices and the dynamic nature of satellite communications. Research should explore advanced algorithms and techniques for dynamic resource allocation, considering factors such as traffic patterns, device

mobility, and varying network loads. This will help maximize the utilization of available resources and improve overall network performance.

Scientific production

Journal publication

- Zheng Zhou, Nicola Accettura, Pascal Berthou. "*A wake-up strategy enabling GNSS-free NB-IoT links to sparse LEO satellite constellations*," 2024 **(Under reviewing)**

International conference publications

- Zheng Zhou, Nicola Accettura, Raoul Prévost, Pascal Berthou. "*Lightweight synchronization to NB-IoT enabled LEO Satellites through Doppler prediction.*" In The 19th International Conference on Wireless and Mobile Computing, Networking and Communications (IEEE WiMob 2023), Jun 2023, Montreal, Canada.

- Zheng Zhou, Nicola Accettura, Pascal Berthou. "*Early detection in random access for Direct-to-Satellite NB-IoT*," 2024 **(Under preparation)**.

Book chapter

- Zheng Zhou, Mohammad Afhamisis, Maria Rita Palattella, Nicola Accettura, Pascal Berthou. "*Pervasive LPWAN connectivity through LEO Satellites: trading off reliability, throughput, latency, and energy efficiency.*" In *Low-Power Wide-Area Networks: Opportunities, Challenges, Risks and Threats*, eds. Ismail Butun and Ian F. Akyildiz, Springer, ISBN: 978-3-031-32934-0.

Bibliography

[3GPP 2015] 3GPP. *3GPP Specifications, Available online: https://3gpp.org/*, 2015. (Cited in pages 1, 12, and 13.)

[3GPP 2018] 3GPP. *3GPP Release 17th*, 2018. (Cited in pages 23 and 36.)

[3GPP 2021] 3GPP. *TR 36.763, Study on Narrow-Band Internet of Things (NB-IoT) / enhanced Machine Type Communication (eMTC) support for Non-Terrestrial Networks (NTN) (Release 17, V17.0.0)*. Technical Report, 3GPP, June 2021. (Cited in pages 49, 51, 52, 53, 54, and 65.)

[3GPP 2023] 3GPP. *TS 36.331, Evolved Universal Terrestrial Radio Access (E-UTRA); Radio Resource Control (RRC); Protocol specification (Release 17, V17.5.0)*. Technical Report, 3GPP, June 2023. (Cited in pages 52, 60, and 85.)

[Afhamisis 2022a] Afhamisis, M., Barillaro, S. and Palattella, M. *A Testbed for LoRaWAN Satellite Backhaul: Design Principles and Validation*. In ICC 2021 - IEEE International Conference on Communications. IEEE, MAY 2022. (Cited in pages 25 and 28.)

[Afhamisis 2022b] Afhamisis, M. and Palattella, M. R. *SALSA: A Scheduling Algorithm for LoRa to LEO Satellites*. IEEE Access, vol. 10, pages 11608–11615, 2022. (Cited in page 24.)

[Al-Fuqaha 2015a] Al-Fuqaha, A., Guizani, M., Mohammadi, M. S., Aledhari, M. and Ayyash, M. *Internet of Things: A Survey on Enabling Technologies, Protocols, and Applications*. IEEE Communications Surveys & Tutorials, vol. 17, pages 2347–2376, 2015. (Cited in page 8.)

[Al-Fuqaha 2015b] Al-Fuqaha, A., Guizani, M., Mohammadi, M., Aledhari, M. and Ayyash, M. *Internet of Things: A Survey on Enabling Technologies, Protocols, and Applications*. IEEE Communications Surveys & Tutorials, vol. 17, no. 4, pages 2347–2376, 2015. (Cited in page 1.)

[Ali 1998] Ali, I., Al-Dhahir, N. and Hershey, J. E. *Doppler characterization for LEO satellites*. IEEE Trans. Commun., vol. 46, 1998. (Cited in pages 38, 39, 40, and 50.)

[Amatetti 2022] Amatetti, C., Conti, M., Guidotti, A. and Vanelli-Coralli, A. *NB-IoT random access procedure via NTN: system level performances*. In ICC 2022 - IEEE International Conference on Communications, pages 2381–2386, 2022. (Cited in page 81.)

[An 2020] An, C. and Ryu, H.-G. *Compensation Systems and Performance Comparison of the Very High Doppler Frequency.* In IEEE ComNet, 2020. (Cited in page 38.)

[Andres-Maldonado 2019] Andres-Maldonado, P., Lauridsen, M., Ameigeiras, P. and Lopez-Soler, J. M. *Analytical Modeling and Experimental Validation of NB-IoT Device Energy Consumption.* IEEE Internet of Things Journal, vol. 6, no. 3, pages 5691–5701, 2019. (Cited in pages 26, 28, 29, and 51.)

[Asaad 2021] Asaad, S. M. and Maghdid, H. S. *A Comprehensive Review of Indoor/Outdoor Localization Solutions in IoT era: Research Challenges and Future Perspectives.* Comput. Networks, vol. 212, page 109041, 2021. (Cited in page 8.)

[Ashton 2009] Ashton, K.*et al. That 'internet of things' thing.* RFID journal, vol. 22, no. 7, pages 97–114, 2009. (Cited in page 8.)

[Atzori 2010] Atzori, L., Iera, A. and Morabito, G. *The Internet of Things: A survey.* Computer Networks, vol. 54, no. 15, pages 2787–2805, 2010. (Cited in page 8.)

[Azari 2020] Azari, A., Stefanović, v., Popovski, P. and Cavdar, C. *On the Latency-Energy Performance of NB-IoT Systems in Providing Wide-Area IoT Connectivity.* IEEE Transactions on Green Communications and Networking, vol. 4, no. 1, pages 57–68, 2020. (Cited in pages 26 and 28.)

[Bankov 2019] Bankov, D., Khorov, E. and Lyakhov, A. *LoRaWAN Modeling and MCS Allocation to Satisfy Heterogeneous QoS Requirements.* Sensors, vol. 19, no. 19, 2019. (Cited in pages 24, 26, 27, 28, and 29.)

[Barbau 2021a] Barbau, R., Deslandes, V., Jakllari, G. and Beylot, A. *An Analytical Model for Evaluating the Interplay Between Capacity and Energy Efficiency in NB-IoT.* In 2021 International Conference on Computer Communications and Networks (ICCCN), pages 1–9, 2021. (Cited in pages 26 and 29.)

[Barbau 2021b] Barbau, R., Deslandes, V., Jakllari, G., Tronc, J. and Beylot, A. *An Analytical Model for Assessing the Performance of NB-IoT.* In ICC 2021 - IEEE International Conference on Communications, pages 1–6, 2021. (Cited in pages 26 and 27.)

[Beltramelli 2018] Beltramelli, L., Mahmood, A., Gidlund, M., Österberg, P. and Jennehag, U. *Interference Modelling in a Multi-Cell LoRa System.* In 2018 14th International Conference on Wireless and Mobile Computing, Networking and Communications (WiMob), pages 1–8, 2018. (Cited in pages 26, 27, and 28.)

[Ben Temim 2022] Ben Temim, M. A., Ferré, G. and Tajan, R. *A New LoRa-like Transceiver Suited for LEO Satellite Communications*. Sensors, vol. 22, no. 5, 2022. (Cited in page 23.)

[Björnson 2018] Björnson, E. and Larsson, E. G. *How Energy-Efficient Can a Wireless Communication System Become?* In 2018 52nd Asilomar Conference on Signals, Systems, and Computers, pages 1252–1256, 2018. (Cited in page 29.)

[Boquet 2021] Boquet, G., Tuset-Peiró, P., Adelantado, F., Watteyne, T. and Vilajosana, X. *LR-FHSS: Overview and Performance Analysis*. IEEE Communications Magazine, vol. 59, no. 3, pages 30–36, 2021. (Cited in page 23.)

[Borgia 2014] Borgia, E. *The Internet of Things vision: Key features, applications and open issues*. Comput. Commun., vol. 54, pages 1–31, 2014. (Cited in page 8.)

[Capez 2022] Capez, G. M., Henn, S., Fraire, J. A. and Garello, R. *Sparse Satellite Constellation Design for Global and Regional Direct-to-Satellite IoT Services*. IEEE Transactions on Aerospace and Electronic Systems, vol. 58, no. 5, pages 3786–3801, 2022. (Cited in page 48.)

[Centenaro 2021a] Centenaro, M., Costa, C., Granelli, F., Sacchi, C. and Vangelista, L. *A Survey on Technologies, Standards and Open Challenges in Satellite IoT*. IEEE Communications Surveys Tutorials, vol. 23, no. 3, pages 1693–1720, 2021. (Cited in page 22.)

[Centenaro 2021b] Centenaro, M., Costa, C. E., Granelli, F., Sacchi, C. and Vangelista, L. *A Survey on Technologies, Standards and Open Challenges in Satellite IoT*. IEEE Communications Surveys & Tutorials, pages 1693–1720, 2021. (Cited in page 1.)

[Chasserat 2020] Chasserat, L., Accettura, N. and Berthou, P. *Short: Achieving Energy Efficiency in Dense LoRaWANs through TDMA*. In 2020 IEEE 21st International Symposium on "A World of Wireless, Mobile and Multimedia Networks" (WoWMoM), pages 26–29, 2020. (Cited in page 29.)

[Chasserat 2021] Chasserat, L., Accettura, N., Prabhu, B. and Berthou, P. *TREMA: A traffic-aware energy efficient MAC protocol to adapt the LoRaWAN capacity*. In 2021 International Conference on Computer Communications and Networks (ICCCN), pages 1–6, 2021. (Cited in page 29.)

[Choudhary 2020] Choudhary, R. K. *Internet of Things: Wildlife Conservation and its Challenges*. Asian Journal of Computer Science and Technology, 2020. (Cited in page 8.)

[Chougrani 2021] Chougrani, H., Kisseleff, S., Martins, W. A. and Chatzinotas, S. *NB-IoT Random Access for Non-Terrestrial Networks: Preamble Detection*

and Uplink Synchronization. IEEE Internet of Things Journal, pages 1–1, 2021. (Cited in page 24.)

[Chougrani 2022] Chougrani, H., Kisseleff, S., Martins, W. A. and Chatzinotas, S. *NB-IoT Random Access for Nonterrestrial Networks: Preamble Detection and Uplink Synchronization.* IEEE IoT Journal, vol. 9, no. 16, 2022. (Cited in page 37.)

[Conti 2020] Conti, M., Andrenacci, S., Maturo, N., Chatzinotas, S. and Vanelli-Coralli, A. *Doppler Impact Analysis for NB-IoT and Satellite Systems Integration.* In ICC, 2020. (Cited in pages 22 and 23.)

[Crisp 2018] Crisp, N. H., Livadiotti, S. and Roberts, P. C. E. *A Semi-Analytical Method for Calculating Revisit Time for Satellite Constellations with Discontinuous Coverage.* ArXiv, vol. abs/1807.02021, 2018. (Cited in pages 51 and 61.)

[Croce 2018] Croce, D., Gucciardo, M., Mangione, S., Santaromita, G. and Tinnirello, I. *Impact of LoRa Imperfect Orthogonality: Analysis of Link-Level Performance.* IEEE Communications Letters, vol. 22, no. 4, pages 796–799, 2018. (Cited in pages 26 and 27.)

[Cruz 2019] Cruz, R., Coelho, A., Campos, R. and Ricardo, M. *A Theoretical Model for Planning NB-IoT Networks.* In 2019 International Conference on Wireless and Mobile Computing, Networking and Communications (WiMob), pages 1–4, 2019. (Cited in pages 26, 27, and 28.)

[Cui 2015] Cui, G., He, Y., Li, P. and Wang, W. *Enhanced Timing Advanced Estimation With Symmetric Zadoff-Chu Sequences for Satellite Systems.* IEEE Communications Letters, vol. 19, no. 5, pages 747–750, 2015. (Cited in page 82.)

[Doroshkin 2019] Doroshkin, A. A., Zadorozhny, A. M., Kus, O. N., Prokopyev, V. Y. and Prokopyev, Y. M. *Experimental Study of LoRa Modulation Immunity to Doppler Effect in CubeSat Radio Communications.* IEEE Access, vol. 7, pages 75721–75731, 2019. (Cited in page 23.)

[ETSI 2018] ETSI. *System Reference document (SRdoc); Technical characteristics for Low Power Wide Area Networks Chirp Spread Spectrum (LPWAN-CSS) operating in the UHF spectrum below 1 GHz.* Technical Report TR 103 526 V1.1.1, Washington, DC, USA, 2018. (Cited in page 12.)

[Fadilah 2022] Fadilah, N., Arifin, M. A., Qonita, A. H., Najati, N., Pratomo, B., Dwiyanto and Nasser, E. N. *Link and Doppler Analysis for LEO Constellation Space-Based IoT.* In IEEE ICARES, 2022. (Cited in page 39.)

[Fang 2021] Fang, X., Feng, W., Wei, T., Chen, Y., Ge, N. and Wang, C.-X. *5G Embraces Satellites for 6G Ubiquitous IoT: Basic Models for Integrated Satellite*

Terrestrial Networks. IEEE Internet of Things Journal, vol. 8, no. 18, pages 14399–14417, 2021. (Cited in page 19.)

[Fernandez 2020] Fernandez, L., Ruiz-De-Azua, J. A., Calveras, A. and Camps, A. *Assessing LoRa for Satellite-to-Earth Communications Considering the Impact of Ionospheric Scintillation.* IEEE Access, vol. 8, pages 165570–165582, 2020. (Cited in page 23.)

[Fraire 2019] Fraire, J. A., Umaña, S. C. and Accettura, N. *Direct-To-Satellite IoT - A Survey of the State of the Art and Future Research Perspectives - Backhauling the IoT Through LEO Satellites.* In Proc. of AdHoc-Now, 2019. (Cited in pages 1, 19, and 53.)

[Gomez 2021] Gomez, C., Darroudi, S. M., Naranjo, H. and Paradells, J. *On the Energy Performance of Iridium Satellite IoT Technology.* Sensors, vol. 21, no. 21, 2021. (Cited in page 23.)

[Gubbi 2012] Gubbi, J., Buyya, R., Marusic, S. and Palaniswami, M. S. *Internet of Things (IoT): A vision, architectural elements, and future directions.* ArXiv, 2012. (Cited in page 8.)

[Guidotti 2017] Guidotti, A., Vanelli-Coralli, A., Caus, M., Bas, J., Colavolpe, G., Foggi, T., Cioni, S., Modenini, A. and Tarchi, D. *Satellite-enabled LTE systems in LEO constellations.* In 2017 IEEE International Conference on Communications Workshops (ICC Workshops), 2017. (Cited in pages 23 and 24.)

[Guidotti 2019] Guidotti, A., Vanelli-Coralli, A., Conti, M., Andrenacci, S., Chatzinotas, S., Maturo, N., Evans, B., Awoseyila, A., Ugolini, A., Foggi, T., Gaudio, L., Alagha, N. and Cioni, S. *Architectures and Key Technical Challenges for 5G Systems Incorporating Satellites.* IEEE Transactions on Vehicular Technology, vol. 68, no. 3, pages 2624–2639, 2019. (Cited in page 22.)

[Guo 2010] Guo, Y. and Zhang, D. *Research on the Reliability of MAC Protocols for Multi-radio Sensor Networks.* In 2010 First International Conference on Pervasive Computing, Signal Processing and Applications, pages 410–413, 2010. (Cited in page 27.)

[Harwahyu 2021] Harwahyu, R., Cheng, R.-G., Liu, D.-H. and Sari, R. F. *Fair Configuration Scheme for Random Access in NB-IoT with Multiple Coverage Enhancement Levels.* IEEE Transactions on Mobile Computing, vol. 20, no. 4, pages 1408–1419, 2021. (Cited in page 15.)

[Hayes 1988] Hayes, E. *Computation of average revisit time for earth-observing satellites.* In 26th Aerospace Sciences Meeting, 1988. (Cited in page 62.)

[Hoglund 2018] Hoglund, A., Van, D. P., Tirronen, T., Liberg, O., Sui, Y. and Yavuz, E. A. *3GPP Release 15 Early Data Transmission.* IEEE Communications Standards Magazine, vol. 2, no. 2, 2018. (Cited in pages 18, 36, and 46.)

[Huang 2021] Huang, Z. *A Pilot-Aided Method of Doppler Offset Estimation and Compensation.* In ICCCS, 2021. (Cited in page 38.)

[Jafari-Nadoushan 2015] Jafari-Nadoushan, M. and Assadian, N. *Repeat ground track orbit design with desired revisit time and optimal tilt.* Aerospace Science and Technology, vol. 40, pages 200–208, 2015. (Cited in page 51.)

[Jamshed 2022] Jamshed, M. A., Ali, K., Abbasi, Q. H., Imran, M. A. and Ur-Rehman, M. *Challenges, Applications, and Future of Wireless Sensors in Internet of Things: A Review.* IEEE Sensors Journal, vol. 22, pages 5482–5494, 2022. (Cited in page 8.)

[Jang 2017] Jang, H. S., Kim, S. M., Park, H.-S. and Sung, D. K. *An Early Preamble Collision Detection Scheme Based on Tagged Preambles for Cellular M2M Random Access.* IEEE Transactions on Vehicular Technology, vol. 66, no. 7, pages 5974–5984, 2017. (Cited in page 82.)

[Janssen 2023] Janssen, T., Koppert, A., Berkvens, R. and Weyn, M. *A Survey on IoT Positioning Leveraging LPWAN, GNSS, and LEO-PNT.* IEEE Internet of Things Journal, vol. 10, no. 13, pages 11135–11159, 2023. (Cited in page 50.)

[Jin 2022] Jin, S., Wang, Q. and Dardanelli, G. *A Review on Multi-GNSS for Earth Observation and Emerging Applications.* Remote Sensing, vol. 14, pages 1–24, 08 2022. (Cited in page 23.)

[Kanj 2020] Kanj, M., Savaux, V. and Guen, M. L. *A Tutorial on NB-IoT Physical Layer Design.* IEEE Communications Surveys & Tutorials, no. 4, 2020. (Cited in page 15.)

[Knight 2016] Knight, M. and Seeber, B. *Decoding LoRa: Realizing a Modern LPWAN with SDR.* Proceedings of the GNU Radio Conference, vol. 1, no. 1, 2016. (Cited in page 10.)

[Kodheli 2018] Kodheli, O., Andrenacci, S., Maturo, N., Chatzinotas, S. and Zimmer, F. *Resource Allocation Approach for Differential Doppler Reduction in NB-IoT over LEO Satellite.* In ASMS/SPSC, 2018. (Cited in pages 36, 42, and 49.)

[Kodheli 2019] Kodheli, O., Maturo, N., Andrenacci, S., Chatzinotas, S. and Zimmer, F. *Link Budget Analysis for Satellite-Based Narrowband IoT Systems.* In Ad-Hoc, Mobile, and Wireless Networks, pages 259–271. Springer International Publishing, 2019. (Cited in page 23.)

[Kodheli 2021] Kodheli, O., Astro, A., Querol, J., Gholamian, M., Kumar, S., Maturo, N. and Chatzinotas, S. *Random Access Procedure Over Non-Terrestrial Networks: From Theory to Practice*. IEEE Access, vol. 9, pages 109130–109143, 2021. (Cited in page 81.)

[Li 2016] Li, J., Zhang, Y., Zhang, Y., Xiong, W., Huang, Y. and Wang, Z. *Fast tracking Doppler compensation for OFDM-based LEO Satellite data transmission*. In IEEE ICCC, 2016. (Cited in page 38.)

[Li 2018] Li, H., Chen, G., Wang, Y., Gao, Y. and Dong, W. *Accurate Performance Modeling of Uplink Transmission in NB-IoT*. In 2018 IEEE 24th International Conference on Parallel and Distributed Systems (ICPADS), pages 910–917, 2018. (Cited in pages 26, 27, and 28.)

[Liberg 2020] Liberg, O., Löwenmark, S. E., Euler, S., Hofström, B., Khan, T., Lin, X. and Sedin, J. *Narrowband Internet of Things for Non-Terrestrial Networks*. IEEE Communications Standards Magazine, vol. 4, no. 4, 2020. (Cited in page 23.)

[Luo 2017] Luo, X., Wang, M., Dai, G. and Chen, X. *A Novel Technique to Compute the Revisit Time of Satellites and Its Application in Remote Sensing Satellite Optimization Design*. Int. J. of Aerospace Engineering, vol. 2017, pages 1–9, 01 2017. (Cited in page 51.)

[Lv 2021] Lv, Z., Chen, D. and Li, J. *Novel System Design and Implementation for the Smart City Vertical Market*. IEEE Communications Magazine, vol. 59, pages 126–131, 2021. (Cited in page 8.)

[Lygouras 2000] Lygouras, J. *Memory reduction in look-up tables for fast symmetric function generators*. Instrumentation and Measurement, IEEE Transactions on, vol. 48, pages 1254 – 1258, 01 2000. (Cited in page 57.)

[Mahmood 2019] Mahmood, A., Sisinni, E., Guntupalli, L., Rondón, R., Hassan, S. A. and Gidlund, M. *Scalability Analysis of a LoRa Network Under Imperfect Orthogonality*. IEEE Transactions on Industrial Informatics, vol. 15, no. 3, pages 1425–1436, 2019. (Cited in pages 26 and 27.)

[Mannoni 2022] Mannoni, V., Berg, V., Cazalens, S. and Raveneau, P. *System Level Evaluation for NB-IoT Satellite Communications*. In 2022 IEEE 95th Vehicular Technology Conference: (VTC2022-Spring), pages 1–6, 2022. (Cited in page 1.)

[Markkula 2019] Markkula, J., Mikhaylov, K. and Haapola, J. *Simulating LoRaWAN: On Importance of Inter Spreading Factor Interference and Collision Effect*. In IEEE International Conference on Communications (ICC), pages 1–7, 2019. (Cited in pages 26, 27, and 28.)

[Martín 2018] Martín, A. G., Leal, R. P., Armada, A. G. and Durán, A. F. *NBIoT Random Access Procedure: System Simulation and Performance.* In 2018 Global Information Infrastructure and Networking Symposium (GIIS), pages 1–5, 2018. (Cited in page 81.)

[Mekki 2019] Mekki, K., Bajic, E., Chaxel, F. and Meyer, F. *A comparative study of LPWAN technologies for large-scale IoT deployment.* ICT Express, vol. 5, 2019. (Cited in page 1.)

[Migabo 2018] Migabo, E., Djouani, K. and Kurien, A. *A Modelling Approach for the Narrowband IoT (NB-IoT) Physical (PHY) Layer Performance.* In IECON - 44th Annual Conference of the IEEE Industrial Electronics Society, pages 5207–5214, 2018. (Cited in pages 26, 28, and 29.)

[Migabo 2020] Migabo, E. M., Djouani, K. D. and Kurien, A. M. *The Narrowband Internet of Things (NB-IoT) Resources Management Performance State of Art, Challenges, and Opportunities.* IEEE Access, vol. 8, pages 97658–97675, 2020. (Cited in page 1.)

[Mohamad Hashim 2023] Mohamad Hashim, I. S. and Al-Hourani, A. *Satellite Based Localization of IoT Devices Using Joint Doppler and Angle-of-Arrival Estimation.* Remote Sensing, vol. 15, no. 23, 2023. (Cited in page 50.)

[Morales 2019] Morales, J., Khalife, J. J., Cruz, U. S. and Kassas, Z. *Orbit Modeling for Simultaneous Tracking and Navigation using LEO Satellite Signals.* Proc. of the 32nd Int. Tech. Meeting of the Sat. Division of The Inst. of Navig. (ION GNSS+ 2019), 2019. (Cited in pages 50 and 58.)

[Mowla 2023] Mowla, M. N., Mowla, N., Shah, A. F. M. S., Rabie, K. M. and Shongwe, T. C. *Internet of Things and Wireless Sensor Networks for Smart Agriculture Applications: A Survey.* IEEE Access, vol. 11, pages 145813–145852, 2023. (Cited in page 8.)

[Neinavaie 2021] Neinavaie, M., Khalife, J. and Kassas, Z. *Blind Doppler Tracking and Beacon Detection for Opportunistic Navigation with LEO Satellite Signals.* In 2021 IEEE Aerospace Conference (50100), 2021. (Cited in page 38.)

[Nurgaliyev 2020] Nurgaliyev, M., Saymbetov, A., Yashchyshyn, Y., Kuttybay, N. and Tukymbekov, D. *Prediction of energy consumption for LoRa based wireless sensors network.* Wireless Networks, vol. 26, no. 5, pages 3507–3520, February 2020. (Cited in pages 26, 28, and 29.)

[Oliveira 2017] Oliveira, R., Guardalben, L. and Sargento, S. *Long Range Communications in Urban and Rural environments.* In IEEE Symposium on Computers and Communications (ISCC), pages 810–817, 2017. (Cited in page 18.)

[Palattella 2018] Palattella, M. R. and Accettura, N. *Enabling Internet of Everything Everywhere: LPWAN with Satellite Backhaul.* In Global Information Infrastructure and Networking Symposium (GIIS), pages 1–5, 2018. (Cited in page 1.)

[Palattella 2021] Palattella, M. R., O'Sullivan, J., Pradas, D., McDonnell, K., Rodriguez, I. and Karagiannis, G. *5G Smart Connectivity Platform for Ubiquitous and Automated Innovative Services.* In IEEE 32nd Annual International Symposium on Personal, Indoor and Mobile Radio Communications (PIMRC), pages 1582–1588, 2021. (Cited in page 19.)

[Pan 2020] Pan, M., Hu, J., Yuan, J., Liu, J. and Su, Y. *An Efficient Blind Doppler Shift Estimation and Compensation Method for LEO Satellite Communications.* In IEEE ICCT, 2020. (Cited in page 38.)

[Paonni 2010] Paonni, M., Anghileri, M., Wallner, S., Avila-Rodriguez, J.-A. and Eissfeller, B. *Performance assessment of GNSS signals in terms of time to first fix for cold, warm and hot start.* Institute of Navigation - International Technical Meeting 2010, ITM 2010, vol. 2, pages 1221–1236, 01 2010. (Cited in page 53.)

[Philip 2021] Philip, M. S. and Singh, P. *Energy Consumption Evaluation of LoRa Sensor Nodes in Wireless Sensor Network.* In Advanced Communication Technologies and Signal Processing (ACTS), pages 1–4, 2021. (Cited in pages 26 and 29.)

[Piyare 2018] Piyare, R., Murphy, A. L., Magno, M. and Benini, L. *On-Demand LoRa: Asynchronous TDMA for Energy Efficient and Low Latency Communication in IoT.* Sensors, vol. 18, no. 11, 2018. (Cited in page 18.)

[Poghosyan 2017] Poghosyan, A. H. and Golkar, A. *CubeSat evolution: Analyzing CubeSat capabilities for conducting science missions.* Progress in Aerospace Sciences, vol. 88, pages 59–83, 2017. (Cited in page 1.)

[Polonelli 2019] Polonelli, T., Brunelli, D., Marzocchi, A. and Benini, L. *Slotted ALOHA on LoRaWAN-Design, Analysis, and Deployment.* Sensors, vol. 19, no. 4, page 838, Feb 2019. (Cited in page 10.)

[Qu 2017] Qu, Z., Zhang, G., Cao, H. and Xie, J. *LEO Satellite Constellation for Internet of Things.* IEEE Access, vol. 5, 2017. (Cited in page 19.)

[Rhodes 2023] Rhodes, B. *Skyfield: High precision research-grade positions for planets and Earth satellites generator*, 2023. (Cited in page 64.)

[Roberts 1975] Roberts, L. *ALOHA Packet System With and Without Slots and Capture.* SIGCOMM Comput. Commun. Rev., vol. 5, pages 28–42, 04 1975. (Cited in page 83.)

[Rouzegar 2019] Rouzegar, H. and Ghanbarisabagh, M. *Estimation of Doppler Curve for LEO Satellites.* Wireless Personal Communications, 2019. (Cited in page 38.)

[Selvaraj 2019] Selvaraj, S. and Sundaravaradhan, S. *Challenges and opportunities in IoT healthcare systems: a systematic review.* SN Applied Sciences, vol. 2, 2019. (Cited in page 8.)

[Semtech 2009] Semtech. *LoRa Alliance, LoRaWAN Specifications, Available online: https://lora-alliance.org/*, 2009. Accessed on 1 September 2021. (Cited in page 1.)

[Sigfox 2010] Sigfox. *Sigfox, Available online:https://www.sigfox.com/en*, 2010. Accessed on 1 May 2022. (Cited in page 1.)

[Soret 2014] Soret, B., Mogensen, P., Pedersen, K. I. and Aguayo-Torres, M. C. *Fundamental tradeoffs among reliability, latency and throughput in cellular networks.* In IEEE Globecom Workshops (GC Wkshps), pages 1391–1396, 2014. (Cited in page 25.)

[Stiller 2020] Stiller, B., Schiller, E., Schmitt, C., Ziegler, S. and James, M. *An overview of network communication technologies for IoT.* Handbook of Internet-of-Things, vol. 12, 2020. (Cited in page 9.)

[Su 2019] Su, Y., Liu, Y., Zhou, Y., Yuan, J., Cao, H. and Shi, J. *Broadband LEO Satellite Communications: Architectures and Key Technologies.* IEEE Wireless Communications, vol. 26, no. 2, pages 55–61, 2019. (Cited in page 48.)

[Sun 2018] Sun, Y., Tong, F., Zhang, Z. and He, S. *Throughput Modeling and Analysis of Random Access in Narrowband Internet of Things.* IEEE Internet of Things Journal, vol. 5, no. 3, pages 1485–1493, 2018. (Cited in pages 26, 29, and 81.)

[Sørensen 2017] Sørensen, R. B., Kim, D. M., Nielsen, J. J. and Popovski, P. *Analysis of Latency and MAC-Layer Performance for Class A LoRaWAN.* IEEE Wireless Communications Letters, vol. 6, no. 5, pages 566–569, 2017. (Cited in pages 26, 27, and 28.)

[Sørensen 2022] Sørensen, A., Wang, H., Remy, M. J., Kjettrup, N., Sørensen, R. B., Nielsen, J. J., Popovski, P. and Madueño, G. C. *Modeling and Experimental Validation for Battery Lifetime Estimation in NB-IoT and LTE-M.* IEEE Internet of Things Journal, vol. 9, no. 12, pages 9804–9819, 2022. (Cited in page 51.)

[Tondo 2021] Tondo, F. A., Montejo-Sánchez, S., Pellenz, M. E., Céspedes, S. and Souza, R. D. *Direct-to-Satellite IoT Slotted Aloha Systems with Multiple Satellites and Unequal Erasure Probabilities.* Sensors, vol. 21, no. 21, 2021. (Cited in page 23.)

[Tuzi 2023] Tuzi, D., Aguilar, E. F., Delamotte, T., Karabulut-Kurt, G. and Knopp, A. *Distributed Approach to Satellite Direct-to-Cell Connectivity in 6G Non-Terrestrial Networks.* IEEE Wireless Communications, vol. 30, no. 6, pages 28–34, 2023. (Cited in page 48.)

[Vatalaro 1995] Vatalaro, F., Corazza, G., Caini, C. and Ferrarelli, C. *Analysis of LEO, MEO, and GEO global mobile satellite systems in the presence of interference and fading.* IEEE Journal on Selected Areas in Communications, vol. 13, no. 2, pages 291–300, 1995. (Cited in page 21.)

[Vomhoff 2023] Vomhoff, V., Raffeck, S., Gebert, S., Geissler, S. and Hossfeld, T. *NB-IoT vs. LTE-M: Measurement Study of the Energy Consumption of LPWAN Technologies.* In 2023 IEEE ICC Workshops, pages 403–408, 2023. (Cited in page 51.)

[Wang 1993] Wang, C.-J. *Structural properties of a low Earth orbit satellite constellation - the Walker delta network.* In Proceedings of MILCOM '93 - IEEE Military Communications Conference, volume 3, pages 968–972 vol.3, 1993. (Cited in page 52.)

[Wang 2019] Wang, W., Tong, Y., Li, L., Lu, A.-A., You, L. and Gao, X. *Near Optimal Timing and Frequency Offset Estimation for 5G Integrated LEO Satellite Communication System.* IEEE Access, vol. 7, 2019. (Cited in pages 36, 38, and 49.)

[Xu 2014] Xu, L., He, W. and Li, S. *Internet of Things in Industries: A Survey.* IEEE Transactions on Industrial Informatics, vol. 10, pages 2233–2243, 2014. (Cited in page 8.)

[Xu 2023] Xu, Y., Jiang, J., He, D. and Zhang, W. *A NB-IoT Random Access Scheme Based on Change Point Detection in NTNs.* IEEE Open Journal of the Communications Society, vol. 4, pages 2176–2185, 2023. (Cited in page 82.)

[Yaqoob 2022] Yaqoob, M., Lashab, A., Vasquez, J. C., Guerrero, J. M., Orchard, M. E. and Bintoudi, A. D. *A Comprehensive Review on Small Satellite Microgrids.* IEEE Transactions on Power Electronics, vol. 37, no. 10, pages 12741–12762, 2022. (Cited in page 1.)

[Yin 2023] Yin, Y., Zhao, D., Li, X. and Zeng, S. *Learning Based Preamble Collision Detection of Cellular Random Access by Physical Layer Features.* In 2023 International Conference on Networking and Network Applications (NaNA), pages 28–33, 2023. (Cited in page 82.)

[You 2022] You, B., Jung, H. and Lee, I.-H. *Survey on Doppler Characterization and Compensation Schemes in LEO Satellite Communication Systems.* In 2022 27th Asia Pacific Conference on Communications (APCC), 2022. (Cited in page 37.)

[Zanella 2014] Zanella, A., Bui, N., Castellani, A. P., Vangelista, L. and Zorzi, M. *Internet of Things for Smart Cities.* IEEE Internet of Things Journal, vol. 1, pages 22–32, 2014. (Cited in page 8.)

[Zhang 2022] Zhang, Z., Wang, D., Liu, L., Wang, B. and Sun, C. *A Frequency Offset Independent Timing Synchronization Method for 5G Integrated LEO Satellite Communication System.* In 2022 IEEE 22nd Int. Conf. on Comm. Tech. (ICCT), pages 423–427, 2022. (Cited in page 49.)

[Zhen 2021] Zhen, L., Zhang, Y., Yu, K., Kumar, N., Barnawi, A. and Xie, Y. *Early Collision Detection for Massive Random Access in Satellite-Based Internet of Things.* IEEE Transactions on Vehicular Technology, vol. 70, no. 5, pages 5184–5189, 2021. (Cited in page 82.)

[Zhu 2024] Zhu, J., Sun, Y. and Peng, M. *Timing Advance Estimation in Low Earth Orbit Satellite Networks.* IEEE Transactions on Vehicular Technology, vol. 73, no. 3, pages 4366–4382, 2024. (Cited in page 82.)

[Zong 2019] Zong, P. and Kohani, S. *Optimal Satellite LEO Constellation Design Based on Global Coverage in One Revisit Time.* International Journal of Aerospace Engineering, vol. 2019, pages 1–12, 2019. (Cited in page 61.)

[Zorbas 2021] Zorbas, D., Caillouet, C., Abdelfadeel Hassan, K. and Pesch, D. *Optimal Data Collection Time in LoRa Networks—A Time-Slotted Approach.* Sensors, vol. 21, no. 4, 2021. (Cited in page 24.)